Economic Geology

BULLETIN OF THE SOCIETY OF ECONOMIC GEOLOGISTS

VOL. 118 August NO. 5

A Reevaluation of the Timing and Temperature of Copper and Molybdenum Precipitation in Porphyry Deposits

Federico Cernuschi,[1,2,†] John H. Dilles,[2] Jaime Osorio,[2] John M. Proffett,[3] and Kalin Kouzmanov[4]

[1]*Eclectic Rock, Calle 18 y 28, Punta del Este 20000, Uruguay*

[2]*College of Earth, Ocean, and Atmospheric Sciences (CEOAS), Oregon State University, Corvallis, Oregon 97331, USA*

[3]*P.O. Box 772066, Eagle River, Alaska 99577, USA*

[4]*University of Geneva, Geneva CH-1205, Switzerland*

Abstract

The timing and temperature at which copper-iron and molybdenum sulfide deposition occurs in porphyry deposits remain controversial. Petrologic estimates indicate that veins and wall-rock alteration zones containing copper-iron sulfides form in a wide temperature range from ~350° to 650°C. Most sulfides are hosted in potassium(K)-silicate–altered rock and quartz A veins or in early-halo alteration selvages formed above ~450°C. In contrast, cathodoluminescence (CL) imaging of A veins indicates that copper-iron sulfides are contained within a primary lucent (bright and gray)-CL quartz and are crosscut by microfractures filled with younger dull (dark and medium-gray)-CL quartz in direct contact with copper-iron sulfides. These observations have been interpreted as supporting late copper-iron sulfide introduction together with dull-CL quartz at moderate temperatures of ~300° to 450°C, based on fluid inclusion estimates.

We provide new CL, QEMSCAN, and petrographic data and images of vein quartz as well as petrologic data of altered wall rock from Haquira East (Peru), Encuentro (Chile), and Batu Hijau (Indonesia) porphyry deposits, which were formed at conditions ranging from deep to shallow (~2–10 km). At all three deposits, dull-CL quartz in microfractures is ubiquitously observed crosscutting all generations of high-temperature lucent-CL quartz veins. Each lucent-CL vein type hosts distinct sulfide populations, crosscuts the others, and coexists in space within the copper and molybdenum ore zones. Within this ore zone, the dull-CL quartz only contains copper-iron sulfides where it transects old A veins and early halos, molybdenite where it transects young molybdenite-bearing quartz veins, and both copper-iron sulfides and molybdenite in younger B veins. Furthermore, where the dull-CL quartz crosscuts igneous or barren (deep) quartz veins, it typically lacks copper and molybdenum. Therefore, dull-CL quartz has no particular spatial or genetic affinity with copper-iron sulfides or molybdenite.

We propose that copper was introduced and precipitated at high temperatures in stability with K-silicate alteration. In shallow porphyry deposits, most copper was introduced with lucent-CL quartz in A veins, likely formed via adiabatic decompression from magmatic lithostatic to hydrostatic conditions at ~450° to 600°C. In deep deposits, most copper is introduced with quartz-poor early halos, likely formed at a temperature range similar to that of A veins but during an early stage of retrograde silica solubility. The inferred timing and temperature of copper precipitation are consistent with available solubility experiments for copper-bearing solutions that suggest copper precipitation may start at a high temperature of ~600°C, and ~90% precipitates before it cools down to ~400°C. Much of the molybdenum is introduced and precipitated with discrete pulses of molybdenite-bearing quartz veins that crosscut and postdate copper-bearing A veins and early halos and, to a lesser degree, with B veins that may carry both copper and molybdenum. Whereas molybdenite-bearing and barren (deep) quartz veins form at relatively high temperatures of ~550° to 650°C, copper-molybdenum–bearing B veins likely form at lower temperatures near ~500°C.

Copper precipitation and local copper remobilization from older veins and halos continued during the formation of copper-iron sulfide veinlets, named C veins, and during the precipitation of dull-CL quartz following K-silicate alteration. C veins and even younger pyrite-rich D veins may have chlorite or sericite selvages and are composed of dull-CL quartz that formed at ~450° and 300° to 450°C, respectively.

Microfractures form through all lucent-CL quartz veins because of the thermal contraction of high-temperature quartz at the onset of sustained cooling after K-silicate alteration has ceased. The fluid that migrated through these microfractures was initially in retrograde silica solubility, which causes dissolution and corrosion of the older lucent-CL quartz. The formation of C veins may overlap in time with the initial stage. At a later

[†]Corresponding author: e-mail, fede@eclectic-rock.com

ISSN 0361-0128; doi:10.5382/econgeo.5032; 35 p.
Digital appendices are available in the online Supplements section.

Submitted: August 22, 2021/Accepted: April 18, 2023

stage and temperatures below <450°C, the fluid precipitates dull-CL quartz in microfractures and dissolution zones within older lucent-CL quartz. In copper-iron sulfide-bearing A and B veins and molybdenite-bearing quartz veins, corroded lucent-CL quartz and the younger dull-CL quartz infill can often be observed in contact with older sulfides because quartz sulfide grain boundaries are preexisting discontinuities, and they are preferentially opened during volume contraction. Collectively, these observations and estimates are consistent with silicate phase petrology and numerous observations that most copper-iron sulfides precipitate in K-silicate alteration zones or in early halos with K-feldspar-muscovite-biotite assemblages.

Introduction

Porphyry deposits are large Cu ± Mo ± Au mineral deposits associated with shallowly emplaced arc-type granitoids typically in convergent tectonic settings. Sulfide mineralization is intimately related to quartz-bearing veins and hydrothermal wall-rock alteration (Seedorff et al., 2005; Sillitoe, 2010). These deposits form where magmatic-hydrothermal fluid separates from an intermediate to silicic magma at some depth below the ore zone and ascends by hydrofracturing the overlying wall rock where it reacts with rock, cools, and depressurizes to form veins and Fe-, Cu-, Mo-, and Au-bearing sulfides. Porphyry deposits are closely associated with magmatic-hydrothermal fluids derived from hydrous, sulfur- and chlorine-rich, intermediate to silicic magmas. There is a strong correlation between the economic ore metal suite and the magmatic composition (Seedorff et al., 2005). Although porphyry dikes are universally associated with porphyry Cu ores, the source magma chamber is not commonly exposed, as it is in some districts like Yerington, Nevada. In most cases, the high-Cu-grade ore is inferred to have developed closely above (<0.5–2 km) the cupolas or tops of the deep granitoid source (Steinberger et al., 2013; Dilles and John, 2021).

The release of magmatic-hydrothermal fluids is synchronous with the emplacement of one or more porphyry dikes and stocks (Fig. 1; e.g., Gustafson and Hunt, 1975; Proffett, 1979; Dilles, 1987; Dilles et al., 2000; Redmond and Einaudi, 2010). Temporal evolution and spatial zoning of ore metals and hydrothermally altered rocks range from the millimeter to kilometer scale. Early porphyry intrusions (older) are commonly associated with higher Cu grades, more quartz veins, and widespread K-silicate alteration (Proffett, 1979; Redmond and Einaudi, 2010). Later porphyries (younger) are associated with lower Cu grades and vein densities. The latest magmatic-hydrothermal events, in some cases postdating all porphyries, are characterized by low Cu/Mo, and are in turn followed by abundant pyrite-rich D veins with sericitic alteration (muscovite). Hydrothermal fluids derived from the associated magmas transport metals as chloride complexes and sulfur species that may react with metals to form sulfides, acids, and alkalis that produce wall-rock alteration from magmatic temperatures of ~350° to 650°C. Hydrostatically pressured nonmagmatic fluids are commonly restricted to <350°C (e.g., Tosdal and Dilles, 2020).

Within this magmatic-hydrothermal history, the timing and temperature of Cu- and Au-bearing sulfide deposition remain contentious and poorly resolved, partly because all Cu-Fe sulfides that precipitated above ~300°C underwent recrystallization at a lower temperature than their original precipitation conditions (Barton and Skinner, 1967). For example, the original Cu-Fe sulfide containing Au in a solid solution might have precipitated as a Cu-rich intermediate solid solution at 500° to 600°C but recrystallized to intergrowths of chalcopyrite-bornite during cooling of the hydrothermal system and the wall rock at <200° to about 300°C.

Currently, two hypotheses are proposed regarding the timing and temperature of the original Cu-Fe sulfide introduction and precipitation.

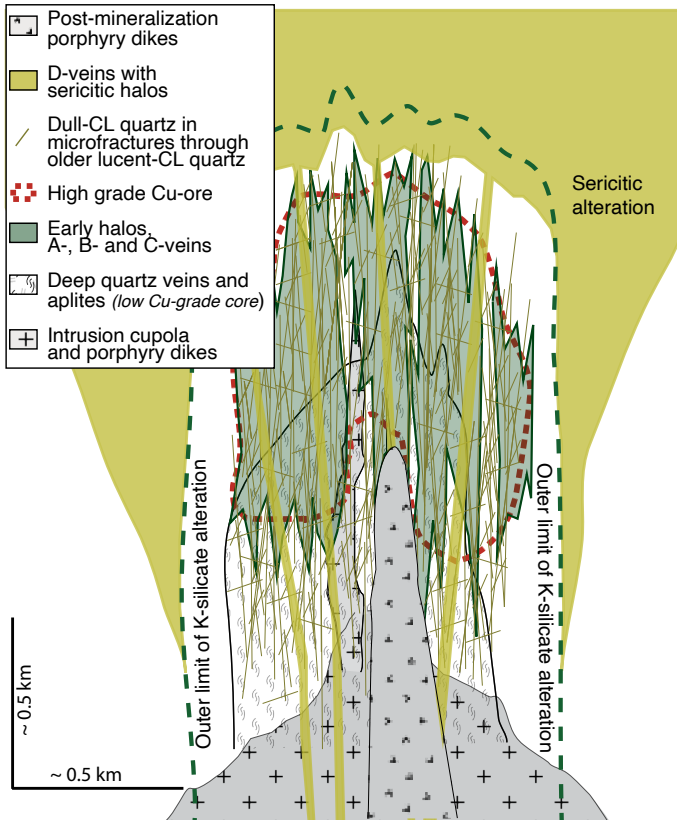

Fig. 1. Schematic zonation model of a porphyry deposit. The high-grade Cu ore correlates with the distribution of Cu-Fe sulfide-bearing early halos and/or A veins and, in some cases, B and C veins. An inverted cup-shaped Cu ore zone sits on top and to the sides of a low-Cu-grade core that may have abundant deep quartz veins, aplite dikes, and postmineralization dikes. The Cu ore and its low-Cu-grade core are included within the limits of the K-silicate alteration zone as mapped by hydrothermal biotite replacements of magmatic hornblende. Dull-CL quartz in microfractures crosscuts all types of lucent-CL quartz in all older vein types and magmatic quartz. Younger sericitic alteration dominates at shallower depths and to the sides of the K-silicate alteration and in structurally controlled D veins and sericitic halos that crosscut the K-silicate–altered zone. Propylitic, sodic-calcic, calcic alteration, and intermediate argillic alteration overprints are not depicted in this cartoon. Microfractures filled with dark-CL quartz are not shown to scale for illustration purposes. Figure modified after Gustafson and Hunt (1975), Seedorff et al. (2005), Sillitoe (2010), and Cernuschi (2015). Abbreviations: CL = cathodoluminescence.

Hypothesis 1: Cu-Fe sulfide is initially deposited early at high to moderate temperature

Early studies noted the close association of ore sulfides with porphyry dike emplacement, quartz A veins, early halos, and rock altered to K-silicate assemblages containing hydrothermal biotite, K-feldspar, and local andalusite thought to form at high temperature based on mineral phase equilibria (450°–~650°C; Fig. 2; Meyer, 1965; Brimhall, 1977; Seedorff et al., 2005; Proffett, 2009). Ti-in-quartz geothermometry of quartz A veins and S isotope thermometry data agree with these mineral phase equilibria estimates (e.g., Field et al., 2005; Seedorff et al., 2005; Rusk et al., 2006; Mercer and Reed, 2013; Maydagan et al., 2015; Osorio, 2017; Cernuschi et al., 2018; Rottier and Casanova, 2021).

Experimental studies on high-temperature transport and on precipitation of Cu cooling below 500° to ~600°C support hypothesis 1 (Brimhall, 1977; Hemley and Hunt, 1992; Hemley et al., 1992). The available fluid inclusion data from older quartz in veins indicate high equilibration temperatures ranging from 450° to >650°C (e.g., A-vein quartz in Roedder, 1984; lucent-CL quartz in Landtwing et al., 2010). Nonetheless, fluid inclusion studies have been hampered by the lack of Cu-Fe sulfides that are demonstrably trapped in older quartz and the scarcity of preserved high-temperature primary fluid inclusions in high-temperature quartz. Similarly, the paucity of hydrothermal quartz that precipitates in the pressure-temperature region of retrograde silica solubility that is traversed by most fluids during ascent, the complexity of numerous superimposed hydrothermal events, and the likelihood of annealing of quartz further complicate the study of primary fluid inclusions in older quartz types (e.g., Audétat and Günther, 1999; Audétat et al., 2008; Bodnar et al., 2014; Monecke et al., 2018).

Hypothesis 2: Cu-Fe sulfide is initially deposited late at a relatively low temperature

Distinct quartz generations within a single quartz vein type have been identified via cathodoluminescence (CL) imaging based on differences in CL brightness and texture (Rusk and Reed, 2002; Redmond et al., 2004). These observations have raised the question of which quartz generations were precipitated synchronously with the observed wall-rock alteration assemblage and which quartz generations are genuinely related to the introduction and precipitation of Cu-Mo-Au–bearing sulfides (Redmond et al., 2004). Because of the close correlation between the scanning electron microscopy (SEM)-CL brightness of quartz and its precipitation temperature (e.g., Huang and Audétat, 2012; Thomas and Watson, 2012), these observations also have implications for the precipitation temperature of sulfides associated with quartz with a range of observed CL brightness. A diverse terminology has been used to describe quartz's different types of CL brightness. Here we simplify the nomenclature into lucent-CL quartz for the more luminescent types and dull-CL for the least luminescent but note that a broad range is observed (see Table 1 and the Methods section for details).

Copper-iron sulfides in lucent-CL quartz of A and B veins were identified in contact with a young and dull-CL quartz generation that crosscuts the older and lucent-CL quartz in all porphyry deposits studied with SEM-CL, including Butte,

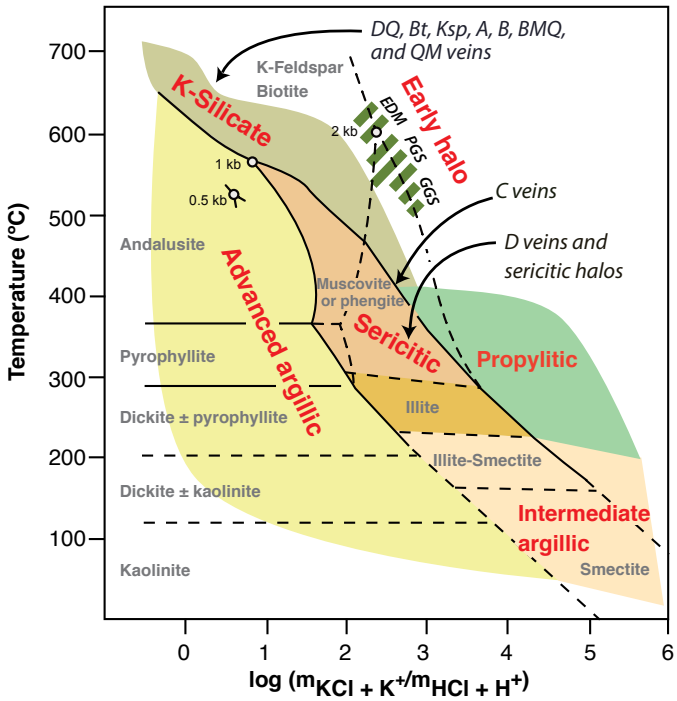

Fig. 2. Phase diagram of hydrothermal mineral stabilities for the system K_2O-Al_2O_3-SiO_2-H_2O-KCl-HCl at quartz saturation as a function of fluid composition and temperature at 1 kbar pressure. Phase equilibria at 0.5 and 2 kbar are only shown at high temperatures. Modified from Hemley and Jones (1964), Montoya and Hemley (1975), Hemley et al. (1980), Seedorff et al. (2005), and Dilles and John (2021). Early halo alteration is equivalent to transitional alteration in the mineralogical terms described by Seedorff et al. (2005). Abbreviations: BMQ = banded molybdenite-quartz, Bt = biotite veinlets, DQ = deep quartz, EDM = early dark micaceous, GGS = green-gray sericite, Ksp = K-feldspar seams, PGS = pale-green sericite, QM = quartz-molybdenite.

Montana (Rusk et al., 2006); El Salvador, Chile (Rusk, 2012); El Teniente, Chile (Klemn et al., 2007); Los Pelambres, Chile (Rusk, 2012); Bingham, Utah (Redmond et al., 2004; Landtwing et al., 2005); Oyu Tolgoi, Mongolia (Müller et al., 2010); Altar, Argentina (Maydagan et al., 2015); Pebble, Alaska (Gregory, 2017); Yulong, China (Sun et al., 2021); Batu Hijau (Schirra et al., 2019, 2022); Santa Rita (Tsuruoka et al., 2021); and Escondida (Jensen et al., 2022). Lucent-CL quartz in microfractures crosscutting older, slightly less lucent-CL quartz has rarely been observed in contact with sulfides (Elatsite, Stefanova et al., 2014). Whereas the Ti content of lucent-CL quartz in older veins commonly ranges from about 20 to >100 ppm, the Ti content of dull-CL quartz is lower and ranges between 1 and 15 ppm (Table 1). Ti-in-quartz and fluid inclusion temperature estimates for lucent-CL quartz commonly indicate precipitation temperatures ranging from 450° to >650°C (e.g., Roedder, 1971, 1984; Landtwing et al., 2010; Rusk, 2012; Maydagan et al., 2015; Osorio, 2017; Cernuschi et al., 2018). The Ti-in-quartz formation temperature of dull-CL quartz is consistently estimated below about 450°C and as low as ~300°C (Rusk, 2012), in agreement with homogenization temperatures of fluid inclusions in this quartz type (e.g., Landtwing et al., 2005, 2010; Klemm et al., 2007; Redmond and Einaudi, 2010; Zwyer, 2010). These observations have been interpreted to mean synchronous deposition of the

Table 1. Wall-Rock Alteration Zones, Vein Types, and SEM-CL Features at Batu Hijau, Encuentro, and Haquira

Alteration type/minerals		Vein/halo type	Abbreviation	Key vein/halo silicate minerals	Vein/halo ore minerals
K-silicate alteration					
Biot-ksp ± alb		Deep quartz veins	DQ	Qtz-ksp ± anh	± Mag-py ± cpy
		A veins	A	Qtz ± ksp	Cpy-bn-dg-py-mag
Early-halo alteration					
Ksp-pheng-biot ± and	Early halos	Early dark micaceous	EDM	Ksp-biot-pheng ± and	Cpy-bn ± py
		Pale-green sericite	PGS	Ksp-pheng-biot	
		Green-gray sericite	GGS	Ksp-pheng ± biot	
K-silicate alteration					
-		Banded molybdenite-quartz veins	BMQ	Qtz	Mb
± Ksp		B veins	B	Qtz ± ksp ± anh	Cpy-bn-py ± mb
-		Quartz-molybdenite veins	QM	Qtz-anh ± ksp	Mb
Chl ± sericite		C veins	C	± Qtz	Cpy-bn ± py
Sericitic alteration					
Chl ± sericite		C veins	C	± Qtz	Cpy-bn ± py
Musc/pheng-chl		D veins and sericitic halos	D	Musc ± qtz	Py ± cpy-bn
Intermediate argillic alteration					
Ill-smec-chl-kaol		Clay selvages and patches		Ill-smec-chl-kaol	± Py ± hm

Note: The SEM-CL column shows the main types and subtype of quartz observed under cathodoluminescence for each vein type; T (°C) shows the average of TitaniQ geothermometry for each vein type, rounded to the nearest 50°C bracket and is summarized from Cernuschi (2015), Osorio (2017), and Cernuschi et al. (2018); dashes indicate not observed or not applicable

Abbreviations: and = andalusite, anh = anhydrite, alb = albite, biot = biotite, bn = bornite, chl = chlorite, cpy = chalcopyrite, dg = digenite, hm = hematite, ill = illite, kaol = kaolinite, ksp = K-feldspar, mag = magnetite, mb = molybdenite, musc = muscovite, pheng = phengitic muscovite, py = pyrite, qtz = quartz, SEM-CL = secondary electron microprobe-cathodoluminescence, smec = smectite

dull-CL quartz and Cu-Fe sulfides at a later time and lower temperature (<450°C) than A veins with lucent-CL quartz (Redmond et al., 2004), consistent with earlier studies on the subject that have also argued for late and low-temperature precipitation of Cu-Fe sulfides (e.g., Norton, 1978; Beane and Titley, 1981; Titley and Beane, 1981; Leach, 1999). Moreover, Cu-Fe sulfide deposition has been proposed to occur during a porphyry to epithermal transition that, in some cases, includes the formation of Cu-Fe sulfide-bearing C veins that locally contain minor amounts of dull-CL quartz and postdate A and B veins as well as early halos (e.g., Monecke et al., 2018; Driesner and Heinrich, 2019).

Testing and reconciliation of the hypotheses

Here, we present data from three study sites that sample the full range of depths of porphyry deposit formation, from deep to shallow. A summary of veins and wall-rock alteration is provided in Table 1, and the deposit paragenesis is further described in the Results section. The first site is the ca. 33 Ma Haquira East deposit of southern Peru, formed in the Eocene Andahuaylas-Yauri batholith at a greater depth of ~8 km based on fluid inclusion data and hornblende barometry (Cernuschi, 2015; Cernuschi et al., 2018). Fluid inclusions are low salinity (intermediate density) and two phase and were therefore trapped in the one-phase part of the water-NaCl system at pressures >1.4 kbar (5-km depth). Fluid inclusion homogenization behavior and phase petrology of host early halos and A veins suggest trapping pressures of ~2.2 to 2.5 kbar (~8–10 km depth; B. Rusk and Y. Zhang, unpub. data, 2015; Cernuschi, 2015; Cernuschi et al., 2018). Haquira East is characterized by a variety of veins and dikes that include—from earliest to latest—early sulfide-poor deep quartz veins (DQ), aplite dikes, and biotite-only veins; Cu-Fe sulfide-rich and quartz-poor early halos and a smaller volume of associated quartz A veins and Cu-Fe sulfide stringers with biotite; banded molybdenite-quartz veins (BMQ); quartz B veins having a centerline infilled with bornite-chalcopyrite ± molybdenite; rare C veins of chalcopyrite ± bornite with no quartz; D veins with pyrite-quartz ± muscovite ± sparse chalcopyrite and alteration selvages composed of muscovite ± pyrite ± quartz and sparse intermediate green/white intermediate argillic selvages with chlorite, smectite, and local kaolinite.

The second site is the ca. 41 Ma Encuentro porphyry Cu-Au-Mo deposit, Centinela district, northern Chile, which formed at an intermediate depth estimated at ~5 km (Osorio, 2017). A veins contain single-phase (intermediate-density) fluid inclusions that homogenize at higher temperatures than ubiquitous brine and vapor-rich inclusions. Inclusion homogenization behavior suggests fluids were trapped at pressures near the brine-vapor solvus or slightly above (Osorio, 2017; Osorio et al., 2018). From earliest to latest and stable with K-silicate alteration, the vein sequence in-

Table 1. (*Cont.*)

	Deep	Intermediate	Shallow	SEM-CL			
Texture	Haquira	Encuentro	Batu Hijau	Type	Subtype	T (°C)	Mineralization
Massive, milky, continuous qtz	Abundant	Some	Trace	Lucent-CL	Bright-CL	~650	-
Sugary qtz, sinuous, discontinuous	Some	Abundant	Abundant	Lucent-CL	Bright- and gray-CL	>550	Cu-Au
Sinous margins, lack centerline infill, associated anastomosing discontinuous veinlets	Abundant (EDM > PGS ± GGS)	Some (EDM)	Rare	Lucent-CL	Rare gray-CL	>500	
Massive, milky, continuous qtz w/ thin mb bands	Abundant	Some	Rare	Lucent-CL	Bright-CL	>600	Mo
Open space, straight-walled, central sulfide infill, qtz growth zoning	Some	Some	Some	Lucent-CL	Bright- and gray-CL	~500	± Cu-(Mo)
Massive, milky, continuous qtz; anhydrite might be abundant	-	Abundant	-	Lucent-CL	Gray-CL	~550	Mo
Sulfide vein, rare qtz	Trace	Trace	Trace	Dull-CL	Medium-gray-CL	~450	± Cu-Au
Sulfide vein, rare qtz	Trace	Trace	Trace	Dull-CL	Medium-gray-CL	~450	± Cu-Au
Central, thin and straight py vein ± qtz with thicker and straight-walled qtz-musc-py halo	Rare	Some	Some	Dull-CL	Dark-CL	~350	-
Veining is rare	Some	-	-	-	-	<300	-

cludes sparse biotite and early halos, Cu-rich and abundant A veins with quartz-K-feldspar-chalcopyrite-bornite, B veins with quartz-chalcopyrite ± molybdenite, quartz-anhydrite-molybdenite ± chalcopyrite veins (QM), and associated and sparse magnetite ± chalcopyrite veinlets. A younger series of veins has hydrothermal muscovite selvages and includes (earliest to latest) rare C veins filled with chalcopyrite-pyrite or chalcopyrite-chlorite-sericite ± pyrite, D veins with pyrite ± chalcopyrite or tourmaline-pyrite ± chalcopyrite, and sericitic halos. A dense stockwork of A veins and sparse early halos contains chalcopyrite and bornite and is associated with the high-grade Cu-Au ore zones (Osorio, 2017; Osorio and Dilles, 2019).

The third site is the ca. 3.7 Ma Batu Hijau Cu-Au deposit on Sumbawa Island, Indonesia, which formed shallowly at an estimated 2-km depth, based on amphibole barometry and (U/Th)/He geochronometry and thickness estimates of the volcaniclastic wall rock that lies above the deposit (see Garwin, 2002, and references therein). It is characterized by a vein sequence, from earliest to latest, of sparse biotite veins; A-family veins (including thick deep quartz veins with magnetite); thin A veins with magnetite-ilmenite; abundant Cu-rich A veins with quartz + bornite + albite ± chalcopyrite; sparse early halos with Cu-Fe sulfides, B veins with quartz, and a centerline infilled by bornite-chalcopyrite ± molybdenite (including banded molybdenite-quartz veins); and rare to sparse C veins containing Cu-Fe sulfide and having chlorite-bearing selvages. Sparse pyrite-rich D veins are associated with selvages of muscovite, local pyrophyllite, or clay minerals (Clode et al., 1999; Garwin, 2002; Setyandhaka et al., 2008; Proffett, 2019). C veins have been argued to be more abundant than previously described, in part based on local petrography and SEM-CL imaging of A-vein quartz (Schirra et al., 2019, 2022).

This study presents petrographic, CL, and quantitative evaluation of minerals by scanning electron microscopy (QEMSCAN) images from the three deposits and documents vein and rock alteration mineralogy and the textures of quartz and sulfides to estimate the timing of hydrothermal alteration, vein formation, and Cu, Fe, and Mo sulfide deposition. Furthermore, we review the petrologic and geochemical data pertinent to estimating temperature conditions to assign broad temperature ranges for older and younger hydrothermal and mineralization events. Based on the results presented below, we argue that Cu-Fe and Mo sulfide introduction and deposition primarily and initially occurred in early veins and hydrothermal alteration mineral zones at high temperatures above 450°C. Furthermore, we conclude that some Cu-Fe sulfide continued to precipitate at a lower temperature but was more extensively remobilized and recrystallized from earlier deposited sulfides.

Methods

Geologic relationships and samples

Detailed core logging using an Anaconda-style system (Einaudi, 1997) recorded the relative ages of veins based on numerous crosscutting observations at Haquira East, Encuentro, and Batu Hijau (Clode et al., 1999; Setyandhaka et al., 2008; Cernuschi et al., 2013; Osorio, 2017). Samples were collected for mineralogical studies from the three porphyry deposits. To provide further context, we review the previously published vein and hydrothermal alteration descriptions and crosscut-

ting observations for other well-studied porphyry deposits elsewhere and compare them with those studied here.

CL and QEMSCAN methodology

Polished sections were examined in transmitted and reflected light using a standard petrographic microscope. SEM-CL images of 30- and 200-µm-thick polished sections were obtained at the Oregon State University Microscopy facility using an FEI Quanta 600FEG with a Gatan mini-CL detector with a wavelength range between 185 and 850 nm (monochromatic). Images were obtained while operating the instrument between 10 and 15 KeV, with a spot size of 6 µm, scanning time between 50 and 200 µs, and resolution of 1,024 × 884 pixels. Before the analyses, thin sections were coated with carbon or gold (<100 nm thick).

Automated mineral analysis and textural imaging of two samples were performed using an FEI QEMSCAN Quanta 650F facility at the Department of Earth Sciences, University of Geneva, Switzerland. The system is equipped with two Bruker QUANTAX light-element energy dispersive X-ray spectrometers. Analyses were conducted at a high vacuum, accelerating voltage of 25 kV, and a probe current of 10 nA on carbon-coated polished thin sections. FieldImage operating mode (Pirrie et al., 2004) was used for analyses. Between 15 and 325 individual fields were measured per sample, with 1,500, 1,000, or 400 pixels per field, depending on the applied point spacing of 5, 3, or 1 µm, respectively. X-ray spectra acquisition time was 10 ms per pixel. Gray-scale level of backscattered electron (BSE) images was calibrated using quartz (42), Cu (130), and Au (232) standards. Data processing was performed using the iDiscover software package. Final results consist of (1) high-quality spatially resolved and fully quantified mineralogical maps enabling basic image analysis, including particle size and shape distribution, mineral assemblages, and mineral proportion definitions, (2) BSE images with resolution identical to that of the mineralogical maps, and (3) X-ray element distribution maps.

SEM-CL nomenclature

A variety of terminology has been previously used to describe the different types of SEM-CL luminescence in quartz veins from porphyry deposits. We use the term lucent-CL for quartz with moderate to intense luminescence and dull-CL for quartz that is barely luminescent to almost nonluminescent (Table 1). Whereas lucent-CL quartz is dominated by bright-CL and gray-CL subtypes (e.g., Rusk and Reed, 2002), dull-CL quartz is dominated by dark-CL and medium-gray-CL subtypes (e.g., Cernuschi et al., 2018). As summarized in Table 1, whereas older and high-temperature quartz in A and B veins, deep quartz veins, molybdenite-bearing quartz veins, phenocrysts in porphyry dikes, and early halos is composed of lucent-CL quartz (Table 1; i.e., bright- to gray-CL), younger and lower-temperature quartz in C and D veins and in microfractures cutting through all the older quartz types is composed of dull-CL quartz (i.e., medium-gray-CL and dark-CL; Rusk, 2012; Maydagan et al., 2015; Osorio, 2017; Cernuschi et al., 2018).

Titanium-in-quartz

The CL intensity of quartz increases with its Ti content. When quartz precipitates in near-equilibrium conditions, it varies with crystallization temperature, enabling an estimate of formation temperatures using Ti geothermometry (e.g., Wark and Watson, 2006). Ti content, however, also increases with pressure and growth rate, complicating the task of providing robust temperature estimates (Huang and Audetát, 2012). Therefore, we focus the presentation of results and discussions on crosscutting relationships of vein types and the different generations of SEM-CL quartz they contain. We employ Ti-in-quartz temperature only to estimate permissible crystallization ranges of lucent-CL and dull-CL quartz.

Previously reported Ti contents from Haquira East, Encuentro, and Batu Hijau (Cernuschi, 2015; Osorio, 2017; Cernuschi et al., 2018) were obtained by electron microprobe analysis and laser ablation-inductively coupled plasma-mass spectrometry. Temperatures were estimated using the appropriate activity of TiO_2 from CL-uniform large zones of quartz or from the most dull-CL zones to avoid rapidly grown Ti-rich zones. The Huang and Audétat (2012) calibration was employed based on a comparison with other calibrations (Mercer et al., 2015; Acosta et al., 2020).

Veining and Hydrothermal Alteration at Haquira East, Encuentro, Batu Hijau, and Other Porphyry Deposits

Below we summarize some of the veining and hydrothermal alteration details of the three deposits studied here and compare them with other porphyry deposits elsewhere. Vein and alteration types are defined in Table 1 (Seedorff et al., 2005; Sillitoe, 2010). Simplified cross sections for the three deposits studied here are shown in Figure 3.

Vein types, wall-rock alteration assemblages, and morphology of orebodies of the porphyry deposit vary with its formation depth, which ranges between ~2 and >8 km (Seedorff et al., 2005; Dilles and John, 2021). The depth at where the magmatic-hydrothermal fluids are released from the source batholith may be the key controlling factor. Proffett (2009) proposed that in shallow porphyry deposits (<3–4 km), most of the Cu-Fe sulfides and ores are hosted in quartz A veins and associated K-silicate alteration, and consequently, he named these A-vein-type porphyry deposits. In contrast, in deep deposits (>3–4 km), most of the Cu-Fe sulfides and Cu ores are hosted in early-halo alteration selvages (see below for definition) with minor quartz, which he named early-halo-type porphyry deposits (cf. Seedorff et al., 2005). Some porphyry deposits, such as Bingham (Redmond and Einaudi, 2010), contain both abundant A veins and early halos in lower abundance and therefore have been named hybrid deposits and are thought to have formed at intermediate depths (~3–5 km; Proffett, 2009; Dilles and John, 2021). The three deposits studied here represent this diversity (Fig. 3); Haquira East is an early-halo-type deposit (Cernuschi et al., 2018), Batu Hijau is an A-vein-type deposit (Clode et al., 1999), and Encuentro is considered hybrid but dominated by A veins (Osorio and Dilles, 2019).

A veins

Thin, sinuous, and commonly discontinuous quartz A veins with Cu-Fe sulfides are characteristic of the Cu ore in shallowly sourced A-vein-type porphyry deposits like El Salvador (Gustafson and Hunt, 1975), Yerington mine (Proffett, 1979),

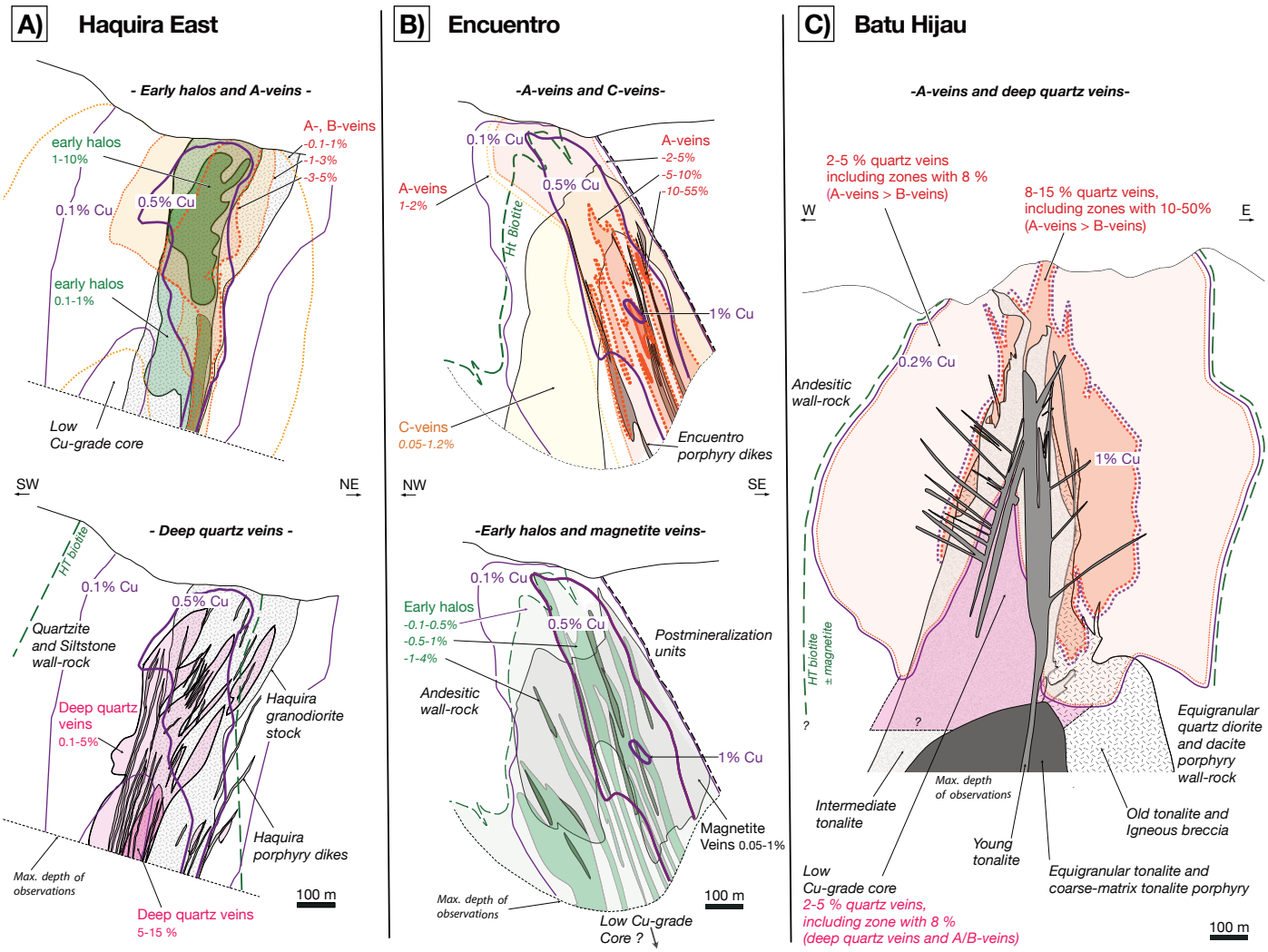

Fig. 3. Simplified cross sections showing the relationships of quartz veins, early halos, K-silicate alteration, and Cu ore for the porphyry copper deposits studied here. A) Haquira East (section 1900NW from Cernuschi, 2015): Cu > 0.1 wt % shows an inverted cup-shaped zone centered near the contact of the Haquira granodiorite and its quartzite/siltstone wall rock. At depth, a low-Cu-grade core (Cu < 0.1 wt %) coincides with the locus of a swarm of thin granodioritic porphyritic dikes that were emplaced close in time with the Cu-bearing veins and early halos. Cu grade is higher in the Haquira granodiorite stock than in wall rock because of the higher Fe content and reactivity of the former (Cernuschi et al., 2013). Deep quartz veins carry little Cu in the low-Cu-grade core, but at shallower depths in the high-Cu-grade shell, they are crosscut by high-density Cu-rich A and B veins and early halos. Both the low-Cu-grade core and the Cu ore shell are enclosed with the zone of hydrothermal biotite replacement of hornblende. B) Encuentro (section 12, from Osorio, 2017): Cu > 0.1 wt % is a vertically elongated zone enclosing the narrower ore zone with Cu > 0.5 wt %. Deep quartz veins are rare. The 0.5 wt % Cu ore shell coincides in space with abundant A veins and sparse early halos. The Cu > 0.1 wt % zone coincides with a zone of early halos and hydrothermal biotite replacement of hornblende that lacks A veins. Chalcopyrite-pyrite C veins with chlorite selvages crosscut early halos and A veins inside the zone of hydrothermal biotite. D veins with sericite (not shown) at shallower levels cut early-halo and A veins and replace hydrothermal biotite. C) Batu Hijau (section 9080N, compiled from Clode et al., 1999; J.M. Proffett, unpub. report, 2003; Setyandhaka et al., 2008). The zone of 0.2 wt % Cu ore has an inverted cup shape and is hosted in wall rock and the central old and intermediate tonalite porphyry intrusions. This zone coincides with the zone of hydrothermal biotite replacement of hornblende and contains up to 8 vol % Cu-bearing A and B quartz veins. Enclosed in the 0.2 wt % Cu zone is a smaller inverted cup-shaped 1 wt % Cu ore shell that contains 8 to 15% Cu-bearing A and B quartz veins and is crosscut by the central intermediate tonalite intrusion. Below the 0.2 wt % zone, a low-Cu-grade core is mostly hosted in the intermediate tonalite intrusion that also contains up to 8 vol % deep quartz veins and less abundant AB veins (Setyandhaka et al., 2008). All Cu zones and A, B, and AB veins are crosscut by the postmineralization young tonalite at the system's center. Abbreviation: HT = hydrothermal.

and Red Chris (Rees et al., 2015) and even much older deposits like Jebel Ohier (Bierlein et al., 2020). The key feature of A veins is that they are composed of quartz grains of aplitic grain size (0.02–0.1 mm). These quartz grains are visible with a typical 20× hand lens and have a sugary texture (Gustafson and Hunt, 1975).

At Batu Hijau, much of the high-grade copper ore is hosted in typical A veins with Cu-Fe sulfide ± magnetite, biotite, oli-

goclase, local albite, and variable amounts of anhydrite (Clode et al., 1999; Fig. 4A; Table 1). At Batu Hijau, morphological variations of sugary quartz veins have been named A-family veins, including slightly thicker and more continuous sugary-textured quartz veins with Cu-Fe sulfides, also called AB veins (Clode et al., 1999, Schirra et al., 2019). Thin A veins with abundant magnetite and fewer Cu-Fe sulfides are older and abundant and are locally crosscut by Cu-Fe sulfide-rich A veins. Elsewhere, similar magnetite-quartz veins are considered A-family veins but have also been named M veins (Seedorff et al., 2005). At Batu Hijau and elsewhere, all A and AB veins predate and are cut by B veins (Gustafson and Hunt, 1975; see below for definition). At Batu Hijau, Cu grade is well correlated with the density of A and AB veins, and to a lesser extent with B veins: whereas the 1 wt % Cu shell is correlated with 8 to 15 vol % of these veins, the broader 0.2 wt % Cu shell correlates with 2 to 5 vol % (Fig. 3D).

Encuentro, a hybrid deposit, has abundant sugary-textured quartz A veins of multiple generations (Fig. 4B) that cut sparse early halos (Fig. 4D; Osorio, 2017; Osorio and Dilles, 2019). Whereas the 0.5 wt % Cu ore shell is well correlated with a 2 to 10 vol % of A veins, early halos contribute up to 0.1 wt % Cu (Fig. 3B).

At Haquira East, A veins are volumetrically minor compared to the more abundant early halos formed at a similar time (Fig. 4C; see next section). Nonetheless, where A veins are present, they carry Cu-Fe sulfides and may have associated K-feldspar halos (Fig. 4G; Table 1). In some cases, these Cu-Fe sulfide-bearing K-feldspar halos are observed with no associated A veins and are reminiscent of the alkali seams previously described at El Salvador, where they are formed at a similar timing to that of A veins (Gustafson and Hunt, 1975). In all the studied deposits, A veins and A-family veins are crosscut by B veins where present, as exemplified at Haquira East (Fig. 4C, H).

Other types of Cu-bearing quartz veins may be present in porphyry copper deposits. For example, banded quartz veins characterized by fluid inclusion-rich dark bands may host Cu-Fe-Au sulfides in shallowly emplaced Au-rich Maricunga-style porphyry deposits (Muntean and Einaudi, 2000, 2001). These veins are commonly observed as a shallow continuation of deeper A veins and may be considered A-family veins because of temporal similarities (Cernuschi et al., in press). However, they are not typically sugary textured, and crosscutting relationships with A veins are poorly constrained. These veins will not be discussed further, because they are not present in the reviewed deposits.

Early halos

In deeply sourced porphyry copper deposits, Cu ore zones have characteristic alteration selvages along a central fracture that commonly lacks a quartz infill (Fig. 4C). These selvages have been named early halos and contain K-feldspar, muscovite (sericite), Cu-Fe sulfides, quartz, and commonly biotite and, in some cases, corundum and andalusite (e.g., Meyer, 1965; Proffett, 2009). Early halos share a characteristic formation timing similar to that of A veins (synchronous or immediately pre- or postdate) and predate B veins and Mo-bearing quartz veins (Proffett, 2009; Cernuschi et al., 2019). Cu-Fe sulfides are mainly disseminated and intergrown with the hydrothermal silicate mineralogy (Fig. 4C-H) and, in many cases, amalgamate into thin, discontinuous, and anastomosing sulfide veinlets that may locally escape from the alteration selvage (Fig. 4I). Magnetite is absent in most early-halo deposits (e.g., Haquira East) with rare exceptions (e.g., Butte; Reed and Dilles, 2020). Early halos host the bulk of the Cu ore in deep early-halo-type porphyry deposits like Butte, Montana (Meyer, 1965; Brimhall, 1972, 1977; Roberts, 1975; Rusk et al., 2008b); Los Pelambres, Chile (Atkinson et al., 1996); Chuquicamata, Chile (Ossandón et al., 2001; Rivera et al., 2012); Taca Taca, Argentina (Benavides, 2017); Copper Cliff, Montana (Uribe-Mogollon and Maher, 2018); and Ann-Mason Pass and Bear, Yerington district, Nevada (Proffett, 2009). At Haquira East, the 0.5 wt % Cu ore shell is well correlated with 1 to 10 vol % of early halos and 3 to 5 vol % of A and B veins hosted in the granodiorite stock (Fig. 3A). The 0.1 wt % Cu shell continues at the quartzite-siltstone wall rock and correlates with the 0.1 to 1 vol % of A and B veins. Early halos are absent in the sedimentary wall rock, and overall Cu grade is lower than at the granodiorite stock because of the limited Fe content and reactivity of the sediments (Cernuschi et al., 2013).

The early-halo hydrothermal mineral assemblages have been previously described as transitional in a mineralogical sense between K-silicate alteration (biotite-K-feldspar) and sericitic or phyllic and muscovite-bearing alteration because of the common coexistence of K-feldspar, biotite, and muscovite (Seedorff et al., 2005). Here, we use the name early halo for this mineral assemblage to avoid the temporal significance of the word transitional (sensu Gustafson and Hunt, 1975). In contrast to younger muscovite (sericitic) halos associated with D veins, which do not have either K-feldspar or biotite, the muscovite in early halos commonly has a phengitic composition (Fe-Mg–rich), regardless of formation position within the porphyry center (e.g., Rusk et al., 2008b; Reed et al., 2013; Cernuschi et al., 2013, 2019; Benavides, 2017; Uribe-Mogollon and Maher, 2018; Alva-Jimenez et al., 2020).

The essential mineralogy of early halos is K-feldspar and muscovite, and the abundance of biotite varies greatly, with a profound impact on the macroscopically observed color. Based on the relative abundance of biotite and for descriptive purposes, early halos can be subdivided into three subtypes (Cernuschi et al., 2019): (1) early dark micaceous, which contains hydrothermal K-feldspar, muscovite, and abundant biotite (Butte: Meyer, 1965; Brimhall, 1977; Haquira: Fig. 4C, G), (2) pale-green sericite, which contains K-feldspar and coarser-grained muscovite but minor biotite (Butte: Reed, 1999; Reed and Dilles, 2020; Los Pelambres, Chile, T4: Atkinson et al., 1996; Copper Creek, Arizona: Riedell et al., 2013; Haquira: Fig. 4E, H), and (3) green-gray sericite, also characterized by K-feldspar and muscovite but only traces of biotite (Los Pelambres, green mica: Atkinson et al., 1996; Haquira: Fig. 4F, I). The green-gray sericite subtype also includes the previously defined dark-green sericitic halos at Butte, Montana, which have chlorite that replaced most hydrothermal biotite (Reed et al., 2013). For consistency, we use the name green-gray sericite to replace the name green sericite used for this subtype of early halo in Cernuschi et al. (2019).

The dominant subtype of early halo varies from one deposit to another and likely reflects wall-rock composition, changes

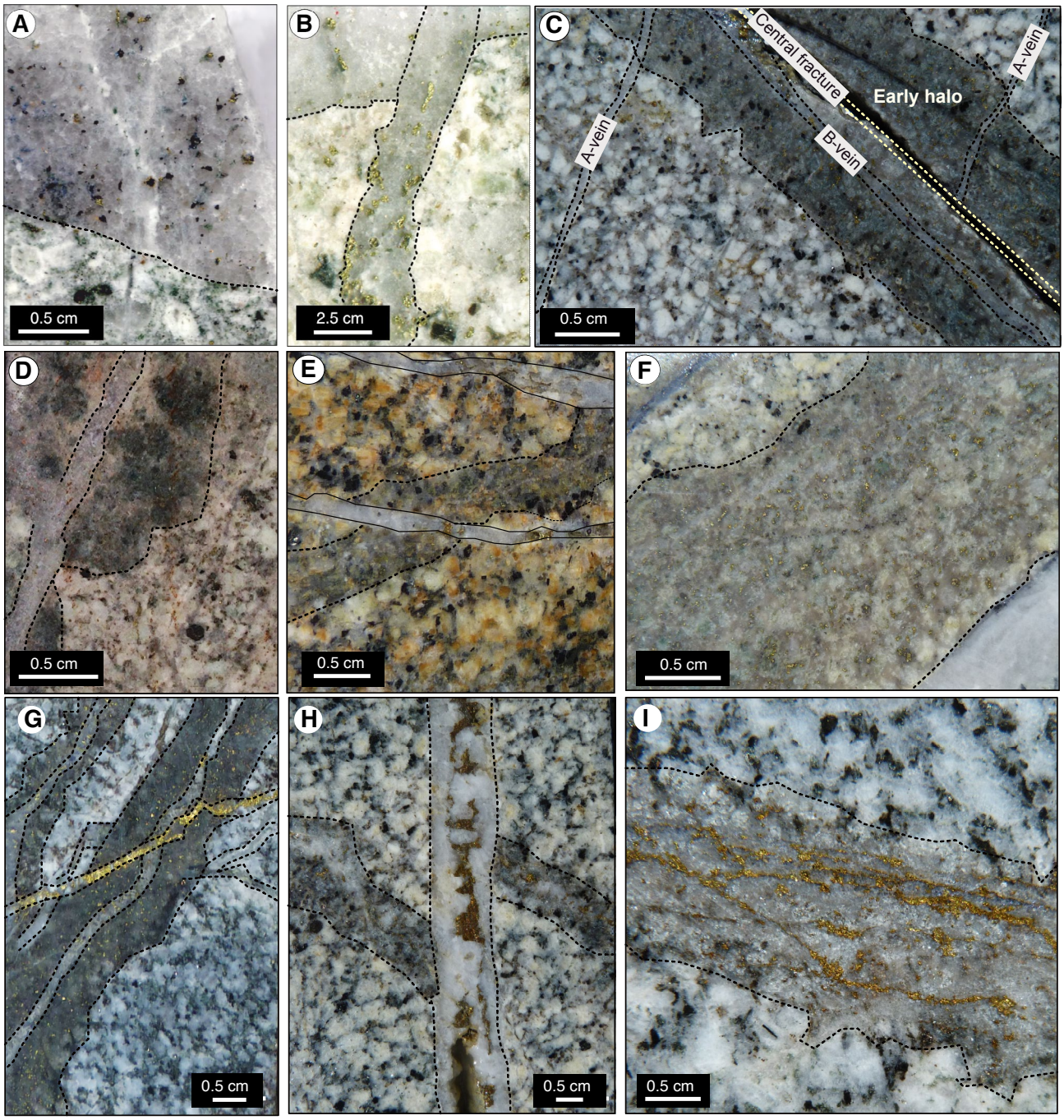

Fig. 4. Examples of key porphyry deposit veins and alteration types mentioned in this manuscript. Photos with no drawing overlays are provided in the Appendix. A) Quartz A vein with bornite and chalcopyrite and typical sugary quartz texture (Batu Hijau, SBD86-873 m, reproduced from Seedorff et al., 2005). B) Quartz A vein with abundant chalcopyrite (A2) crosscuts and displaces an older and thicker A vein (A1; Encuentro, JVC29-787.4 m). C) An early halo of the early dark micaceous subtype with disseminated bornite-chalcopyrite crosscuts and displaces a quartz A vein with bornite-chalcopyrite and a narrow K-feldspar halo. A younger B vein with Cu-Fe sulfides and some molybdenite crosscuts the A vein and reopens the early halo at the side of its central fracture (Haquira East, AHAD98A-125.8 m). D) Early halo of the early dark micaceous subtype with minor Cu-Fe sulfide is crosscut by a narrow quartz-anhydrite-molybdenite vein (Encuentro, JVC152-670.8 m). E) Early halo of the pale-green sericite subtype with chalcopyrite and traces of bornite is crosscut and displaced by a quartz B vein with chalcopyrite (Haquira East, AHAD098A-157.5 m). F) Early halo of the green-gray sericite type and chalcopyrite replaces rock containing older barren deep quartz veins (Haquira East, AHAD098A-130 m). G) Early halos of the early dark micaceous subtype alter the wall rock along older quartz A veins. Both early halos and A veins contain disseminated chalcopyrite and are crosscut by a chalcopyrite C vein (Haquira East, AHAD185-515.3 m). H) Early halo of the pale-green sericite subtype with disseminated chalcopyrite alters rocks with discontinuous quartz A veins. A quartz B vein with a chalcopyrite centerline crosscut and displaced the early halo (Haquira East, AHAD127-474 m). I) Anastomosing chalcopyrite veins within an early halo of the green sericite subtype that contains disseminated chalcopyrite (Haquira, AHAD127-655.4 m).

in fluid/rock ratio with time, and the acidity increase associated with cooling and HCl or H_2SO_4 dissociation. Early dark micaceous and pale-green sericite types of early halos with abundant biotite are common in igneous wall rock of intermediate composition and, therefore, relatively high iron content, as exemplified at Butte. Similarly, at Haquira East, early dark micaceous halos are the most abundant subtype (Fig. 4C, G), pale-green sericite halos are volumetrically minor (Fig. 4E, H), and green-gray sericite early halos are very rare (Fig. 4F, I). Green-gray sericite early halos with very little biotite are more abundant in igneous and sedimentary wall rock of more felsic composition (Los Pelambres, green mica: Atkinson et al., 1996; Chuquicamata, Chile: Ossandón et al., 2001; Rivera et al., 2012; Taca Taca, Argentina: Benavides, 2017; Copper Cliff, Montana: Uribe-Mogollon and Maher, 2018). Therefore, the muscovite/biotite ratio of the dominant subtype of early halos appears to be controlled by the availability of Fe in the wall rock (Cernuschi et al., 2019).

Early halos are, in some cases, zoned. A single early halo may have an outer early dark micaceous zone and an inner pale-green sericite zone, which suggests that temporal increases in the fluid/rock ratios also control the muscovite/biotite ratio (e.g., Butte, Haquira East, Copper Creek, Reed et al., 2013; Cernuschi et al., 2019). In other cases, early-halo assemblages may be zoned spatially and in time throughout a deposit. Butte has a spatial and temporal zonation from deeper and older early dark micaceous halos to shallower and younger pale-green sericite halos (Rusk et al., 2008b; Reed et al., 2013). At Haquira East, a deposit-scale zonation is not documented, and all subtypes of early halos are formed at a similar timing with no obvious crosscutting relationship (Cernuschi et al., 2013). Nonetheless, the very top of the high-Cu-grade shell has been eroded (Cernuschi, 2015). At both Haquira East and Butte, in the deepest areas of the high-Cu-grade shell, early halos grade into very thin and discontinuous biotite and chalcopyrite veinlets along a central fracture with associated K-feldspar that have been named biotite crackles (Brimhall, 1977; Reed and Dilles, 2020). In some of these deep zones, the biotite veinlets are very discontinuous, and most Cu sulfides precipitate together with shreddy biotite after magmatic hornblende, giving the appearance of disseminated mineralization.

Most importantly, the critical characteristic of all subtypes of early halos is that they are paragenetically early. They are emplaced close in time with A veins and predate banded molybdenite-quartz veins, B veins, C veins, and D veins. Therefore, in the following sections of this manuscript, we use early halo to refer to all subtypes.

A veins are absent in some early-halo-type deposits like Butte but might be present in small volumes in other deposits like Haquira East, which also carry some Cu-Fe sulfides (Table 1; Fig. 4C; Cernuschi et al., 2013). In all cases, A veins are minor contributors to the Cu ore in early-halo-type deposits, where early halos are abundant. At Haquira East, A veins have various and sometimes contradictory crosscutting relationships with early halos: the central fracture of early halos may crosscut and displace A veins (Fig. 4C), A veins may crosscut and displace early halos (Fig. 4E), and in many cases, early halos may be observed as local selvages along A veins (Fig. 4G). These relationships suggest several early halo and A-vein events at Haquira East. This is similar to Bingham, where several documented hydrothermal events include an early-halo stage cut by A veins (Redmond and Einaudi, 2010). At Haquira East, B veins crosscut and displace all early halos and commonly reopen them (Fig. 4H), often offsetting the original central fracture and demonstrating that early halos are not selvages of B veins (Fig. 4C). Both A veins and early halos may include local and discontinuous Cu-Fe sulfide-only stringers that escape outward of the veins and halos. When these stringers are observed in the periphery of the A veins and early halos, they are still stable with K-feldspar and biotite (Fig. 4I). These stringers are part of the A-vein and early-halo formation, predate B veins, and are, therefore, much younger than C veins Cu sulfide stringers that cut them (see below).

Early halos may be locally present in some A-vein-type porphyry deposits but in small volume and, therefore, are insignificant contributors to the Cu ore. This is the case at Batu Hijau, where sparse early halos are present and have been inferred to form close in time with A veins (early dark micaceous-like from Clode et al., 1999). At El Salvador, similar Cu-Fe sulfide-rich selvages of alkali feldspar, green muscovite, biotite, chlorite, anhydrite, andalusite, corundum, and sphene were recognized at depth as being closely related to A veins. Because of the lack of crosscutting observations with B veins, these zones were named andalusite and corundum alteration by Gustafson and Hunt (1975). Some of these halos were later split into early biotite and younger C veins based on tentative differences in crosscutting relationships with B veins by Gustafson and Quiroga (1995). However, the authors describe that both halos are composed of a similar assemblage of K-feldspar, biotite, and green muscovite, which are easily confused in hand samples. Hybrid deposits like Encuentro (discussed in the section above) and Bingham are dominated by A veins; however, early halos have a more significant volume than in typical A-vein-type deposits and contribute some Cu to the ore.

Deep quartz veins

At Haquira East, there is a deep and low-grade or barren core with abundant sulfide-poor, milky, and thick quartz veins with some feldspar and varying amounts of anhydrite, locally named deep quartz veins (Table 1; Figs. 3A, 5A; Haquira: Cernuschi et al., 2012). The deep quartz veins in this K-silicate alteration zone that range from slightly older to synchronous with the overlying zone of high-grade copper sulfides in early halos have mutually crosscutting relationships with aplite dikes and commonly form composite vein dikes of aplite and quartz veins (Fig. 5B, C). Deep quartz veins are present in lower abundance at a shallower depth in the Cu ore zone, where Cu-Fe sulfide-bearing A veins commonly crosscut and displace deep quartz veins that lack Cu-Fe sulfides (Figs. 3A, 5E).

Similar quartz veins have been recognized as distinct from typical sugary quartz A veins in porphyry deposits elsewhere. At Butte, these quartz veins have been named barren quartz veins. They transition upward to narrow quartz-chalcopyrite veins with early-halo selvages (early dark micaceous), which further suggests broad synchronicity of the two vein types (Rusk et al., 2008b). Similar veins have been named barren stockwork quartz veins and described as abundant at the bar-

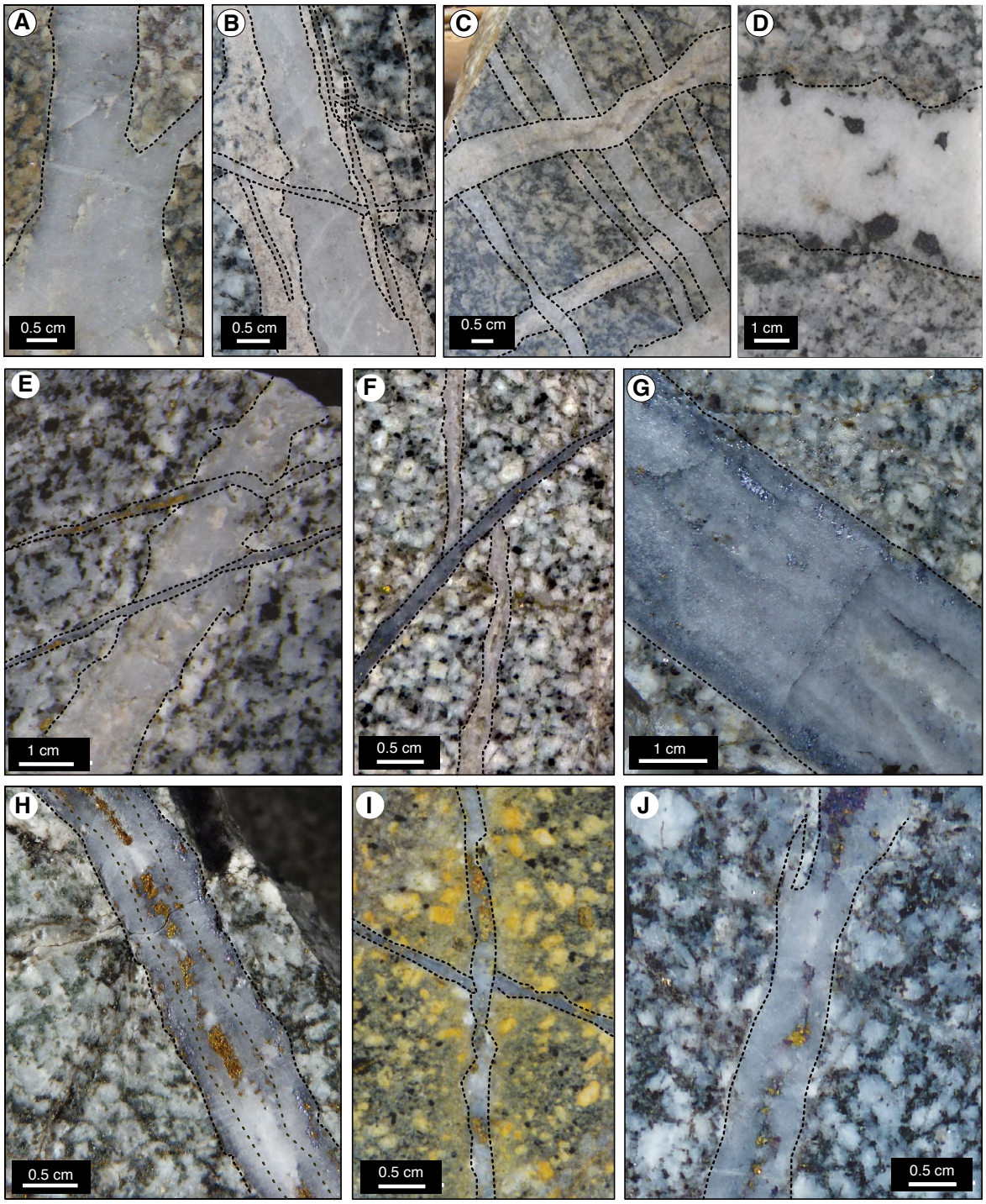

Fig. 5. Examples of key porphyry copper deposit vein and alteration types mentioned in this manuscript. Photos with no drawing overlays are provided in the Appendix. A) Deep quartz vein composed of milky and massive quartz (Haquira East, AHAD224-478 m). B) A deep quartz vein reopens a pink aplite dike (i.e., vein dike); both are crosscut by sugary-textured quartz A veins (Haquira East, AHAD098A-500 m). C) Pink aplite dikes and gray deep quartz veins have mutually crosscutting relationships (Haquira East, AHAD132-632 m). D) Deep quartz vein with milky quartz and magnetite (Batu Hijau, SBD256-942 m, from Setyandhaka et al., 2008). E) Thin and sugary-textured quartz A veins with chalcopyrite crosscuts a thicker milky deep quartz vein with K-feldspar and no sulfides (Haquira East, AHAD102-346.5 m). F) A thin, gray banded molybdenite-quartz vein crosscuts and displaces a pink deep quartz vein (Haquira East, AHAD098A-125.4 m). G) A thick banded molybdenite-quartz vein with typical semicontinuous molybdenite-bearing bands at the edges of the vein (Haquira East, AHAD098A-127.7 m). H) Banded molybdenite-quartz vein with molybdenite on margin reopened by a quartz B vein with chalcopyrite-rich centerline (Haquira East, AHAD185-834.55 m). I) Chalcopyrite-rich quartz B vein crosscuts and displaces a gray banded molybdenite-quartz vein (Haquira East, AHAD185-245 m). J) Quartz B vein with a chalcopyrite-bornite centerline (Haquira East, AHAD185-570 m).

ren core of Bingham (Porter et al., 2012). These quartz veins have also been called barren A or A-family veins (e.g., Clode et al., 1999). However, deep quartz veins do not contain sugary quartz like A veins and are commonly coarser grained, milky, thicker, less sinuous, and much more continuous than A veins (e.g., Haquira East; Fig. 4A-F; Cernuschi, 2015). Furthermore, deep quartz veins are typically most abundant below the zone where typical sugary-textured quartz A veins are most abundant. This spatial distribution might occur at El Salvador, where Gustafson and Quiroga (1995) noted sugary-textured A veins with sulfides in the shallower parts of the deposit and described deeper quartz veins as nonsugary, coarser grained, and having approximately the same age constraints as shallower A veins.

At Batu Hijau, deep quartz veins are observed in the deeper parts of the deposit and were included in the A-family vein category (Clode et al., 1999). These veins are massive, milky, and commonly thicker and more continuous and straight walled than the sugary-textured, thinner, and sinuous A and AB veins with Cu-Fe sulfides observed at shallower depths (Fig. 5D; Setyandhaka et al., 2008). Both deep quartz veins and A/AB veins contain magnetite and have poorly constrained relative ages based on crosscutting relationships. Nonetheless, some of the deep quartz veins at the low-Cu-grade core are hosted in the intermediate tonalite and therefore have to be younger than the A veins hosted above in the old tonalite and its wall rock (Fig. 3D). Both the 0.2 wt % Cu shell and its low-Cu-grade core are located in a rock volume containing 2 to 5 vol % of quartz veins. However, whereas within the inverted cup-shaped 0.2 wt % Cu shell, most quartz veins are of the A, AB, and B types; in the low-grade core, deep quartz veins are the dominant vein type (Fig. 3D; Setyandhaka et al., 2008).

The roots of Encuentro have not been drilled; therefore, deep quartz veins are rarely observed. Nonetheless, where observed, they crosscut sugary A veins. A low-Cu-grade core is presumed to be concealed at some depth below the current limit of drilling and along the projected axis of the deposit, as evidenced by the inverted cup-shaped distribution of magnetite veinlets at a shallower depth (Fig. 3B; Osorio, 2017).

Deep quartz veins are characteristic at the roots of both A-vein-type and early-halo-type deposits; however, based on published descriptions, they are more abundant in the latter. Nonetheless, deep quartz veins may not have been distinguished everywhere from A veins in shallow deposits. In contrast, they are easily recognized compared to overlying quartz-poor early halos in deeper deposits. Furthermore, late to postmineral stocks intrude the low-Cu-grade core of many A-vein-type porphyry deposits (e.g., El Salvador: Gustafson and Quiroga, 1995; Alumbrera: Proffett, 2003; Fig. 3D, Batu Hijau: Clode et al., 1999). In those cases, if dense, deep quartz veining existed at depth, it had been destroyed by the late intrusions. These late intrusions may be responsible for temporal differences in veining observed between the two deposit types. Whereas in early-halo-type deposits, deep quartz veins are older to synchronous with shallower early halos and A veins (e.g., Butte, Haquira); in A-vein-type and hybrid deposits, deep quartz veins may be synchronous to or younger than shallower A veins (e.g., Batu Hijau, Encuentro). This is because most preserved deep quartz veins are hosted in intrusions that are younger and deeper than the ones that host the A veins and Cu ore above. Because of these genetic differences, whereas the most intense quartz veining zones are correlated in space with the Cu ore in A-vein-type deposits such as Batu Hijau (Fig. 3C), the highest intensity of quartz veining lies below the Cu ore in early-halo-type deposits like Haquira East (Fig. 3A).

Other hydrothermal features such as biotite veins and breccias (early biotitic or EB of Gustafson and Quiroga, 1995), magnetite veinlets, and anhydrite veins, as well as magmatic features such as aplites and hybrid features such as vein dikes and unidirectional solidification textures (USTs), are also found at some barren cores below the ore zones and indicate broadly synchronous emplacement of magma and aqueous fluid (Kirkham and Sinclair, 1988; Seedorff et al., 2005; Cernuschi et al., 2013). Nonetheless, some types of USTs are observed at shallower depths within the Cu ore zone. These may occur at the top of porphyry dikes or along their contacts with the wall rock and may host significant Cu-Au mineralization (Müller et al., 2023).

Molybdenite-bearing veins and B veins

Because of the crosscutting relationships reported below, we discriminate older banded molybdenite-quartz veins that carry molybdenum (Mo) and lack Cu-Fe sulfides from younger B veins that carry Cu-Fe sulfides and minor molybdenite. Banded molybdenite-quartz veins, such as those observed at Haquira East (Table 1; Fig. 5G, F; Cernuschi et al., 2013), are quartz veins that have molybdenite principally forming bands along the vein margins and in some internal vein-parallel streaks. We restrict the definition of B veins (Table 1; Gustafson and Hunt, 1975) to straight-walled veins lined by drusy quartz crystals in which the centerline is partially open or filled with Cu-Fe sulfide, K-feldspar, biotite, anhydrite, and local minor molybdenite, as illustrated for Haquira (Fig. 5J) and Encuentro (Fig. 6C). To a lesser degree, Cu-Fe sulfides and trace molybdenite might occur as disseminations outside the centerline and contained within the quartz crystals forming the B vein. Quartz-molybdenite veins that postdate B veins are present at Encuentro (Fig. 6D) but are not as frequently observed in porphyry deposits as the older Mo-bearing quartz veins described above.

At Haquira East, banded molybdenite-quartz veins lack Cu-Fe sulfides and are the main contributor of Mo to ore, as their abundance is well-correlated with Mo grade (Cernuschi et al., 2013). Similar banded molybdenite-quartz veins have been described as significant Mo contributors in shallow, deep, and hybrid porphyry deposits, including Butte (banded quartz-molybdenite veins, Proffett, 1973), Chuquicamata (Rivera et al., 2012), Alumbrera (Proffett, 2003), Bingham (Redmond and Einaudi, 2010), and El Teniente (type 6a and 6b from Vry et al., 2010). In all cases where crosscutting relationships have been documented, banded molybdenite-quartz veins lack selvages but are stable with K-silicate alteration and postdate early halos and A veins (e.g., Butte, Meyer et al., 1968; Alumbrera, Proffett, 2003; Bingham, Redmond and Einaudi, 2010; Chuquicamata, Rivera et al., 2012).

At Haquira East, banded molybdenite-quartz veins (Fig. 5G) crosscut deep quartz veins (Fig. 5F) and early halos (Fig. 6A) and are, in turn, crosscut and displaced by B veins that con-

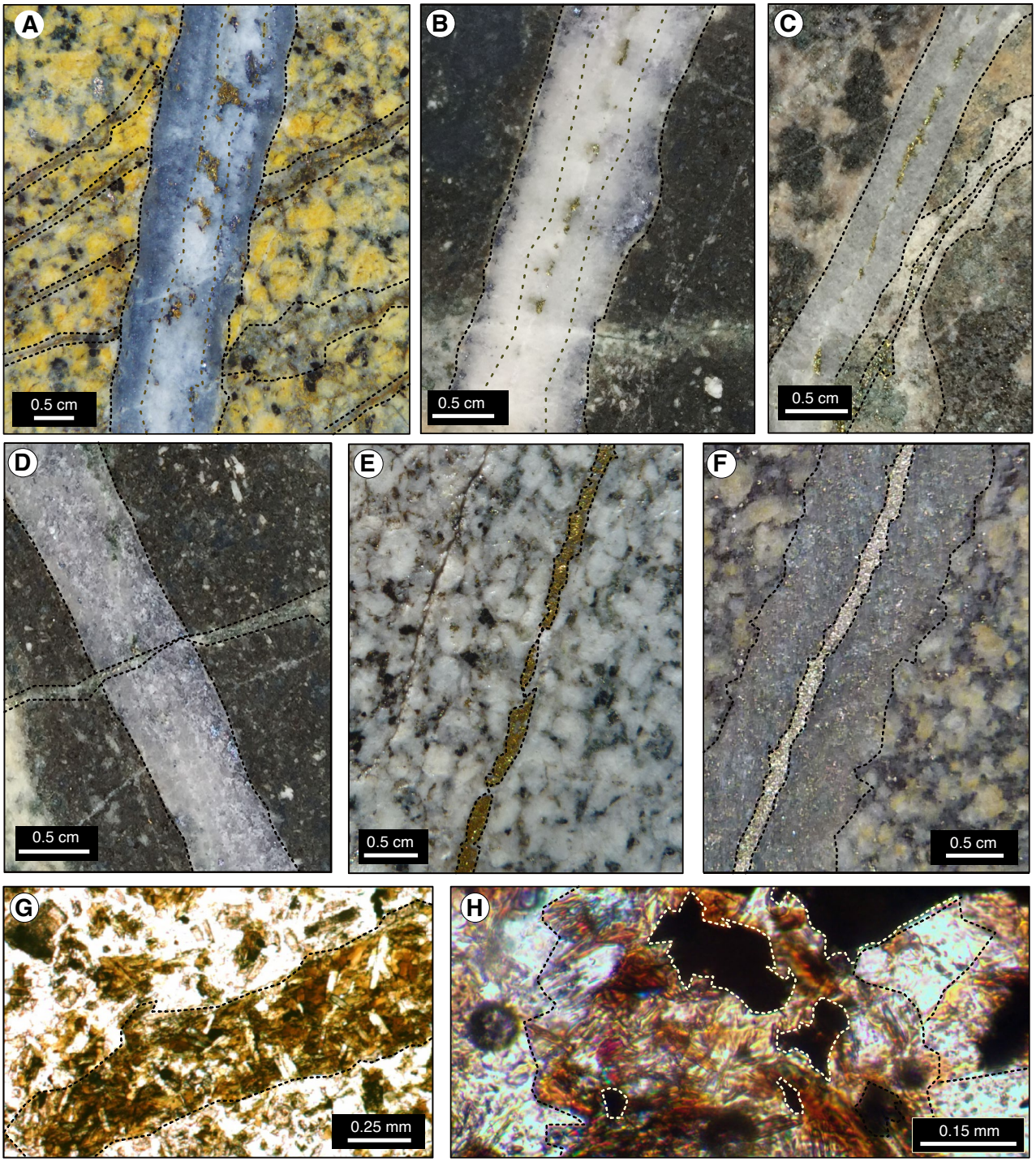

Fig. 6. Examples of key porphyry deposit veins and alteration types mentioned in this manuscript. Photos with no drawing overlays are provided in the Appendix. A) Narrow and discontinuous sugary-textured quartz A veins with chalcopyrite have associated thin early-halo selvages in some areas. These veins and halos are crosscut by a banded molybdenite-quartz vein with two outer bands of quartz rich in molybdenite. The banded molybdenite-quartz vein was reopened by a central chalcopyrite-rich quartz B vein with traces of molybdenite (Haquira East, AHAD185-234 m). B) Banded molybdenite-quartz vein reopened by a quartz B vein with central chalcopyrite (Encuentro, JVC148-872.5 m). C) Quartz B vein with a chalcopyrite-rich centerline. Note the narrow D-type pyrite-chalcopyrite vein with a sericitic halo on the right side (Encuentro, JVC148-610 m). D) Quartz-anhydrite-molybdenite vein from Encuentro. Note that molybdenite is disseminated throughout the vein (JVC148-851 m). E) A chalcopyrite C vein has no associated quartz or alteration halos (Haquira East, AHAD98A-378 m). F) A pyrite D vein with a sericitic halo composed of muscovite, pyrite, and quartz (Haquira East, AHAD175-537 m). G) Transmitted-light microscopy image of hydrothermal (shreddy) biotite that completely replaced magmatic hornblende from the Haquira East granodioritic stock (AHAD098A-180 m). H) Hydrothermal (shreddy) biotite with intergrown chalcopyrite and bornite (AHAD159-662 m).

tain chalcopyrite ± bornite ± pyrite ± molybdenite (Fig. 5I; Table 1; Cernuschi et al., 2013). Therefore, the banded molybdenite-quartz veins are introduced after the Cu-bearing early halos and A veins but before the formation of B veins with both Cu-Fe and Mo sulfides. Furthermore, at Haquira East, banded molybdenite-quartz veins are commonly reopened by Cu-Mo–bearing quartz B veins in shallower areas of the deposit where both B veins and banded molybdenite-quartz veins occur (Cernuschi et al., 2013; Figs. 5H, 6A). Banded molybdenite-quartz veins also occur at deeper parts of some porphyry deposits where B veins are scarce. The reopening of older banded molybdenite-quartz veins by younger B veins results in a banded molybdenite-quartz margin infilled with a central chalcopyrite-rich B vein. The central chalcopyrite vein observed inside some type 6 banded molybdenite-quartz veins described at El Teniente may be a similar occurrence (Vry et al., 2010; Spencer et al., 2015). This quartz vein morphology was originally described as a single B-vein generation at El Salvador by Gustafson and Hunt (1975). Nonetheless, these authors recognized some of the deeper molybdenite-bearing veins that lack Cu-Fe sulfides as potentially different from the more typical B veins. These fit the definition of banded molybdenite-quartz veins used here (B veins with no centerline; see Gustafson and Quiroga, 1995). Nonetheless, the relative abundance of banded molybdenite-quartz veins and B veins varies between deposits, and some, like Butte, have abundant banded molybdenite-quartz veins but lack B veins (Mercer and Reed, 2013).

At Batu Hijau, banded molybdenite-quartz veins have been documented as a distinct vein type but are grouped with B veins containing Cu-Fe sulfide in a single generation of veins (e.g., fig. 3a from Schirra et al., 2022). Nonetheless, most of the logged B veins do not have outer molybdenite bands, consistent with observed low abundances of banded molybdenite-quartz veins and Mo ore at Batu Hijau (Clode et al., 1999).

Encuentro has abundant B veins (Fig. 6C), and banded molybdenite-quartz veins are minor and consistently associated with B veins (Fig. 6B; Osorio and Dilles, 2019). However, the bulk of the Mo ore is hosted by a younger generation of quartz-molybdenite veins that crosscut both older banded molybdenite-quartz veins and B veins (Fig. 6D; Osorio, 2017; Osorio and Dilles, 2019). These quartz-molybdenite veins are not banded, but instead molybdenite occurs disseminated and in patches in the vein quartz and can be accompanied by variable amounts of anhydrite (Table 1; see quartz-anhydrite-molybdenite [QAM] from Osorio, 2017). In other porphyry deposits, these young molybdenite-bearing veins are more rarely observed than the older generation of banded molybdenite-quartz veins that predate B veins. Nonetheless, young quartz-molybdenite veins have been documented as significant contributors to Mo ore in other porphyry deposits like El Teniente (type 7, Vry et al., 2010). Because they postdate B veins, these younger quartz-molybdenite veins lack the central reopen and infill by chalcopyrite common in older banded molybdenite-quartz veins.

K-silicate alteration

Deep quartz veins, biotite veins, A veins, B veins, molybdenite-bearing veins, and early halos lie in zones of pervasively altered wall rock characterized by K-silicate alteration with hydrothermally added biotite and less K-feldspar (Figs. 1, 2; e.g., Roberts, 1973, 1975; Gustafson and Hunt, 1975; Seedorff et al., 2005). In granodiorite porphyries, K-feldspar and sparse biotite are also igneous minerals in the aplitic groundmass but can be altered.

We note that whereas the hydrothermal assemblage observed within the early halos includes muscovite together with K-feldspar and biotite, these halos are enclosed in a larger volume of wall rock characterized by typical K-silicate alteration (K-feldspar and biotite). Therefore, the K-silicate zone in early-halo-type deposits is similar in mineralogy and volume to the K-silicate–altered wall rock that contains quartz veins in A-vein-type porphyry deposits. In these K-silicate–altered zones, hydrothermal (shreddy) biotite has replaced primary mafic mineral sites (Fig. 6G), and K-feldspar may partially replace plagioclase feldspar. Minor albite can form in K-silicate alteration because of the leftover sodium after the alteration of magmatic anorthite to hydrothermal K-feldspar. In high-Cu-grade zones, shreddy biotite is observed intergrown with Cu-Fe sulfides in rock adjacent to Cu-bearing A veins and early halos in both deep and shallow porphyry deposits (Fig. 6H). These zones of pervasive K-silicate alteration result from the amalgamation of narrow (<0.1–30 mm) K-silicate alteration selvages along early biotite veins, deep quartz veins, anhydrite veins, A veins, and possibly the precursor fractures to early halos (e.g., Seedorff et al., 2005; Redmond and Einaudi, 2010).

Chlorite is commonly present in K-silicate–altered zones; however, it is debatable whether it is formed with K-feldspar and biotite (e.g., Tsuruoka et al., 2021) or produced by the alteration of biotite by younger fluids (Seedorff et al., 2005). Mineral phase equilibria indicate that both scenarios could occur, as chlorite has a wide temperature stability range and could be stable with both K-silicate assemblages at high temperatures and sericitic assemblages at lower temperatures (Dilles and John, 2021; Tosdal and Dilles, 2020). For example, B veins at Batu Hijau have biotite along the centerline; however, in many cases, it has been replaced by chlorite (see fig. 4b from Schirra et al., 2022).

The intimate spatial relationship of A veins and early halos with large bodies of K-silicate hydrothermal wall-rock alteration and the high-grade copper ore shell is well-documented through core logging and cross sections in many porphyry deposits, including (1) early-halo-type porphyry deposits like Los Pelambres, Chile (Atkinson et al., 1996; Perelló et al., 2012); Chuquicamata, Radomiro Tomic, and Mina Ministro Hales, Chile (Rivera et al., 2012); Taca Taca, Argentina (Benavides, 2017), Copper Cliff, Montana (Uribe-Mogollon and Maher, 2008); and Haquira East, Peru (Cernuschi et al., 2013); (2) A-vein-type porphyry deposits like El Salvador, Chile (Gustafson and Hunt, 1975); Yerington mine, Nevada (Proffett, 1979); Alumbrera, Argentina (Proffett, 2003); Batu Hijau, Indonesia (Clode et al., 1999); El Teniente, Chile (Vry et al., 2010); and Red Chris (Rees et al., 2015); and (3) hybrid porphyry deposits like Encuentro, Chile (Osorio, 2017; Osorio and Dilles, 2019) and Bingham, Utah (Redmond and Einaudi, 2010). This spatial zonation is illustrated at Haquira East, Encuentro, and Batu Hijau in the cross sections shown in Figure 3.

As described above, deep quartz veins, biotite veins, A veins, early halos, and banded molybdenite-quartz veins commonly have a characteristic spatial distribution and temporal sequence based on crosscutting relationships. However, this vein sequence may repeat after each new porphyry dike emplacement event and therefore produce a variety of crosscutting relationships with previous generations of veins, also known as vein reversals (Proffett, 1979; Carten, 1986; Seedorff and Einaudi, 2004; Redmond and Einaudi, 2010; Spencer et al., 2015). These vein reversals tend to be much less common after the B- and C-vein stages at the waning stages of K-silicate alteration and rare or maybe absent after the D-vein stage and the onset of sericitic alteration.

C veins

C veins are characterized by a vein fill of chalcopyrite ± bornite ± pyrite with little to no quartz and possible narrow selvages of chlorite ± muscovite where K-feldspar may remain stable but biotite is not (Fig. 3D; Dilles and Einaudi, 1982; Monecke et al., 2018). The diagnostic feature of C veins is that they crosscut B veins and older veins and are, in turn, crosscut by D veins. Therefore, C veins are likely formed at the waning stages of K-silicate alteration and the onset of sericitic alteration. Nonetheless, the term C vein has been used previously with some ambiguity. Older Cu-Fe sulfide-only stringers, spatially and temporally related to A veins, early halos, and biotite crackles and stable with hydrothermal biotite, predate B veins and are therefore not considered C veins, because they do not fit the mineralogical and timing criteria (Fig. 4I; see above). Some of the micaceous halos at El Salvador were named C veins (Gustafson and Quiroga, 1995); however, at least some fit the temporal and mineralogical definition of early halos (Gustafson and Hunt, 1975). The ubiquitous presence of biotite, K-feldspar, and green muscovite in these halos is described by Gustafson and Hunt (1975) and Gustafson and Quiroga (1995). This mineralogy departs from the chlorite ± muscovite with relict K-feldspar mineralogy associated with C veins that has been documented to crosscut B veins elsewhere. At the Ann-Mason porphyry deposit (early-halo type; Nevada; Proffett, 2009), three varieties of sulfide-rich veins that fit the timing of C veins were described: one containing chalcopyrite ± quartz ± chlorite with K-feldspar ± muscovite selvages, a second containing epidote-quartz-chalcopyrite ± chlorite ± bornite or pyrite with epidote ± albite ± chlorite ± muscovite selvages, and a rare third containing chlorite-quartz; the epidote and chlorite veins are likely formed by both magmatic and nonmagmatic brines, and we do not consider them C veins here (Dilles and Einaudi, 1992).

C veins, as used here, commonly make a small contribution to the Cu ore according to previously published maps and cross sections, with some exceptions in shallowly sourced porphyry deposits like El Teniente (Vry et al., 2010; Spencer et al., 2015) and local areas of Alumbrera (Proffett, 2003).

At Batu Hijau, core logging and cross sections indicate rare C veins (Fig. 3D; Clode et al., 1999). Nonetheless, C veins might be locally more abundant at the eastern flank of the deposit, where extensive low-temperature overprint and recrystallization have been previously documented. However, the 0.2 and 1 wt % Cu shells shown in the cross section of Figure 3D show no spatial relationship with the areas with documented C veins. There are no significant differences in Cu grade between the eastern and western flanks. However, based on petrographic work, Schirra et al. (2022) argued that C veins are more widely present than previously recognized and can be essential contributors to Cu ore—in particular, a thinner subcategory named paint veins (cf. Fournier, 1967). Some of these are documented as thin veinlets of dull-CL quartz within older lucent-CL quartz A veins (see microfracture discussion below). Nonetheless, some older early halos may have been incidentally included in the younger C-vein category. This may be the case with green and narrow chlorite-sericite halos containing disseminations and Cu-Fe sulfide stringers. These are documented to crosscut A and AB veins; however, crosscutting relationships with B veins are not established (see paint vein crosscutting AB vein in fig. 3d from Schirra et al., 2022). It is possible that some of these halos predate B veins and are early halos stable with hydrothermal biotite, where most of the biotite has been altered to chlorite as previously described by Clode et al. (1999).

At Encuentro, C veins are volumetrically minor chalcopyrite-pyrite veinlets with chlorite halos constituting 0.05 to 1.2 vol %, whereas deeper chalcopyrite-pyrite veins with no halos are 0.05% and locally reach 2.0 vol %. Both types are observed overlapping and above the A-vein–bearing K-silicate zone but with no spatial coincidence with the high-Cu-grade ore. C veins appear to grade into D veins with sericitic halos at a shallower depth and outboard the K-silicate alteration zone (Fig. 3B; Osorio, 2017).

At Haquira East, C veins are rare (Figs. 4G, 6E; Cernuschi et al., 2013). Nonetheless, some of the younger Cu-Fe sulfide veins that appear to infill the B-vein centerline crosscut the B-vein margin into the wall rock, where they become a Cu-Fe sulfide-rich vein with no quartz. Therefore, in some cases, the Cu-Fe sulfide centerline of a B vein can be considered to result from a B vein that was later reopened and infilled by C-vein sulfides. Similar observations are reported in other porphyry deposits elsewhere (Driesner and Heinrich, 2019; Dilles and John, 2021).

D veins and sericitic alteration

Veins associated with K-silicate alteration and slightly younger C veins are crosscut and postdated by D veins associated with sericitic alteration in most porphyry deposits. This transition is likely produced by the cooling of magmatic-hydrothermal fluids from the K-feldspar-biotite stability field to the sericite (muscovite) stability field (Reed et al., 2013; Dilles and John, 2021; Table 1; Fig. 2). D veins contain a vein fill of pyrite ± quartz ± traces of muscovite and commonly have characteristic sericitic alteration selvages (Fig. 6F). D veins also postdate K-silicate–related Cu and Mo ore formation because they crosscut all the previously mentioned Cu-Fe sulfide-bearing veins and halos, including C veins (Gustafson and Hunt, 1975; Seedorff et al., 2005; Sillitoe, 2010; Schirra et al., 2022). The sericitic halos associated with D veins are alteration selvages of millimeter to centimeter width in which quartz, muscovite, local chlorite, anhydrite, and pyrite have completely replaced magmatic and hydrothermal biotite and K-feldspar, plagioclase, and ferromagnesian minerals (Fig. 2; Seedorff et al., 2005; Rusk et al., 2008a). Where D-vein halos lack feldspar, the sericite

is commonly pure muscovite in composition, whereas in the outermost zones of some D-vein halos or in distal partial sericitic alteration zones that contain relict feldspar, the muscovite contains significant iron and magnesium and is phengitic (Halley et al., 2015). Thus, D-vein halos with pervasive sericite are white to bright gray and somewhat distinct from pale-green to gray phengites of early halos (Cernuschi et al., 2019). In addition to pyrite, many D veins contain minor Cu-Fe sulfide (chalcopyrite). Still, because they have a low chalcopyrite to pyrite ratio, they generally do not constitute high-grade Cu ore. Nonetheless, chalcopyrite-rich D veins are common where they crosscut high-Cu-grade zones with early halos or A veins (Gustafson and Hunt, 1975; Osorio and Dilles, 2019), and potentially they derive relatively high Cu contents via local remobilization of Cu deposited in the earlier high-Cu-grade sulfides as in Chuquicamata, Mina Ministro Hales (Sillitoe et al., 1996; Ossandón et al., 2001), and Resolution (Hehnke et al., 2012).

At Haquira East, D veins are narrow, volumetrically minor, and crosscut older veins in the center of the K-silicate alteration (Cernuschi et al., 2013). At Batu Hijau, D veins are most abundant at the periphery of the K-silicate zone (Clode et al., 1999). At Encuentro, they overlap and extend above the upper part of the northwest zone of the K-silicate–altered wall rock (Fig. 3B; Osorio, 2017).

Other types of veins and associated wall-rock alteration

Quartz-bearing veins younger than D veins are rare. Advanced argillic alteration zones (Fig. 2) may be present in the upper parts of porphyry alteration zones, form either before sericitic alteration (Sepp, 2022) or afterward, and are superimposed in telescoped systems (e.g., Sillitoe, 2010). Low-temperature (<350°C) quartz sulfide veins are commonly formed in Cordilleran base metal lodes and the epithermal environment but not in porphyry deposits (Dilles and John, 2021). Different types of magmatic and magmatic-hydrothermal breccias form in all the alteration zones described above and, in many cases, contribute to economic ore (Proffett, 2009; Sillitoe, 2010). Intermediate argillic alteration characterized by a variety of smectite, vermiculite (hydrobiotite), illite, chlorite, and kaolinite minerals is commonly the lowest-temperature hypogene alteration (<220°C). Intermediate argillic alteration may be associated with fractures containing local pyrite or as patchy overprints to older K-silicate alteration as observed at Haquira East (Cernuschi, 2015). In these cases, the K-silicate–altered center is usually overprinted much more intensely than its sericitic periphery. In some deposits, the intermediate argillic overprint is intense and locally replaces older K-silicate mineral assemblages pervasively, which makes it difficult to recognize the relict high-temperature alteration (e.g., Vendaval Central, Cernuschi et al., in press).

Sodic-calcic, sodic, calcic, and propylitic alteration and related veins lie in the peripheral parts of many porphyry deposits and, in some cases, overlap the K-silicate center but are not discussed herein (see Seedorff et al., 2005; Sillitoe, 2010; Cernuschi et al., in press). Veins and altered rock in both SiO_2-poor alkalic porphyry deposits and Mo porphyry deposits differ somewhat from the veining paragenesis described above and will not be reviewed here.

Petrographic Observations

We present textural and paragenetic data of key vein and halo types from Haquira East, Encuentro, and Batu Hijau to assess the timing of Cu-Fe sulfide and molybdenite precipitation relative to the hydrothermal assemblages and the different generations of lucent-CL and dull-CL quartz. We focus on the relative timing of veins containing lucent-CL versus dull-CL quartz and only estimate the pressure and temperature conditions of formation. The key observations are summarized under the four subtitles listed below and are illustrated in the four panels of Figure 7.

Cu-Fe sulfides are observed in contact with both lucent- and dull-CL quartz or are unrelated to quartz

Most of the Cu-Fe sulfide grains in early halos from Haquira East (Fig. 8A) are not in contact with quartz, indicating that Cu-Fe sulfides can precipitate without any associated quartz (Fig. 7A). QEMSCAN images of early halos in Cu ore zones from Haquira East reveal Cu-Fe sulfide intergrowths with hydrothermal K-feldspar (Fig. 8B, D), muscovite, biotite, and minor quartz (Fig. 8D). Similar mineralogy in contact with Cu-Fe sulfides and minor quartz has been described for early halos at Los Pelambres (Atkinson et al., 1996; Perelló et al., 2012), Encuentro (Osorio, 2017), and Butte (Meyer, 1965). At Butte, andalusite is, in some cases, also present (Mercer and Reed, 2013).

Volumetrically minor quartz A veins with K-feldspar halos are associated with early halos at Haquira East. In these A veins, QEMSCAN images show Cu-Fe sulfides in contact with K-feldspar (Fig. 8A), and SEM-CL images show Cu-Fe sulfides in contact with both the older main vein fill of lucent-CL quartz and with dull-CL quartz in younger microfractures (gray-CL in A-type vein, Fig. 9A, B). Similarly, Cu-Fe sulfides are observed in contact with K-feldspar in alkali seams considered contemporaneous with the A veins (Fig. 8A, C).

At porphyry deposits where A veins are a primary host of the Cu-Fe sulfides, dull-CL quartz has been reported to contact or contain Cu-Fe sulfides in all the previously published SEM-CL studies (see detailed reference list in the introduction). In this study, we also observe that dull-CL quartz commonly contacts or contains Cu-Fe sulfides in the A-vein samples from the three studied deposits. However, we also observe the A-vein lucent-CL quartz contacting Cu-Fe sulfides (Fig. 7A) and locally containing them (Fig. 9E, F).

At the hybrid-type Encuentro porphyry deposit, SEM-CL images of A veins reveal Cu-Fe sulfides that mainly contact lucent-CL quartz with K-feldspar and anhydrite (Fig. 9C). Dull-CL quartz is sparse and contacts lucent-CL quartz, K-feldspar, anhydrite, and Cu-Fe sulfides. In another sample from Encuentro, the A-vein mosaic-textured lucent-CL quartz is overgrown by dull-CL quartz (Fig. 9D), and most Cu-Fe sulfides are in contact with dull-CL quartz and only locally in contact with lucent-CL quartz. However, dull-CL quartz is not always in contact with Cu-Fe sulfides, such as planar fractures cutting lucent-CL quartz (Fig. 9D).

At Batu Hijau, A veins with lucent-CL quartz are cut by abundant dull-CL quartz in microfractures that contact Cu-Fe sulfides as imaged by SEM-CL (Fig. 9E, F). In many cases, as in the central zone of the imaged A vein, this dull-

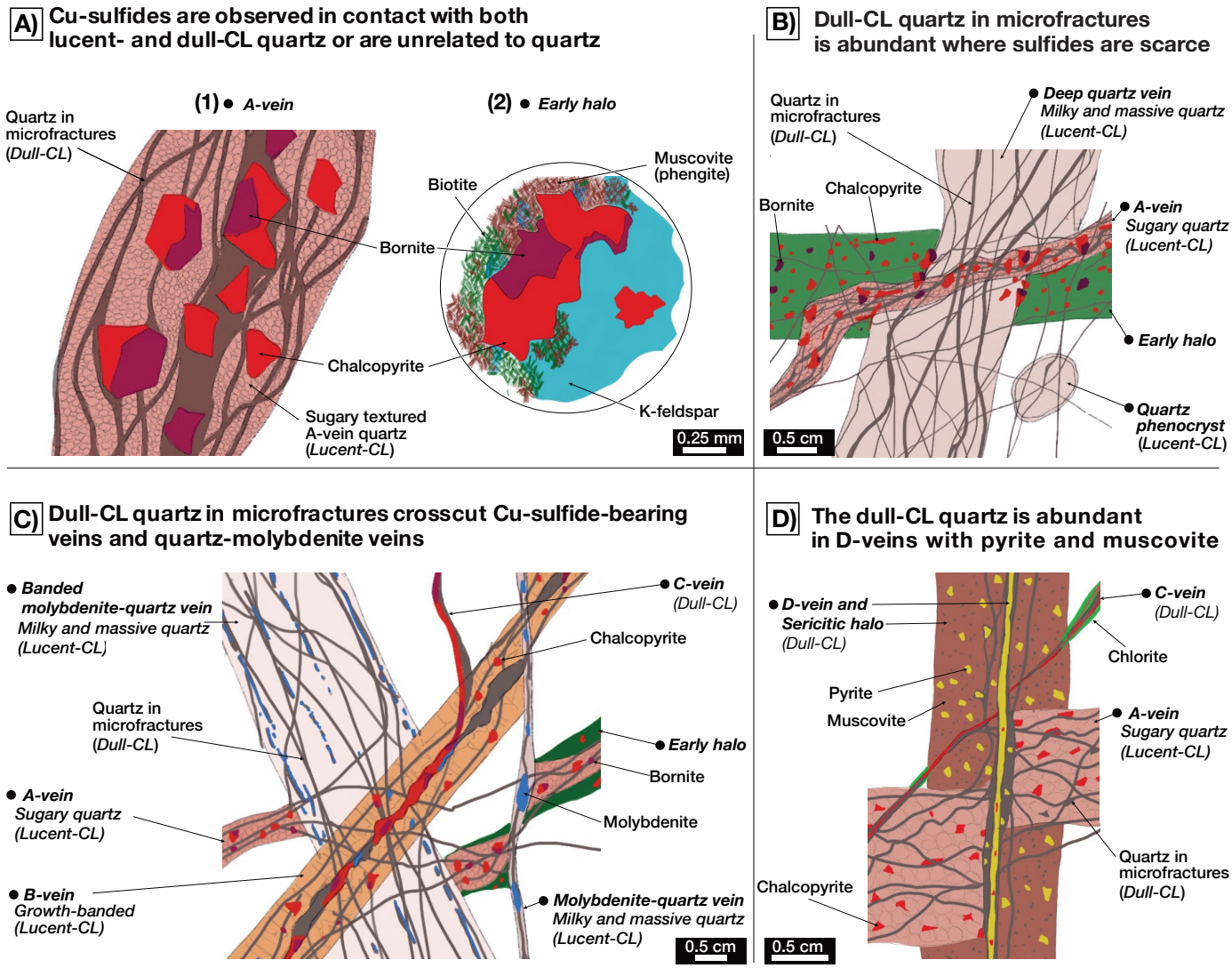

Fig. 7. Schematic cartoon of crosscutting relationships of different vein types, early halos, and their relationships with Cu-Fe sulfides, molybdenite, pyrite, and lucent- and dull-CL quartz. A) Cu-Fe sulfides in ore-forming veins and halos: A1) Sugary-textured lucent-CL quartz A vein contains Cu-Fe sulfides and is crosscut by dull-CL quartz filling microfractures. Both types of quartz are in contact with Cu-Fe sulfides. A2) Early halo composed of hydrothermal K-feldspar, muscovite, biotite, chalcopyrite, and bornite replacing a magmatic feldspar. Quartz is absent, and the hydrothermal silicate mineralogy contains Cu-Fe sulfides. B) A sulfide-poor deep quartz vein (with massive and milky quartz) is crosscut by a sugary-textured quartz A vein and transected by an early halo containing Cu-Fe sulfides. The deep quartz vein only contains sulfides locally where the A vein and the early halo crosscut it. All vein types and a nearby quartz phenocryst at the hosting intrusion are crosscut by dull-CL quartz in microfractures. The dull-CL quartz is only observed in contact with Cu-Fe sulfides in the A vein and the early halo and is barren in the deep quartz vein and the quartz phenocryst. C) A banded molybdenite-quartz vein is composed of massive and milky quartz containing narrow bands with molybdenite and lacking Cu-Fe sulfides. This vein crosscuts and displaces older sugary quartz A vein and an associated early halo, both containing Cu-Fe sulfides and lacking molybdenite. A younger quartz B vein crosscuts the banded molybdenite-quartz vein and comprises euhedral crystalline quartz with growth bands. The B vein contains both Cu-Fe sulfides and molybdenite; a significant part of the Cu-Fe sulfides is located along a centerline. These sulfides depart from the centerline and form a sulfide-only C vein with rare quartz in other parts of the vein. A younger (nonbanded) quartz-molybdenite vein lacks Cu-Fe sulfides, crosscuts the B vein, and predates the C vein. All veins are composed of lucent-CL quartz, except the C vein, with local dull-CL quartz. Dull-CL quartz is observed filling microfractures through all lucent-CL veins. It is in contact with molybdenite in the molybdenite-bearing veins, with Cu-Fe sulfides in the Cu-Fe sulfide-bearing veins and halos and with both Cu-Fe sulfides and molybdenite in the B veins. D) A pyrite ± quartz D vein with a sericitic halo composed of muscovite-pyrite-quartz crosscuts an older quartz A vein that contains chalcopyrite. The D vein only has local Cu-Fe sulfides where it crosscuts the A vein. A chalcopyrite-rich C vein with local chlorite selvages crosscuts the A vein and predates the D vein. Dull-CL quartz is observed in all vein types and is in contact with chalcopyrite in the A and C vein and pyrite-muscovite in the D vein. Abbreviation: CL = cathodoluminescence.

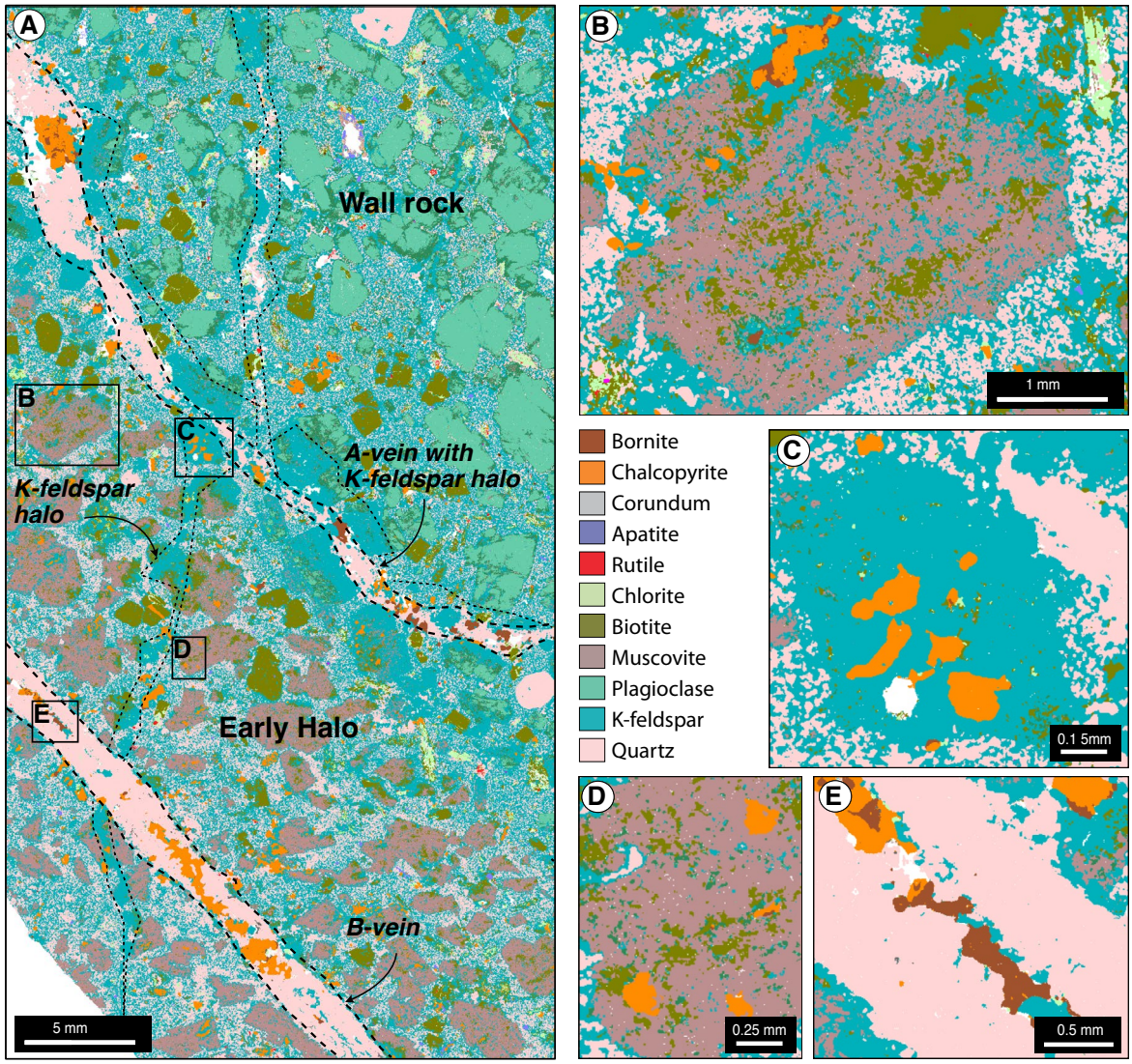

Fig. 8. QEMSCAN images of the mineralogy of veins and altered wall rock. Images with no drawing overlays are provided in the Appendix. A) A bornite-chalcopyrite–bearing early halo of the early dark micaceous subtype, composed of hydrothermal K-feldspar, muscovite, biotite, quartz, and rare corundum that preferentially replaces feldspar sites of the Haquira granodiorite stock together with quartz A veins that contain disseminated bornite-chalcopyrite and have K-feldspar halos. A K-feldspar halo (alkali seam) with minor quartz also carries chalcopyrite. The early halo is reopened by a quartz B vein with K-feldspar-bornite-chalcopyrite along a centerline. B) Hydrothermal K-feldspar, biotite, muscovite, quartz, and corundum replace plagioclase phenocrysts in the early halo. Cu-Fe sulfides in the halo are not in contact with quartz but are in contact with K-feldspar. C) K-feldspar halo contains Cu-Fe sulfides and has minor quartz. D) Hydrothermal K-feldspar, biotite, muscovite, quartz, and corundum replace a plagioclase phenocryst contained within the early halo. Cu-Fe sulfides in the early halo are not in contact with quartz but are in contact with K-feldspar, biotite, and muscovite. E) Quartz B vein with a semicontinuous Cu-Fe sulfide/K-feldspar centerline where sulfides are in contact with quartz and K-feldspar.

CL quartz completely contains the Cu-Fe sulfides. However, at the margins of the central dull-CL quartz zone, bornite is mainly contained within the lucent-CL quartz of the A vein and is rarely in contact with dull-CL quartz (Fig. 9E, F).

In younger B-vein quartz from Haquira East, Cu-Fe sulfides are in contact with K-feldspar (Fig. 8E) and with both lucent- and dull-CL quartz (gray-CL to bright-CL, Fig. 9G, H). In some of the SEM-CL images referenced above, the textures suggest lucent-CL quartz dissolution prior to deposition of Cu-Fe sulfides or dull-CL quartz (e.g., Fig. 9H). Similar observations of some lucent-CL quartz in contact with Cu-Fe sulfides and erosion of lucent-CL quartz have been previously reported at Santa Rita (Tsuruoka et al., 2021) and can be observed in previously published SEM-CL images from Bingham (Redmond et al., 2004) and Escondida (Jensen et al., 2022). Dissolution is more frequently observed in B veins than in A veins, possibly because dissolution disrupts the more obvious internal banding in the former.

The observations presented here show the intrinsic relationship between Cu-Fe sulfides and the older quartz-poor K-feldspar, muscovite, and biotite early-halo mineralogy. In quartz A and B veins, however, Cu-Fe sulfides can be ob-

served in contact with both the older lucent-CL quartz and the younger and crosscutting dull-CL quartz (Fig. 7A).

Dull-CL quartz in microfractures is abundant where sulfides are scarce

Dull-CL quartz in microfractures is not only present in Cu-Fe sulfide-bearing A and B veins but also abundant in quartz veins where Cu-Fe sulfide is scarce. At Haquira East, dull-CL quartz is not as volumetrically abundant as in shallow porphyry deposits like Batu Hijau. However, it is ubiquitously observed crosscutting all types of older quartz, including deep quartz veins that are poor in Cu-Fe sulfide and stable with K-silicate alteration (Fig. 9I) and quartz phenocrysts in the granodiorite porphyry (Fig. 10F). In these veins and phenocrysts, dull-CL quartz is rarely in contact with Cu-Fe sulfide. For example, a quartz phenocryst cut by dull-CL quartz microfractures lacks Cu-Fe sulfides, whereas in the same drill hole intercept, nearby early halos, A veins, and later B veins carry abundant Cu-Fe sulfides (Fig. 10F). Both A and B veins have dull-CL quartz microfractures with SEM-CL characteristics identical to those cutting the quartz phenocrysts; however, the former dull-CL quartz contacts Cu-Fe sulfides, but the latter does not. Similarly, older deep quartz veins lack Cu-Fe sulfides and are crosscut by younger Cu-Fe sulfide-bearing A and B veins at shallow depths (Fig. 3A). All of these lucent-CL quartz vein generations are crosscut by dull-CL quartz in microfractures; however, dull-CL quartz does not contact Cu-Fe sulfide where it cuts deep quartz veins, whereas it does contact Cu-Fe sulfides where it cuts quartz in A and B veins. These crosscutting relationships and the types of CL quartz they contain are schematically illustrated in Figure 7B.

Similar observations of dull-CL quartz in barren veins have been described for deep and shallow porphyry deposits. Magmatic quartz from the Butte granite and quartz phenocrysts from the Modoc porphyry at Butte have dull-CL quartz microfractures similar to those cutting quartz phenocrysts at Haquira East, and all lack sulfide (Mercer and Reed, 2013). Dull-CL quartz in microfractures is ubiquitous in several porphyry copper deposits and also cuts low-grade-Cu to barren quartz veins (e.g., Rusk, 2012). For example, deep barren stockwork quartz (deep quartz) veins at Bingham have dull-CL quartz-filled microfractures, similar to those described in Cu-Fe sulfide-bearing A veins, but lack Cu-Fe sulfide (Landtwing et al., 2010). Similarly, barren quartz veins from Grasberg, Papua New Guinea, and Henderson, Colorado, and quartz veins with only minor pyrite from Gaby Sur, Chile, are cut by abundant dull-CL quartz in microfractures that lack Cu-Fe sulfides (Rusk, 2012).

In summary, the late and dull-CL quartz is ubiquitously observed in different types of old lucent-CL quartz, including both Cu-poor deep quartz veins and porphyry phenocrysts, as well as in younger and Cu-rich A and B veins. From these, dull-CL quartz in microfractures only occurs with Cu-Fe sulfides in A and B veins, and it is barren in deep quartz veins and porphyry phenocrysts (Fig. 7B).

Dull-CL quartz in microfractures also crosscuts quartz-molybdenite veins that lack Cu-Fe sulfides

Dull-CL quartz is not unique to Cu-Fe sulfide-bearing and barren veins but is also commonly observed filling fractures that cut molybdenite-bearing quartz veins that lack Cu-Fe sulfides. At Haquira East, dull-CL quartz in microfractures is observed in contact with molybdenite in banded molybdenite-quartz veins hosted in lucent-CL quartz (Fig. 10A, B). Dull-CL quartz in microfractures cutting through molybdenite-bearing veins (i.e., cobweb texture, Rusk and Reed, 2002) that do not contain ore-forming Cu-Fe sulfides appears to be a ubiquitous feature as previously reported in several deep and shallow porphyry deposits such as Butte, Montana (Mercer and Reed, 2013); Bingham, Utah; Gaby Sur and El Abra, Chile (Rusk, 2012); and Altar, Argentina (Maydagan et al., 2015); and porphyry molybdenum deposits elsewhere (Henderson, Colorado: Rusk, 2012; Dabaoshan, China: Mao et al., 2017).

At Haquira East, older early halos and A veins with Cu-Fe sulfides are crosscut by younger banded molybdenite-quartz veins with no Cu-Fe sulfides and are all equally crosscut by dull-CL quartz in microfractures. Similar observations were made at Encuentro, where dull-CL quartz is also volumetrically minor (Osorio, 2017). Still, it is ubiquitously observed cutting both A veins with Cu-Fe sulfides (Fig. 9C, D) and younger quartz-molybdenite veins with sparse Cu-Fe sulfides (Fig. 10C). At Haquira East and Encuentro, the different types of lucent-CL quartz veins described above coexist in the same deposit areas. Where they crosscut each other, they systematically preserve their distinct Mo- or Cu-rich sulfide populations (Cernuschi et al., 2013; Osorio, 2017).

These observations indicate that dull-CL quartz in microfractures crosscuts several generations of crosscutting lucent-CL quartz veins that overlap in space within the high-Cu-Mo-grade ore but host different sulfide populations (Fig. 7C). Dull-CL quartz is observed in contact with Cu-Fe sulfides in early halos and A veins, with molybdenite in banded molybdenite-quartz veins, and with both Cu-Fe sulfides and molybdenite in younger B veins.

Dull-CL quartz is abundant in D veins with pyrite and muscovite

At Haquira East and Encuentro, D veins are composed of dull-CL quartz, lack lucent-CL quartz, and cut K-feldspar- and biotite-bearing K-silicate alteration zones and replace these minerals in selvages of sericite (muscovite, Fig. 10G-I). This timing, mineralogy, and quartz type have been observed for D veins elsewhere (e.g., Rusk et al., 2006; Rusk, 2012; Maydagan et al., 2015).

The CL intensity, Ti content, and oxygen isotope composition of quartz in D veins are similar to those of dull-CL quartz in microfractures that crosscut older and lucent-CL veins. Two types of dull-CL quartz can be distinguished in D veins and microfractures: one type of dull-CL quartz is not luminescent in SEM-CL, has a Ti content <5 ppm, and has been named dark-CL quartz (Redmond et al., 2004; Rusk, 2012). The second type of dull-CL quartz in microfractures is weakly luminescent, as observed in high contrast in SEM-CL, has Ti content of 5 to 15 ppm, and has been named medium-gray-dark-CL quartz (Table 1; Rusk, 2012; Cernuschi et al., 2018). At Haquira East, oxygen isotope compositions measured in situ by ion probe of both types of dull-CL quartz is identical in D veins ($\delta^{18}O$ ~11.2‰ for medium-gray-CL and ~12.6‰ for dark-CL), and in microfractures cutting through older lucent-CL quartz ($\delta^{18}O$ ~11.3‰ for medium-gray-CL; 12.4‰ for

dark-CL, and ~10.6‰ for lucent-CL; Cernuschi et al., 2018). The SEM-CL and Ti compositional similarities between dull-CL quartz in microfractures and quartz in D veins are well-documented in porphyry deposits elsewhere (e.g., Rusk and Reed, 2002; Rusk, 2012). The dull-CL quartz in D veins is commonly observed in contact with pyrite and only minor Cu-Fe sulfides, except where D veins crosscut zones with older Cu-Fe sulfide-bearing A and B veins.

Besides the compositional similarities between dull-CL quartz in D veins and microfractures cutting older veins, crosscutting relationships suggest a similar formation timing. For example, D veins at Encuentro contain mainly pyrite and anhydrite and only sparse or rare quartz. However, where D veins crosscut early lucent-CL quartz in A veins, dull-CL quartz occurs along the margins of the pyrite-rich D veins, likely because the dull-CL quartz results from recrystallization of the older lucent-CL quartz of the A vein (Fig. 10I). This crosscutting relationship results in narrow dull-CL quartz zones contained within lucent-CL quartz. Furthermore, in this sample, dull-CL quartz microfractures crosscut lucent-CL quartz in zones lacking sulfide and extending away from the sulfide-bearing D vein that amalgamate with dull-CL overgrowth zones at the periphery of lucent-CL quartz grains (Fig. 10I).

At Haquira East, Encuentro, and Batu Hijau, C veins crosscut and therefore postdate B veins and are in turn crosscut by D veins (Figs. 6E, 7D). C veins studied in several porphyry deposits rarely have quartz, but where they do, it is of the dull-CL type, and similar to D veins, they completely lack lucent-CL quartz (e.g., Spencer et al., 2015; Driesner and Heinrich, 2019). For example, at At Batu Hijau, SEM-CL imaging of Cu-Fe sulfide-rich C veins with chlorite and muscovite (i.e., paint veins) shows minor amounts of the brighter subtypes of dull-CL quartz (Schirra et al., 2019, 2022).

These observations suggest that the dull-CL quartz in microfractures that crosscuts different generations of older lucent-CL quartz in various veins may have a composition and formation timing similar to that of the dull-CL quartz observed in younger C and D veins, as illustrated in Figure 7D.

Discussion

In the studied porphyry deposits, a diversity of quartz veins and alteration halo types is observed within the K-silicate–altered high-Cu-Mo-grade ore shells and their roots (Figs. 1, 3). These veins and halos include, in order of relative age, Cu-Mo sulfide-poor deep quartz veins, Cu-Fe sulfide-bearing quartz A veins and early halos with minor quartz, banded molybdenite-quartz veins that lack Cu sulfides, and Cu-Fe sulfide and molybdenite-bearing quartz B veins. The quartz in these veins and halos is of the lucent-CL type. However, all lucent-CL quartz veins are crosscut by a similarly dense network of microfractures infilled with dull-CL quartz (Fig. 7). This quartz is comparable to the dull-CL quartz that forms younger C veinlets with Cu-Fe sulfide, chlorite, muscovite, and even younger pyrite-bearing D veins with sericitic halos (Table 1; Fig. 11). Both C and D veins lack lucent-CL quartz. There is no evidence that dull-CL quartz is formed between different lucent-CL generations. Dull-CL quartz is systematically observed crosscutting all lucent-CL quartz. The opposite crosscutting relationship, lucent-CL quartz crosscutting dull-CL quartz, is not observed in the three studied deposits and is rarely reported elsewhere. Therefore, dull-CL quartz postdates the whole crosscutting sequence of older lucent-CL veins. The observations discussed above suggest that the system remained hot and that upflowing fluid produced lucent-CL quartz until protracted cooling occurred at the waning stages of the magmatic system. At this point, lucent-CL quartz precipitation ended, and dull-CL quartz began forming.

In early halos, where quartz is rare, the mineralogical observations reported above show that Cu-Fe sulfides formed together with the hydrothermal K-feldspar, muscovite, and biotite that constitute the alteration halo. This indicates early and relatively high temperature sulfide introduction and precipitation. However, the formation timing of Cu-Fe sulfides

Fig. 9. QEMSCAN, scanning electron microscopy-cathodoluminescence (SEM-CL), and reflected microscopy images of key vein types. Images with no drawing overlays are provided in the Appendix. A) QEMSCAN image of a plagioclase site in an early halo is replaced by hydrothermal K-feldspar, biotite, muscovite, quartz, and corundum. Cu-Fe sulfides in the halo are not in contact with quartz but are in contact with K-feldspar. An associated quartz A vein above this feldspar site has bornite-chalcopyrite in contact with K-feldspar and quartz (Haquira East, AHAD98A-262 m). B) SEM-CL image of the same area. In the A-vein quartz, chalcopyrite is in contact with K-feldspar and both lucent- and dull-CL quartz. C) SEM-CL image of a quartz A vein that contains a central band made of a fine-grained aggregate of quartz and K-feldspar; both anhydrite and chalcopyrite are contained by lucent-CL quartz. Dull-CL quartz is sparse and present only in microfractures (Encuentro, JVC29-787 m). D) SEM-CL image of a quartz A vein. Cu-Fe sulfides and anhydrite are in contact with the mosaic-textured lucent-CL quartz and overgrowth zones with dull-CL quartz. The latter are interconnected with planar microfractures infilled with dull-CL quartz that do not contain Cu-Fe sulfides (Encuentro, JVC29-787 m). E) Reflected-light microscopy image and F) SEM-CL image of a lucent-CL mosaic-textured quartz A vein with incipient wavy concentric banding. The dull-CL quartz in microfractures and the lucent-CL quartz of the A vein are in contact with bornite and chalcopyrite (red arrows). Three bornite grains at the sides of the central zone are enclosed in lucent-CL quartz (green arrows) and are only locally in contact with dull-CL quartz in microfractures (Batu Hijau: SBD86-873 m). G) Backscattered electron image and H) SEM-CL image of a chalcopyrite-bearing quartz B vein. Chalcopyrite is in contact with the B-vein lucent-CL quartz (red arrows) and dull-CL quartz in microfractures and overgrowth zones (Haquira East, AHAD-185-229 m). I) SEM-CL image of lucent-CL quartz of a deep quartz vein with abundant dull-CL filled microfractures with no Cu-Fe sulfides (Haquira East, AHAD127-739 m). Abbreviations: Biot = biotite, Bn = bornite, Cpy = chalcopyrite, Cor = corundum, K-fdsp = K-feldspar, Musc = muscovite, Plg = plagioclase, Qtz = quartz.

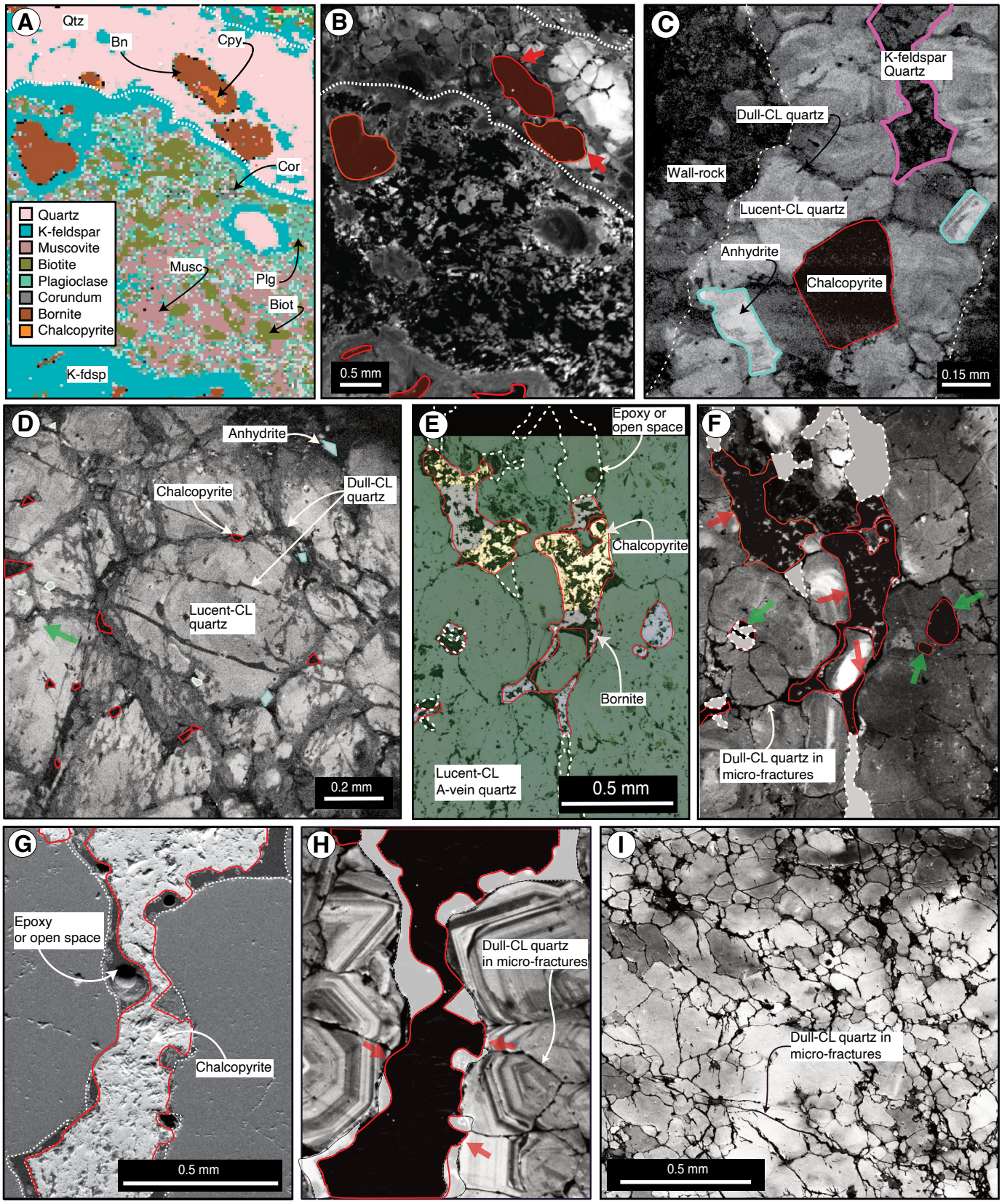

hosted in lucent-CL quartz veins cannot be readily resolved by studying SEM-CL vein textures, because sulfides contact both the lucent-CL quartz that forms the vein and the dull-CL quartz that crosscuts them. Nonetheless, piecing together deposit-scale vein crosscutting relationships with quartz SEM-CL textures of different vein types can constrain the Cu-Fe sulfide introduction and precipitation timing in quartz veins. Each lucent-CL vein type hosts distinct Cu-Fe, Mo, and Fe sulfide populations or lacks sulfides (Figs. 7, 11). These distinct sulfide contents are maintained where different generations of lucent-CL quartz veins crosscut each other (e.g., Fig. 5I), and despite that, they are all similarly crosscut and reopened by young dull-CL quartz in microfractures (Fig. 7). This can be interpreted to indicate that the sulfide populations could be related to the original formation of each vein type and are not significantly modified by younger events. The dull-CL quartz is only observed with Cu-Fe sulfides in a few lucent-CL vein types, such as A and B veins. Dull-CL quartz is present in other veins, such as deep quartz veins, where it is not associated with any sulfides, and in banded molybdenite-quartz veins, where it contacts molybdenite but no Cu-Fe sulfides (Figs. 7, 11). These observations further suggest that sulfides in lucent-CL veins, or lack thereof, were formed before the dull-CL quartz introduction (Fig. 11). Dull-CL quartz is likely introduced in several young events; however, because of their low Ti content, different dull-CL quartz generations are difficult to distinguish with SEM-CL imaging. Nonetheless, because all dull-CL quartz is young, crosscutting relationships with older veins will be similar if there are one or multiple generations. Because dull-CL quartz is not particularly associated with Cu-Fe sulfides or molybdenite but equally crosscuts all the older generations of lucent-CL quartz veins, dull-CL quartz precipitation postdates both the lucent-CL quartz veins and likely most of the Cu-Fe and Mo sulfides they contain. If not, the discussed observations would require that some generations of the young dull-CL quartz-forming fluid were Cu rich, whereas others were Cu poor. The young and Cu-rich fluid would have to percolate selectively through only a few lucent-CL quartz vein types (A and B veins) but not through older and younger lucent-CL quartz vein types that were present during the young fluid input (i.e., deep quartz veins and banded molybdenite-quartz veins). This selective fluid infill would have to occur systematically to A and B veins across different deposit areas while avoiding deep quartz veins and banded molybdenite-quartz veins (Fig. 11). We consider it unlikely that such a heterogeneous and uneven process occurred.

We argue that dull-CL quartz in microfractures is introduced late in a series of young events that crosscut all older types of quartz veins and take advantage of permeability both created by volume contraction upon sustained cooling after K-silicate alteration ceased and enhanced by quartz dissolution in the area of retrograde silica solubility (e.g., Figs. 9D, 11). Because the Cu-Fe sulfide/quartz interface is a preexisting discontinuity, open space will be generated at these contacts during volume contraction and can be infilled by dull-CL quartz. This potentially explains why observations of dull-CL quartz in contact with or containing Cu-Fe sulfides are more common than observations of relict lucent-CL quartz contacting the Cu-Fe sulfides that were originally precipitated with it (Figs. 7A, 9E, F).

Below we describe a reconciled scenario for vein and hydrothermal alteration formation, Cu and Mo introduction, and sulfide precipitation, and the relationship of this scenario with lucent-CL and dull-CL quartz formation in the context of crosscutting and textural observations reported above. We also discuss previously published temperature constraints from mineral stability estimates and Ti-in-quartz geothermometry to provide broad permissible ranges for high-, moderate-, and low-temperature hydrothermal events.

Cu-Fe sulfides precipitate in lucent-CL A-vein quartz and in early halos associated with K-silicate alteration, early and at high temperature

The first stage of Cu introduction and Cu-Fe sulfide precipitation occurs early and in stability with K-silicate alteration together with the formation of A-vein and/or early halos. Therefore, temperature estimates for lucent-CL quartz formation in A veins and for the silicate mineralogy of early halos may indicate the temperature of the precipitation of the sulfides they contain (Fig. 12).

Fig. 10. Scanning electron microscopy-cathodoluminescence (SEM-CL) images of key vein types. Images with no drawing overlays are provided in the Appendix. A) Reflected-light microscope image and B) SEM-CL image of molybdenite in contact with the lucent-CL (bright-CL) quartz band of a banded molybdenite-quartz (BMQ) vein. Molybdenite is locally in contact with later dull-CL quartz in microfractures (Haquira East, AHAD108-80 m). C) Molybdenite is enclosed in lucent-CL quartz of a B vein with anhydrite and chalcopyrite. Dull-CL quartz in microfractures crosscuts the lucent-CL quartz and is locally in contact with molybdenite (Encuentro, JVC155-458 m). D) Reflected-light microscope image and E) SEM-CL image of molybdenite grains in lucent-CL (bright-CL) quartz band of a banded molybdenite-quartz vein crosscut by a slightly darker lucent-CL quartz of a B vein (gray-CL). Cu-Fe sulfides are never in contact with the bright-CL quartz in banded molybdenite-quartz veins and are only included in the gray-CL quartz of the B vein that crosscuts and reopens the banded molybdenite-quartz vein. Dull-CL quartz in microfractures crosscuts the lucent-CL of both vein types and is locally in contact with the molybdenite in the banded molybdenite-quartz vein and the Cu-Fe sulfides in the B vein (AHAD108-80 m). F) SEM-CL image of quartz phenocryst in a granodioritic synmineralization porphyry dike. A set of dull-CL quartz in microfractures with no Cu-Fe sulfide intensely crosscuts both the quartz phenocryst and aplitic groundmass (AHAD-98A-125.8 m). The porphyry dike that hosts this quartz phenocryst is crosscut by Cu-bearing early halos and quartz A and B veins. G) Reflected-light microscope image and H) SEM-CL image shown at higher SEM-CL contrast than all previous CL images. Both subtypes of dull-Cl quartz are observed (medium-gray- and dark-CL) in contact with muscovite and pyrite-chalcopyrite in a quartz D vein (Haquira East, AHAD-98A-545 m). I) SEM-CL image of a D vein with pyrite-chalcopyrite crosscutting a quartz A vein. D veins at Encuentro contain minor or lack quartz; however, abundant dull-CL quartz forms along the vein when it crosscuts older lucent-CL quartz with mosaic texture. Quartz in microfractures through the lucent-CL quartz is equally dull-CL as the D-type vein quartz and appears to emanate from it (Encuentro, JVC97-461 m). Abbreviations: Cpy = chalcopyrite, Py = pyrite.

Temperature estimates for lucent-CL quartz in A veins based on Ti-in-quartz geothermometry and fluid inclusions from a variety of A-vein-type, early-halo-type, and hybrid porphyry deposits range from 500° to ~650°C (Batu Hijau: Cernuschi, 2015; Schirra et al., 2017; Haquira East: Cernuschi et al., 2018; Bingham: Roedder, 1971; Irwin and Roedder, 1995; Redmond et al., 2004; Landtwing et al., 2010; Encuentro: Osorio, 2017; Osorio et al., 2018; El Teniente: Klemm et al., 2007; Butte: Rusk et al., 2008b, Mercer and Reed, 2013; Altar: Maydagan et al., 2015). The available formation temperature estimates agree with mineral phase equilibria estimates for the K-silicate alteration (hydrothermal biotite and K-feldspar) that accompanies A veins above ~550°C (Fig. 2; Seedorff et al., 2005) and other chemical stability estimates (Titley and Beane, 1981; Brimhall et al., 1985; Reed et al., 2013; Monecke et al., 2018; Dilles and John, 2021).

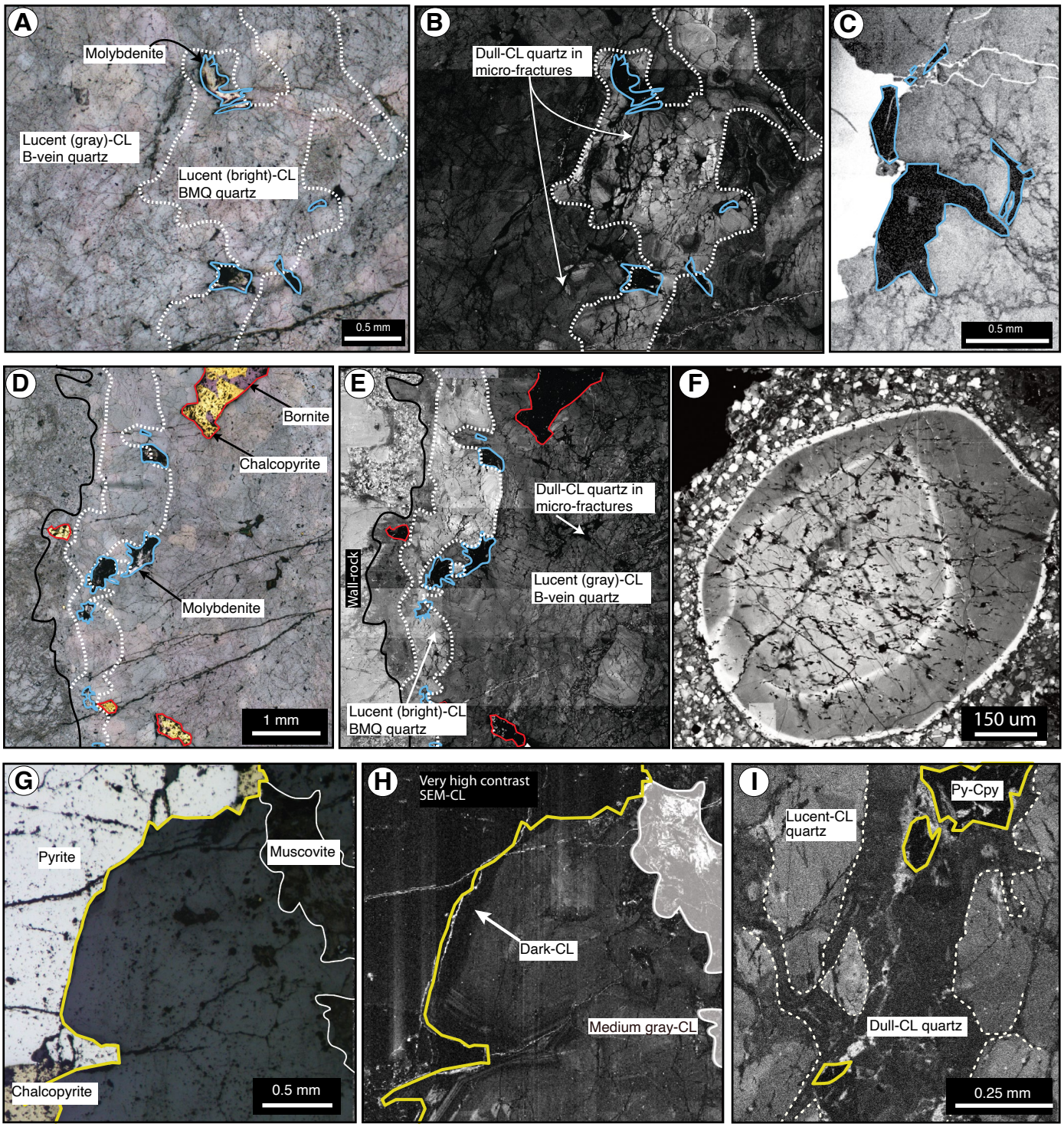

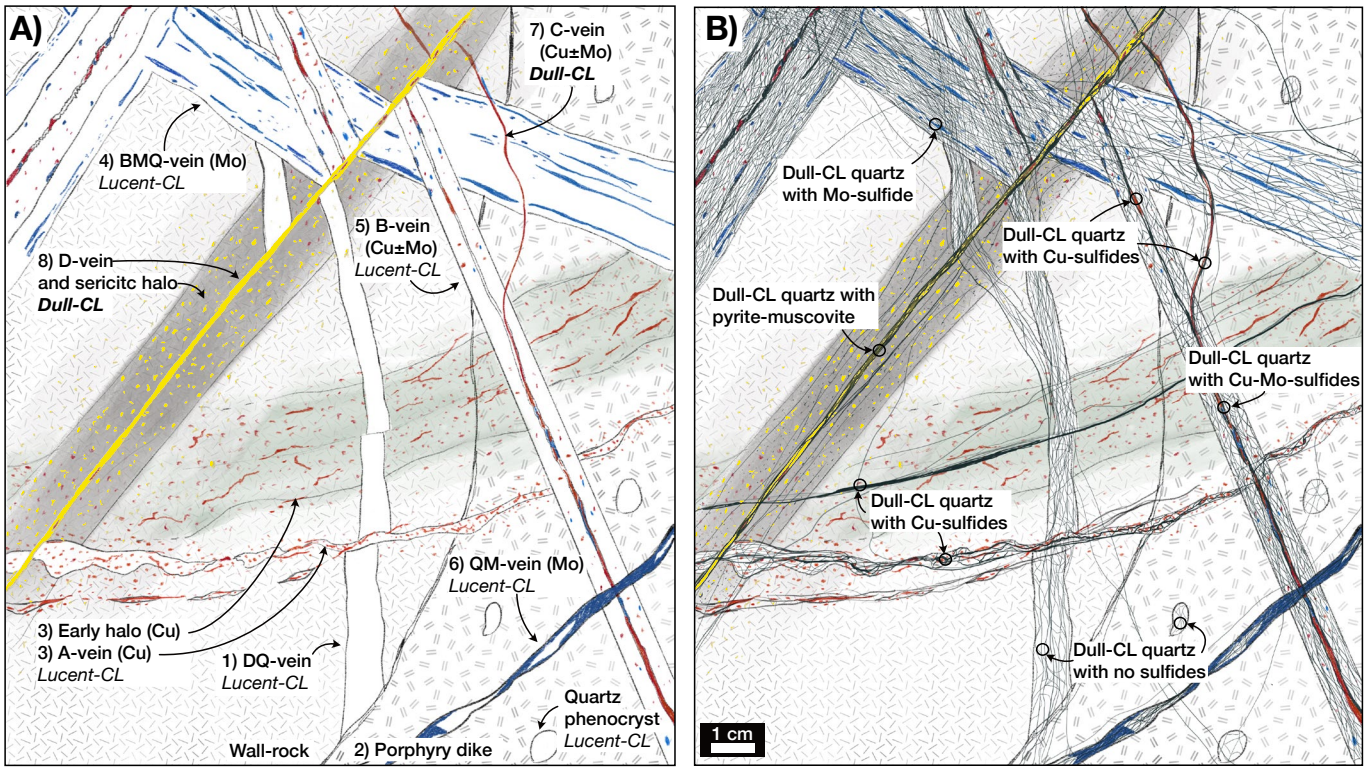

Fig. 11. A) Schematic cartoon of key veining stages in some porphyry copper deposits. Whereas veins 1 to 6 are composed of lucent-CL quartz, veins 7 to 8 are composed of dull-CL quartz. B) During the formation of veins 7 and 8, hydrothermal fluid percolates microfractures formed by thermal contraction in older lucent-CL quartz and can precipitate dull-CL quartz. Through this process, dull-CL quartz is precipitated in contact with older Cu and Mo sulfides contained in some of the older lucent-CL quartz veins. Multiple generations of dull-CL quartz exist; however, they are all younger than the lucent-CL quartz of veins 1 to 6. Reverse crosscutting relationships are commonly observed, mostly in veins 1 to 4. Abbreviations: BMQ = banded molybdenite-quartz, CL = cathodoluminescence, DQ = deep quartz, QM = quartz- molybdenite.

Silicate mineral phase equilibria in all subtypes of early halos indicate a broad temperature range of 450° to ~600°C for K-feldspar-muscovite-biotite ± andalusite ± chlorite alteration assemblages (Figs. 2, 11; Seedorff et al., 2005) and support the same formation temperatures of the Cu-Fe sulfides found intergrown with these silicates. Biotite-rich, early halos from Butte contain local andalusite (Meyer, 1965; Roberts, 1973; Brimhall, 1977) formed at 550° to ~600°C and pressures ranging from 0.70 to 2 kbar, i.e., lithostatic to hydrostatic (Fig. 2). Based on Figure 2, early halos lacking andalusite likely formed below the temperature stability of andalusite (450°–~550°C). Similarly, hydrothermal biotite and rutile in biotite veins and early dark micaceous halos that commonly contact chalcopyrite yield temperature estimates of 450° to 680°C (Mercer and Reed, 2013), and muscovite-alkali feldspar equilibrium yield temperatures of 600° to 700°C (Brimhall, 1977). As previously noted, some minor mineralogical differences in early halos are likely related to the available Fe content of the wall rock and fluid/rock ratios and not solely to their formation temperature (Cernuschi et al., 2019).

Thus, early halos and A veins, dominant in deep and shallow porphyry deposits, respectively, form at high temperatures associated with K-silicate alteration. Therefore, the intergrown Cu-Fe sulfides likely also formed at these temperatures. Sulfur isotope fractionation estimates for coexisting anhydrite-chalcopyrite in early dark micaceous halos at Butte give sulfide equilibration estimates of 480° to ~575°C, which are minimum estimates for precipitation (Field et al., 2005). The presence of sulfide and anhydrite also necessitates the presence of sufficient H_2S and H_2SO_4 at these high temperatures.

The overlapping formation temperature estimates of both early halos and A veins reaffirm that the key differences in the dominant Cu ore-forming vein/halo style are not simply controlled by temperature but rather by the depth of magmatic fluid release from the underlying batholith cupolas, as discussed below.

Retrograde solubility of quartz at high pressure favors the formation of early halos in deep porphyry copper deposits

The magmatic-hydrothermal fluid that produces veins and hydrothermal alteration in porphyry deposits ascends from a deep and lithostatically pressured magma and depressurizes to hydrostatic pressures near the surface. Although some authors have argued that the brittle-ductile transition at ~350° to 400°C marks the boundary between deep lithostatic and shallow hydrostatic fluid pressures (cf. Fournier, 1985), the magmatic fluids have sufficient mechanical energy to hydrofracture the rock in the ductile zone (Burnham, 1985) and rapidly ascend from lithostatic to hydrostatic pressure at great depth and relatively high temperature (Tosdal and Dilles, 2020). Figure 13 illustrates three adiabatic (i.e., isoentropic

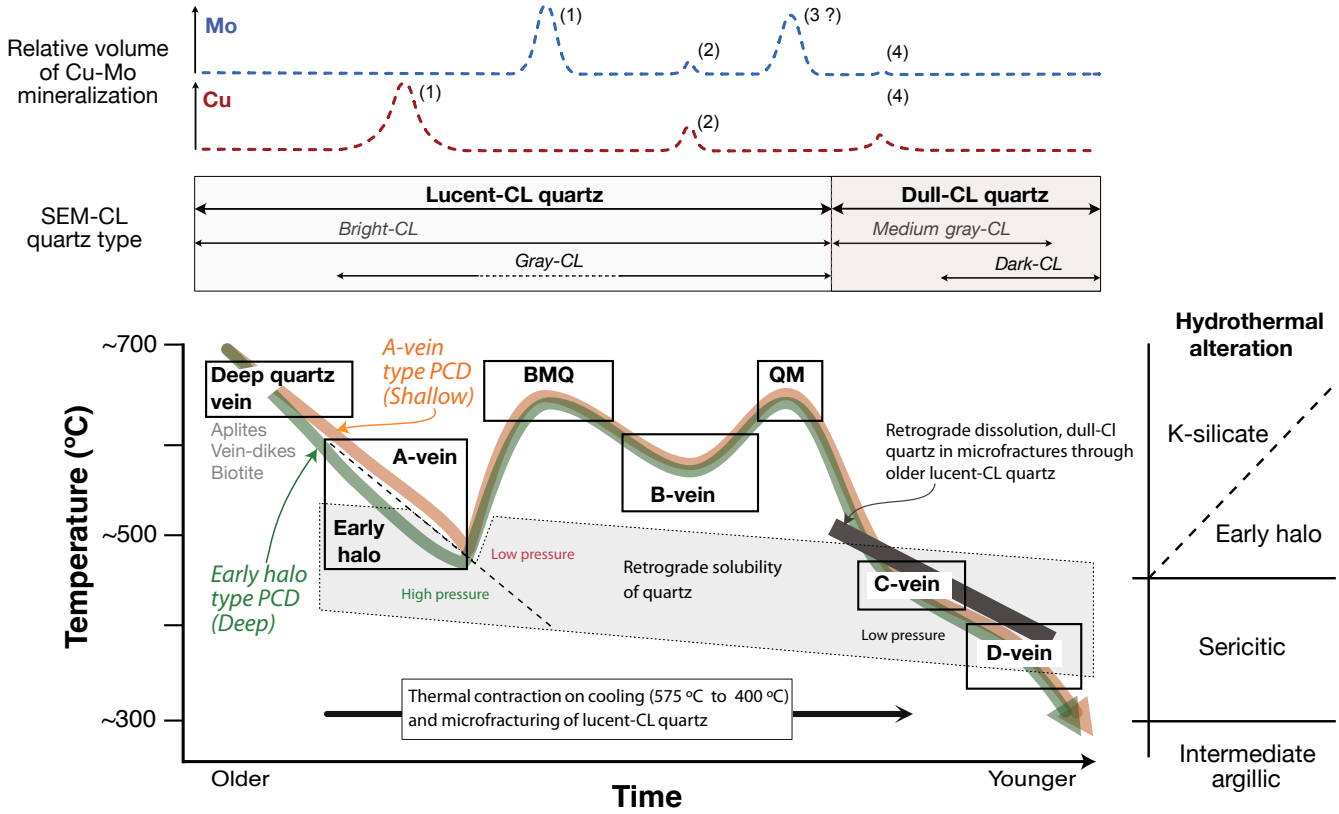

Fig. 12. Schematic temperature versus time diagram of a porphyry deposit evolution. Cu-Fe sulfide is introduced in stability with K-silicate alteration and quartz A veins in shallowly sourced porphyry copper deposits (orange line) or K-silicate/muscovite alteration in early halos in deeply sourced porphyry deposits (green line). Deeply sourced fluids experience retrograde silica solubility at high pressure during the formation of early halos. Mo mineralization is also introduced during K-silicate alteration but with later banded molybdenite-quartz (BMQ) veins. Minor Cu and Mo can be introduced or remobilized from older sulfides with B and C veins. Some porphyry deposits have significant Mo mineralization in nonbanded quartz-molybdenite (QM) veins that postdate B veins. After cooling, thermal contraction affects all high-temperature lucent-CL quartz, creating a network of microfractures. Lower-temperature fluids flood these microfractures in retrograde silica solubility and produce dissolution and erosion. Later at lower pressure and temperature, fluids precipitate dull-CL quartz. This stage may coincide with the formation of C veins at the waning stages of K-silicate alteration. Dull-CL quartz continues precipitating with pyrite and muscovite in D veins in stability with sericitic alteration. Both deep and shallowly sourced fluids experience retrograde silica solubility at low pressure at some stage during the formation of C and D veins and the introduction of dull-CL quartz in microfractures. Abbreviations: CL = cathodoluminescence, PCD = porphyry copper deposit, SEM-CL = scanning electron microscopy-cathodoluminescence.

with no heat added or lost from fluid) ascent paths for water derived from deep, intermediate, and shallow magmatic sources. These paths are shown in Figure 13 as green, blue, and red curved lines, respectively, and start at 700° to 740°C in lithostatic pressure and end at 530° to 560°C in hydrostatic pressure (~one-third lithostatic). The silica solubility illustrates that these paths lead to saturation and precipitation of 85, 94, and 95 mass % of silica as quartz veins along the three paths (pink field), respectively, as initially suggested by Rusk and Reed (2002). Once fluids reach hydrostatic pressures, they ascend further on hydrostatic gradients and pass through the retrograde solubility (green field) area, where quartz is not precipitated, and the fluid may dissolve silica between 350° and ~540°C. Therefore, quartz is absent or rare in vein conduits formed in this temperature range (e.g., early-halo, C, and D veins).

Both deep and shallow systems may precipitate most quartz in deep veins during the initial depressurization (red field) at temperatures too high to precipitate Cu-Fe sulfides. This result is consistent with low Cu grades in the deep core of porphyry deposits with abundant Cu-Fe sulfide-poor deep quartz veins (Figs. 1, 3; e.g., Landtwing et al., 2005; Weis et al., 2012). However, the deep and shallow paths differ significantly as fluids ascend and pressure decreases. Whereas the deep ascent path (green line) traverses the zone of retrograde quartz solubility from 410° to ~540°C, the shallow ascent path (red line) continues to precipitate quartz throughout much of this temperature range. It traverses the zone of retrograde quartz solubility from 350° to ~475°C. Therefore, deep hydrothermal systems may produce quartz-poor early halos because of the high-pressure retrograde solubility of quartz at a temperature range in which shallow systems produce quartz in A veins. Therefore, Cu-rich A veins and early halos form above the hot zone where deep and Cu-poor quartz veins precipitate. These fluid ascent paths result in the observed inverted cup-shaped high-Cu-grade shells that mimic the steep geothermal gradient caused by the hot hydrothermal upflow (Figs. 1, 3; e.g., Weis et al., 2012). As new and younger fluid

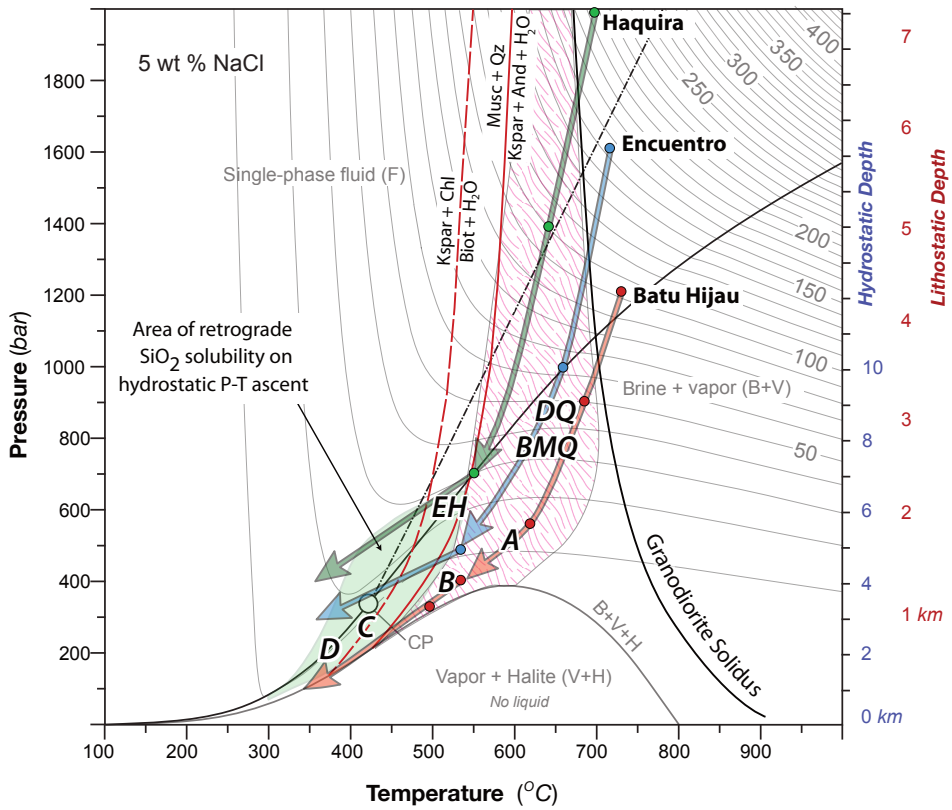

Fig. 13. Pressure-temperature (P-T) conditions of key veins and hydrothermal alteration types from porphyry deposits were plotted on the quartz solubility diagram for 5 wt % NaCl equiv water (Monecke et al., 2018). Also shown are the reactions bounding the stability of andalusite (Frank et al., 1998) and biotite (estimated by Dilles and John, 2021). Fluid derived from porphyry deposit magmas at deep, moderate, and shallow conditions (green, blue, red curves) depressurizes during rapid ascent from lithostatic to hydrostatic conditions (Rusk and Reed, 2002). Here, we approximate ascent paths from lithostatic to hydrostatic pressure with the adiabatic curves for water (Henley et al., 2015). At temperatures below ~450° to 550°C, hydrostatic conditions are assumed. The field of retrograde silica solubility (green field) is indicated for hydrostatically pressured fluids cooling along the linear pressure-temperature paths illustrated. The quartz solubility curves are from Monecke et al. (2018) (cf. Fournier, 1985). The fluids from the deepest magmatic sources (>2 kbar) stay in the single-phase field (F), whereas all others enter the brine and vapor (B + V) field. The fluids from the shallowest sources ascend and cool along the three-phase boundary of brine, vapor, and halite (B + V + H, red curve at <450°–500°C; Lecumberri-Sanchez et al., 2015). During the rapid adiabatic depressurization from lithostatic to hydrostatic conditions, quartz in veins begins to precipitate (pink field), including deep quartz veins and banded molybdenite-quartz veins. In shallow porphyry systems, the low-pressure path continues to precipitate quartz and forms Cu-bearing A veins as it crosses the brine-vapor and brine-vapor-halite fields (red line in the red field). In deep porphyry systems, the ascending fluid at high pressure may experience silica retrograde solubility between 410° to ~540°C and therefore favor the production of quartz-poor early halos instead of A veins as quartz precipitation is inhibited (green line through the green field). In these shallow systems, the field of retrograde solubility of quartz is not intercepted at this stage, and it is crossed later between <350° and ~475°C, as younger fluid inputs are sourced from greater depth (area between red and blue lines in the green field). Hybrid porphyry systems are formed at intermediate depths where the fluid fluctuates between both fields (blue line). In all deposits, both A veins and early halos are cut by local sulfide-rich (C) and pyrite-rich (D) veins with chlorite and muscovite (sericite) selvages, respectively. These may also partially form during retrograde silica solubility between <350° and ~475°C. See text for further explanation and Table 1 for vein and alteration mineralogy. Abbreviations: And = andesite, Biot = biotite, Chl = chlorite, CP = critical point, DQ = deep quartz, EH = early halos, Kspar – K-feldspar, Musc = muscovite, Qz = quartz.

ascends from slightly deeper zones, both deep and shallow systems may experience low-pressure retrograde solubility of quartz at the C- and D-vein stages, as the ascent path does not intercept the brine-vapor-salt boundary in both shallow and deep systems (blue and green lines in Fig. 13).

The critical magmatic-hydrothermal source depth for the transition between A-vein-type and early-halo-type porphyry deposits has been inferred at ~5 km (Proffett, 2009). This depth marks the boundary between single-phase fluid and two-phase brine plus vapor, illustrated in Figure 13 (e.g., Bodnar, 1995; Driesner and Heinrich, 2007). Similarly, the formation depth for the boundary between porphyry deposits containing an altered rock with A veins and deeper deposits with early halos was estimated at 3 to 4 km based on hydrostatic pressures of ~300 to 400 bar (Dilles and John, 2021). The single-phase fluid dynamic is evidenced in the deeply sourced Haquira East fluids, where fluid inclusions do not show unmixing (intermediate-density two-phase inclusions, ~2.2–2.5 kbar; B. Rusk and Y. Zhang, unpub. data, 2015; Cernuschi, 2015). Nonetheless, we note that the deeply sourced Butte fluids (≥2.2 kbar lithostatic pressure; Rusk et al., 2006) ascended and locally depressurized and

unmixed to brine + vapor, and the Ann-Mason early halos formed entirely in the field of brine + vapor (Dilles and Einaudi, 1992; Proffett, 2009). Therefore, rapid pressure fluctuations may have reached transient conditions that enabled early-halo formation.

Molybdenite precipitates in high-temperature lucent-CL quartz veins after the bulk of the Cu ore formation

Molybdenite precipitated with lucent-CL quartz veins with molybdenite after most of the Cu-Fe sulfide-bearing A veins and early halos formed but before the introduction of the dull-CL quartz (banded and nonbanded quartz veins with molybdenite; Figs. 11, 12). Temperature estimates for Mo-bearing veins are scarce. At Haquira East, Ti-in-quartz estimates suggest precipitation temperatures of ~650°C for quartz in banded molybdenite-quartz veins (Cernuschi et al., 2018). The younger nonbanded quartz-molybdenite veins at Encuentro have lucent-CL quartz with both high and moderate Ti content (~130 and ~70 ppm), which yields titanium-in-quartz estimates of >550°C (Osorio, 2017; Osorio et al., 2018). Fluid inclusions in molybdenite-bearing veins at Bingham yield estimates of up to ~580°C (Seo et al., 2012). Anhydrite-molybdenite sulfur isotope compositional pairs at Butte yield equilibration temperature estimates of 545° to 630°C with an average of 605°C (Field et al., 2005). These high-temperature estimates suggest that molybdenite might have precipitated during inputs of new high-temperature fluids attending thermal reversals (Fig. 12; Cernuschi et al., 2018). These thermal and temporal differences may explain why inverted cup-shaped Mo ores are concentric with the older inverted cup-shaped Cu ore shell but not coincident, as both Cu and Mo shells respond to hydrothermal fluid upflow from the same source but at a different time, temperature, and possibly source depth and therefore a slightly different hydrothermal pressure-temperature gradient (e.g., Haquira East: Cernuschi, 2015; Encuentro: Osorio, 2017; Bingham: Porter et al., 2012).

Some Cu-Fe and Mo sulfides continue to precipitate at a lower temperature in B veins

A relatively small volume of Cu-Fe sulfides and molybdenite is found in B veins in some porphyry deposits. B veins formed after A veins and early halos and between different generations of quartz-molybdenite veins, where these crosscutting relationships are documented (Figs. 11, 12). Ti-in-quartz geothermometry yields estimates of ~550°C for the precipitation of lucent-CL quartz in B veins (Rusk et al., 2006; Cernuschi et al., 2018). Other B-vein estimates indicate 375° to ~500°C (e.g., Monecke et al., 2018). These estimates suggest a lower precipitation temperature for Cu-Fe sulfides and molybdenite in B veins than in the primary and earlier Cu-Mo–mineralization events. Still, the vein mainly formed stable with K-silicate mineral assemblages (Fig. 2). In some cases, the sulfides that fill the B veins centerline may have been deposited significantly after B-vein quartz deposition by younger and lower-temperature fluids possibly associated with C veins (see below). Such relationships are observed at Haquira East and other deposits, where C veins are locally observed to cut wall rock and then enter the centerline of several B veins (Cernuschi, 2015; Driesner and Heinrich, 2019).

Early and lucent-CL quartz is fractured upon cooling after K-silicate alteration has ceased and before dull-CL quartz introduction and precipitation

All the early high-temperature veins, including deep quartz, A veins, early halos, varieties of quartz-molybdenite, and B veins, are crosscut and reopened by microfractures filled with low-temperature dull-CL quartz. In part, the late microfractures in older quartz were likely formed by the thermal contraction of quartz during cooling. An abrupt volume reduction of ~0.8% occurs during cooling through 573°C at the transition from alpha (α) to beta (β) quartz (Fig. 14; Skinner, 1966; Dilles, 1984). An additional ~1.8 vol % reduction follows cooling from 573° to ~400°C. This volume reduction can potentially produce a net of microfractures throughout the high-temperature quartz and explains why microfractures abundantly cut all lucent-CL quartz in both veins and phenocrysts. In addition, because quartz sulfide grain boundaries are preexisting discontinuities, they are preferentially opened as microfractures during quartz volume contraction. As a result, relatively low temperature ascending fluids can easily permeate along both preexisting sulfide-quartz contacts and microfractures through older quartz. This mechanism explains why observing dull-CL along the interface between Cu-Fe sulfide and lucent-CL quartz and microfractures in lucent-CL quartz may be so common in all older vein types. If dull-CL quartz is abundant, this model predicts that the observation of dull-CL quartz in contact with Cu-Fe sulfide will be more common than the observation of relict lucent-CL quartz with Cu-Fe sulfides. Additionally, anhydrite, K-feldspar, and molybdenite grain boundaries with lucent-CL quartz are also reopened, as demonstrated by lucent-CL quartz locally rimmed by dull-CL quartz in contact with those minerals (Figs. 7, 9A, C, E). Dull-CL quartz precipitated and possibly locally recrystallized the earlier lucent-CL quartz as different subtypes of dull-CL quartz depending on the degree of dissolution and fluid volume. This may explain why some fractures through lucent-CL quartz are filled with dull-CL quartz of the dark-CL subtype in some areas and the medium-gray-CL subtype in others (e.g., Fig. 9D).

Dissolution and erosion of older lucent-CL quartz also occur during this period, as some of the fluid upflow at and below ~450°C intercepts the area of retrograde silica solubility (Fig. 13; Fournier, 1985; Monecke et al., 2019). As a result, the cooling and depressurizing fluids that percolate through the microfractures will locally dissolve the host lucent-CL quartz, enhancing the creation of microfractures and precluding them from sealing. In this process, microfracture widths may have widened, and erosion and truncation features will be created in the early lucent-CL quartz. This erosion and truncation are mainly observed where SEM-CL images reveal growth bands in B veins, but it is likely present in all types of old lucent-CL quartz. Because this fluid upflow may also happen along preexisting discontinuities between quartz and other mineral phases, we expect lucent-CL quartz to show erosion and dissolution against Cu-Fe sulfides and other minerals (e.g., Fig. 9H; Tsuruoka et al., 2021).

The creation of microfractures through older lucent-CL quartz may only happen after the system experienced sustained cooling, likely after the main stage of porphyry dike emplacement and magmatic fluid release have ceased or

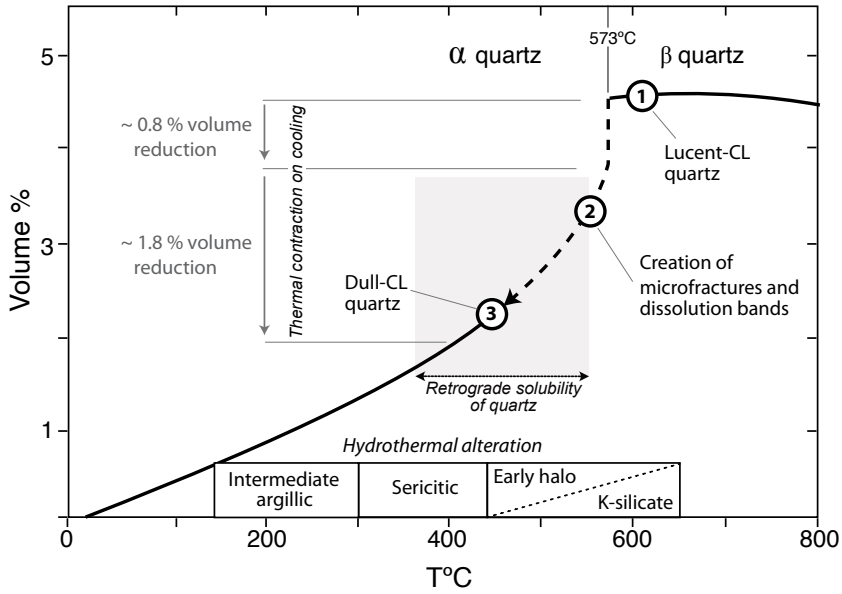

Fig. 14. Thermal expansion of quartz versus temperature (T) relative to α quartz at 20°C, reproduced from Dilles (1984) and data from Skinner (1966). High-temperature β quartz (1) experiences considerable volume reduction upon cooling, significantly below the 573°C α-β phase transformation and down to about 400°C, which is accommodated by the creation of microfractures (2). This event coincides with the silica retrograde solubility area; therefore, microfractures cannot be sealed by quartz precipitation, and dissolution bands may be formed. Therefore, hydrothermal fluid can penetrate these microfractures at a younger and lower temperature stage (3) and precipitate dull-CL quartz. Quartz solubility is pressure dependent; thus, a broad approximate range is depicted in the diagram (Fournier, 1985). Abbreviation: CL = cathodoluminescence.

greatly diminished. In the earlier period before sustained cooling, fluctuations in temperature were governed by quick depressurization upon fluid release and hydrofracturing, followed by sealing of permeability by lucent-CL quartz vein precipitation, quickly restoring lithostatic pressure while the temperature of the system remained high (Fig. 13; Tosdal and Dilles, 2020). Therefore, if microfractures were created before the system experienced sustained cooling, between the formation of different generations of lucent-CL quartz veins, the fractures were rapidly healed, precluding fluid inflow and infill precipitation.

We propose that the creation of open microfractures attended rapid cooling and largely followed K-silicate alteration. Later and moderate-temperature fluids precipitated dull-CL quartz in the microfractures.

Some Cu-Fe sulfides may be reprecipitated in C veins during lower-temperature events and the onset of dull-CL quartz formation

At many porphyry deposits, C veins carry Cu-Fe sulfides and rare molybdenite, postdate B veins, and predate D veins (Figs. 11, 12; e.g., Spencer et al., 2015). C veins contain minor amounts of brighter types of dull-CL quartz that have been interpreted as primary and deposited together with Cu-Fe and Fe sulfides (e.g., Batu Hijau: Schirra et al., 2019, 2022). Ti-in-quartz estimates for C-vein formation indicate temperatures up to ~450°C (medium-gray-CL quartz; Table 1). Similarly, Monecke et al. (2018) estimated 375° to 450°C for the formation of C veins, and Driesner and Heinrich (2019) estimated <400°C based on fluid inclusions. These conditions suggest that C-vein formation occurred at the end of K-silicate alteration (Seedorff et al., 2005) and are consistent with the observation that most C veins appear locally stable with adjacent K-silicate–altered wall rock. Whereas K-feldspar is apparently stable in vein selvages, biotite is commonly replaced by chlorite ± sericite (Table 1; Figs. 2, 9). Based on these data, we suggest that the bulk of Cu-Fe sulfide precipitation in C veins likely occurred with quartz at ~400°C during the waning stages of K-silicate alteration and that as temperature decreased, late fluids converted biotite to chlorite ± sericite.

The Cu-Fe sulfides present in C veins and possibly some of the B-vein centerlines may be a product of a late copper input from a magmatic-hydrothermal fluid source. Alternatively, the copper could be remobilized from older Cu-Fe sulfides in higher-temperature A veins and early halos. We suggest that remobilization is the most likely and dominant source of copper in these C veins in many porphyry deposits, based on the paucity of Cu-Fe sulfides in all types of younger veins outside the Cu ore zones where Cu-Fe sulfides are initially introduced in A veins and early halos (e.g., Encuentro, Fig. 3B). Nonetheless, the late introduction of Cu-Fe sulfides may be significant in other deposits. Local dissolution must have occurred to some of the original Cu-Fe sulfides during the younger remobilization events. However, dissolution textures are not preserved, because all Cu-Fe sulfides that precipitated above ~300°C undergo recrystallization during cooling of the hydrothermal system and the wall rock from ~300° to <200°C, resulting in bornite and chalcopyrite assemblages (Barton and Skinner, 1967). Therefore, all the observed Cu-Fe sulfides have recrystallized at a lower temperature than their original high-temperature deposition and later moderate-temperature dissolution, local remobilization, and reprecipitation.

At Batu Hijau, C veins are most abundant on its eastern flank, and in this area, A veins host more dull-CL quartz in

microfractures, and chalcopyrite is more recrystallized than elsewhere. This asymmetry of the zonation suggests that the eastern flank of the deposit experienced a more significant late fluid overprint than the western flank, causing remobilization and reprecipitation of Cu-Fe sulfides. This remobilization must be local at Batu Hijau and other porphyry deposits elsewhere because the bulk of C veins is spatially associated with older A and B veins and early halos. Therefore, remobilization must be local, and substantial transport is unlikely.

C veins and the first stage of dull-CL quartz precipitation in microfractures through older lucent-CL quartz might occur at similar timing, as suggested by vein crosscutting relationships (Figs. 11, 12). At Haquira East, Ti-in-quartz geothermometry estimates of dull-CL quartz in microfractures range from ~450°C for the medium-gray-CL subtype to ~350°C for the dark-CL subtype (Cernuschi et al., 2018), in agreement with temperature estimates for similar dull-CL quartz filling microfractures in older lucent-CL quartz in porphyry deposits elsewhere (e.g., Rusk, 2012; Monecke et al., 2018) and homogenization temperatures of fluid inclusions in dull-CL quartz (e.g., Altar: Maydagan et al., 2015; Bingham: Landtwing et al., 2005, 2010; Redmond et al., 2004; Batu Hijau, Q2 quartz: Zwyer, 2010; Schirra et al., 2017; Dabaoshan: Mao et al., 2017). These temperature estimates of the first and medium-gray-CL subtype of dull-CL quartz in microfractures overlap with the temperature range estimated for C-vein formation (350°–~450°C).

Dull-CL quartz precipitation continues during D-vein formation and sericitic alteration

Crosscutting relationships at many porphyry deposits indicate that D veins with quartz-sericite-pyrite halos crosscut all earlier veins hosted in K-silicate alteration zones throughout the vertical extent of the deposit (Fig. 1; e.g., Seedorff et al., 2005; Sillitoe, 2010). At this stage, the bulk of the Cu-Fe sulfides already precipitated (Figs. 11, 12).

D veins are formed by dull-CL quartz, both medium-gray-CL and dark-CL subtypes. In D veins from Haquira, both quartz types commonly enclose muscovite grains and yield Ti-in-quartz temperature estimates of ~450° and ~350°C, respectively (Cernuschi et al., 2018), consistent with the stability of muscovite between ~300° to ~450°C and other temperature estimates for D veins elsewhere (e.g., Seedorff et al., 2005; Rusk, 2012; Monecke et al., 2018). Similarly, as reported above, the Ti content and oxygen isotope compositions of both subtypes of dull-CL quartz are similar for quartz in D veins and quartz in microfracture fillings through lucent-CL quartz in older veins, suggesting possible genetic relationships (Cernuschi et al., 2018).

Oxygen isotope data further support the percolation of late and moderate-temperature fluids through older and high-temperature quartz veins. At Haquira East, lucent-CL quartz in early halos, as well as in A and B veins, yields oxygen isotope compositions ($\delta^{18}O$ ~ 10.5‰) that indicate equilibration temperatures at ~450°C, which is consistent with equilibration with water ($\delta^{18}O$ ~ 11.2‰) at the temperatures estimated for the formation of the medium-gray-CL subtype of dull-CL quartz (Cernuschi et al., 2018). The ubiquity of dull-CL quartz in older quartz veins from deep and shallow portions of the system and the oxygen isotope reequilibration suggest a late-stage upflow of magmatic-hydrothermal fluid permeated through the whole vertical section at a moderate temperature of ~450°C (Fig. 1; Cernuschi et al., 2018).

These observations indicate that the initial introduction of dull-CL quartz in microfractures through older lucent-CL quartz veins started following K-silicate alteration during the formation of C veins, and dull-CL quartz continued to precipitate during the later D-vein formation and sericitic alteration. After lucent-CL quartz precipitation ceased and only dull-CL quartz was being precipitated, there was an apparent progression from alternating medium-gray-CL and dark-CL subtype to only dark-CL subtype, which might be related to the progressive cooling of the system at its waning stages.

Copper solubility experiments suggest that most Cu-Fe sulfide precipitates at high temperatures

The experimental solubility of copper in aqueous chloride solutions provides direct evidence for the precipitation of copper sulfide at high temperatures due to solution cooling (Barnes, 1979; Hemley and Hunt, 1992; Hemley et al., 1992). The pioneering studies of Hemley et al. (1992) measured the solubility of copper at sulfide saturation in 1 molal chloride solutions (5.8 wt % NaCl equiv at 300°–500°C). Here, we extend the solubility relationships to 600° to 650°C and up to 2 molal chloride (11.6 wt % NaCl equiv) from data of Lerchbaumer and Audétat (2012) and into the two-phase region of brine plus vapor, as summarized in Figure 15.

The copper solubility in sulfide-saturated solutions is directly proportional to chloride content and increases with temperature (Barnes, 1979; Hemley et al., 1992). The chloride content relationship is due to the complexation of cupric (Cu^+) ion with Cl^- ion as $CuCl_{aq}$ (i.e., $[Cu^+]_{aq} + [Cl^-]_{aq} = [CuCl]_{aq}$), which at a constant concentration of $[Cu^+]_{aq}$ requires that $[CuCl]_{aq}$ content is directly proportional to $[Cl^-]_{aq}$ (i.e., $\log [CuCl]_{aq} = \log [Cl^-]_{aq} + \log K_{eq} + \log [Cu^+]_{aq}$ and because the last two terms are fixed, $\log [CuCl]_{aq} = \log [Cl^-]_{aq} + C$, where K and C are constants). This relationship allows us to interpolate data collected at various chloride concentrations to 1 and 2 molal chloride, the typical range of porphyry-type fluids (Audétat et al., 2008). In the two-phase region of brine and vapor, the bulk salinity can be estimated by summing the mass fraction of brine multiplied by the molality of chloride in brine and the mass fraction of vapor multiplied by the molality of chloride in vapor. When we use the mass ratio of vapor to brine of 4:1 to 9:1 for porphyry copper fluids of Lerchbaumer and Audétat (2012), experiment copper solubilities at 600° to 650°C lie along the projection of the Hemley et al. (1992) solubilities at 300° to 500°C (Fig. 15). Note that copper solubilities vary slightly as the vapor to brine ratio decreases from 4 to 9, as illustrated, because of decreased salinity of the bulk mixture. Similar copper solubilities are derived from the experimental data of M.R. Frank at 500° to 700°C in single-phase and brine-vapor mixtures (writ. commun., 2022). We note that under the proposed adiabatic depressurization paths illustrated in Figure 13, low- and moderate-pressure fluids derived from granitic melts at 700° to 750°C lie in the single-phase field initially but, upon depressurization, enter the two-phase brine plus vapor field at 600° to ~740°C and remain in that field until 400°C or lower. In contrast, high-pressure flu-

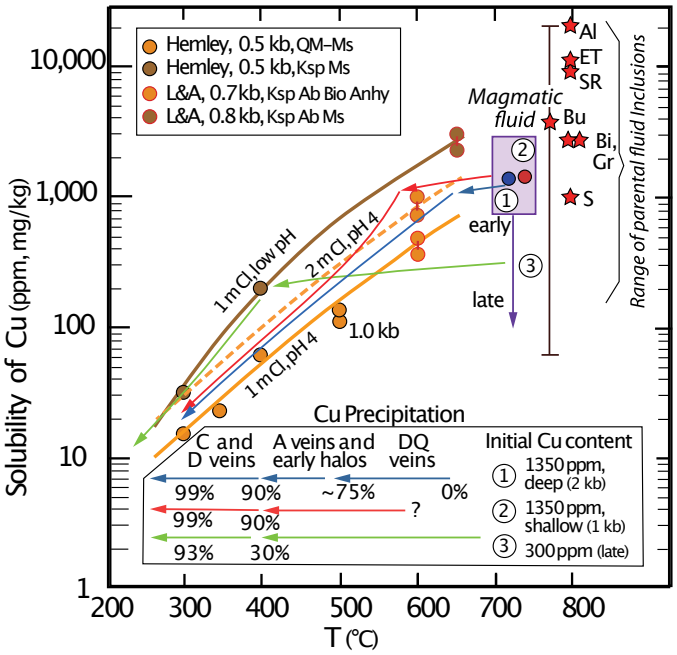

Fig. 15. Temperature versus copper solubility from experiments of Hemley et al. (1992) and Lerchbaumer and Audétat (2012; L&A) (see text). Two sets of solubility curves were constructed, one for slightly acidic conditions buffered by K-feldspar-albite-muscovite ± biotite (e.g., early halos and K-silicate alteration) and a second one for more acidic conditions buffered by K-feldspar-muscovite (e.g., quartz-sericite alteration). Temperatures are shown for sulfide-saturated assemblages. The copper solubilities for acidic fluids are illustrated for 1 molal chloride solutions with 5.8 wt % NaCl equiv, and slightly acidic fluids are illustrated for 1 and 2 molal chloride (5.8 and 11.6 wt % NaCl equiv). These are similar to the range of porphyry copper magmatic-hydrothermal fluid salinities. The maximum copper contents of the magmatic fluids can be estimated using low-salinity fluid inclusions (red stars), little affected by posttrapping modification: Butte (Bu) from Rusk et al., 2006) and Alumbrera (Al), El Teniente (ET), Santa Rita (SR), Butte (Bu), Bingham (Bi), Grasberg (Gr), and Stronghold (S) from Audetat et al. (2008). With initial inputs of 1,350 ppm Cu in chloride solution and sufficient reduced sulfur, the arrows suggest >90% of Cu sulfide precipitates at >400°C and most at 400° to 600°C. The blue arrowed line indicates the likely cooling path for ascending fluids derived from a deep granite (2 kbar). With an initial 1,350 ppm Cu content and sufficient H_2S, deeply derived fluids that form early halos saturate in chalcopyrite at ~650°C during adiabatic decompression from lithostatic to hydrostatic conditions while remaining in the single-fluid field (Fig. 13). Similar fluids derived from a low-pressure granite (1–1.5 kbar, red line) decompress adiabatically and at high temperature (~650°C), enter the brine plus vapor field, and unmix. Chalcopyrite does not initially precipitate in deep quartz veins but does with further cooling below ~560°C in A veins at near-hydrostatic conditions. Late Cu-poor fluids (green line) derived from great depth ascend into the previously altered rock to produce C and D veins with sericitic and chloritic alteration and minor chalcopyrite, mostly at <400°C. Abbreviations: Ab = albite, Anhy = anhydrite, Bio = biotite, DQ = deep quartz, Ksp = K-feldspar, Ms = muscovite, QM = quartz-molybdenite.

ids remain entirely in the single-phase field (e.g., Butte: Rusk et al., 2008b; Haquira East: Cernuschi et al., 2018).

We illustrate two general solubilities in Figure 15: one for more neutral pH (4–5) conditions based on the Hemley et al. (1992) 1 molal chloride experiments at 0.5 kbar and 300° to 500°C buffered by quartz monzonite (quartz-K-feldspar-plagioclase-muscovite ± biotite) with sulfides (pyrrhotite-pyrite-magnetite-chalcopyrite-sphalerite-galena) and for pH ~4 experiments of Lerchbaumer and Audétat (2012) at 0.7 kbar and 600°C buffered by albite-K-feldspar-(orthoclase)-biotite-chalcopyrite-anhydrite-bornite. The latter experiments calibrate an approximated curve for 2 molal solutions. A second solubility curve for assemblages lacking Ca-bearing plagioclase and biotite at 1 molal chloride is calibrated by experiments of Hemley et al. (1992) buffered by K-feldspar-muscovite-quartz-sulfides at 0.5 kbar and 300° to 400°C and by the low-pH (≤0.3 at 25°C) experiments of Lerchbaumer and Audétat (2012) at 0.8 kbar and 650°C buffered by albite-orthoclase-muscovite-topaz-chalcocite. The solubility of copper in sulfide-saturated solution is appropriate to veins buffered by K-silicate and sericitic alteration and is estimated by mildly acidic conditions (450°–650°C) and acidic conditions (300°–400°C), respectively.

In order to use these experimental data, the solutions must be sulfide saturated. Most sulfur in source magmas is likely present as anhydrite (Ohmoto and Rye, 1979; Streck and Dilles, 1998; Field et al., 2005; Chambefort et al., 2008; Hutchinson and Dilles, 2019), and upon fluid release, anhydrite breaks down to supply SO_2 gas to the aqueous fluids. In deep porphyry deposits such as Butte, Montana, sulfur isotope compositions of anhydrite, Cu and Mo sulfide, and pyrite pairs yield equilibration temperatures of 500° to 630°C (Field et al., 2005) that are similar to temperature estimates of 475° to 700°C from associated potassic alteration and early-halo veins based on feldspar-mica-biotite compositions as well as Ti-in-quartz and Zr-in-rutile geothermometers (Brimhall, 1977; Mercer and Reed, 2013). Similarly, for shallow porphyry deposits, the sulfur isotope data from anhydrite, Cu and Mo sulfide, and pyrite pairs at El Salvador yield equilibration temperatures of 360° to 560°C, stable with potassic alteration (Field and Gustafson, 1976; Field et al., 2005). These data are consistent with sufficient H_2S supply to form sulfide via disproportionation of SO_2 into water ($4SO_2 + 4H_2O = H_2S + 3H_2SO_4$) at temperatures as high as 650°C. Although this reaction is thought to react all SO_2 by 400°C (Ohmoto and Rye, 1979), the reaction is shifted toward the products at high pressure. Alternatively, the reaction of SO_2 gas directly with Ca plagioclase produces the same 1:3 proportion of H_2S to H_2SO_4 and may occur at temperatures above 700°C (Blundy et al., 2015; Henley et al., 2015).

Magmatic fluids are estimated to contain 910 to 2,730 ppm Cu, calculated using the silicate melt-fluid partition coefficient of 9.1 molality of chloride in fluid (Candela and Holland, 1984), initial melt contents of 100 to 150 ppm copper, and 1 to 2 molal chloride. These copper contents are similar to those from fluid inclusions trapped at high temperatures in the single-phase field, which can be modified by a copper increase because of posttrapping indiffusion (Audetat et al., 2008; Lerchbaumer and Audetat, 2012). As documented by the Mole granite and modeled by Candela and Holland (1984) and Cline and Bodnar (1991), early fluids evolved from magma are Cu rich and deplete the remaining magma's Cu content, and therefore, late fluids are Cu poor.

Within this context, three fluid evolution paths illustrate the separation of fluids from deep magmas, shallow magmas, and late fluids (1, 2, and 3, in Fig. 15). The copper solubility relationships predict that in early fluids, about 90% of copper sulfide precipitates in the range of 400° to 650°C in K-silicate alteration and associated early-halo and/or A veins,

although as noted above, geologic data suggest that in shallow-sourced fluids, sufficient sulfide to precipitate copper sulfide may become available at ~560°C. Late fluids ascend from great depth and are, therefore, a single phase, reaching the ore zone at ~400°C. However, these fluids have less copper (~100–400 ppm). For example, it is plausible for an early fluid with 2,000 ppm Cu to evolve into a late fluid with 200 ppm Cu (Fig. 15). Such a late fluid would saturate in Cu-Fe sulfide at a relatively low temperature of ~420°C and precipitate 90% of its Cu by ~280°C. Consequently, such late, Cu-poor fluids would be undersaturated with respect to Cu-Fe sulfide and would be expected to dissolve Cu from earlier deposited Cu-Fe sulfides and then, with further cooling below ~420°C would precipitate minor amounts of Cu-Fe sulfide. Therefore, the passage of late fluids predicts late and local Cu remobilization from early veins and halos and the occurrence of reprecipitated Cu-Fe sulfide in C and D veins in the range of 300° to 450°C. Nonetheless, more data and studies are needed to properly evaluate Cu remobilization mechanisms at low temperatures.

Conclusions

The following evolution can reconcile the two alternate hypotheses for Cu-Fe sulfide precipitation in porphyry deposits. One or more early and high-temperature events occur where most Cu-Fe sulfide is initially introduced and precipitated as per hypothesis 1 (>450°C). This event is followed by a later, more moderate-temperature event in which additional but lesser amounts of Cu-Fe sulfide are introduced, and previously precipitated copper is locally remobilized and reprecipitated in line with the observations that sustain hypothesis 2 (<450°C). At this late stage, a network of microfractures is created through all the older lucent-CL quartz types by volume contraction and dissolution upon cooling. The bulk of dull-CL quartz is pervasively introduced through these microfractures. It may precipitate in contact with older sulfides hosted in lucent-CL quartz because the interfaces between different minerals are preexisting discontinuities sensitive to detachment during the volume contraction of quartz. This mechanism explains why it is more common to observe Cu-Fe sulfides in contact with young dull-CL quartz than with the relict lucent-CL quartz that formed with them.

In this reconciled hypothesis, the bulk of Cu-Fe sulfides is introduced through a series of early events at high temperatures (>450° and <650°C) characterized either by A veins containing lucent-CL quartz at lower pressure or by early halos at higher pressures, both of which formed together with wall-rock hydrothermal K-silicate alteration zones containing K-feldspar, biotite, and local muscovite and andalusite (Figs. 11, 12). Below the ore zone, in the roots of the porphyry system, a low-Cu-grade or barren core is formed by a zone containing deep quartz veins (Figs. 1, 3), aplite dikes, and biotite veins that formed at higher temperatures (>650°C) and in stability with K-silicate alteration. There, Cu-Fe sulfide precipitation is likely inhibited by high temperatures and the limited availability of H_2S.

In some porphyry deposits, a smaller volume of Cu-Fe sulfides with some molybdenite can be introduced in B veins with lucent-CL quartz that are also stable with K-silicate alteration. However, the bulk of the molybdenite usually precipitates at higher temperatures in banded molybdenite-quartz veins that are older than B veins or, in some cases, in nonbanded quartz-molybdenite veins that are younger than B veins. Both molybdenite-bearing veins are also stable with K-silicate alteration (Figs. 11, 12). This veining paragenesis indicates that porphyry deposits produce Cu mineralization without Mo first (A veins and early halos), then Mo mineralization without Cu (banded quartz-molybdenite veins). Where present, smaller volumes of both Cu and Mo may be introduced or reprecipitated later (B and C veins), and a few porphyry deposits produce younger Mo mineralization without Cu (nonbanded quartz-molybdenite veins; Figs. 11, 12). This may be related to temporal changes in Cu/Mo ratios in the magmatic-hydrothermal fluid due to magmatic processes in the parental batholith, as well as changes in fluid temperature.

Widespread microfractures are created by volume contraction of older lucent-CL quartz upon cooling below the quartz alpha-beta transition at 573°C and continue with cooling down to about 400°C. During this process, the microfractures are enhanced by dissolution due to fluid entering the silica retrograde field at ~450°C (Figs. 13, 14). This volume reduction occurs after K-silicate alteration has ceased and when the system experiences protracted cooling, likely due to the retraction of the magmatic system at depth. The microfractures through lucent-CL quartz crosscut all older lucent-CL quartz types throughout the vertical extent of the porphyry system, from the deep low-Cu-grade core to the shallower and peripheral Cu-Mo–bearing zone, and are later filled with younger dull-CL quartz. In this way, the bulk of the moderate-temperature dull-CL quartz postdates the bulk of the Cu-Fe sulfide and molybdenite precipitation (Fig. 11). Nonetheless, this moderate-temperature event overlaps with the formation of sparsely abundant C veins containing Cu-Fe sulfides and maybe with Cu-Fe sulfide that infills some B vein centerlines. Additional Cu-Fe sulfides may be introduced with these moderate-temperature magmatic-hydrothermal fluids but in significantly lesser amounts compared to earlier high-temperature introduction. The Cu-Fe sulfides in moderate-temperature veins are likely locally remobilized and reprecipitated from previously deposited Cu-Fe sulfide. The flooding of dull-CL quartz at a lower temperature in microfractures through older quartz continued through the beginning stages of D-vein formation and sericitic alteration (Figs. 11, 12).

Deeply formed early-halo-type porphyry deposits like Haquira or hybrid deposits like Encuentro have less dull-CL quartz in microfractures than more shallowly formed A-vein-type porphyry deposits like Batu Hijau. These differences in the low-temperature overprint between early-halo-type and A-vein-type deposits may be related to the pressure dependence of the temperature range of retrograde silica solubility (Fig. 13). Whereas in deep early-halo-type deposits, the bulk of the Cu is precipitated during the early stages of fluid cooling in the zone of retrograde silica solubility when quartz precipitation is inhibited (i.e., in early halos that have little quartz), in shallow A-vein-type deposits, the bulk of Cu is precipitated as fluids cool through the normal prograde solubility zone and precipitate abundant quartz in A veins. Therefore, later fluids in the retrograde solubility window will percolate through a much larger volume of quartz veins with Cu-Fe sulfides in A-vein-type deposits than in early-halo-type deposits and are therefore able to dissolve and reprecipitate more quartz in the former than in the latter.

Despite the diversity of vein and alteration types that is described for porphyry deposits from different areas and ages, there is a fundamental commonality in the key vein or halo types, timing, and associated hydrothermal alteration across porphyry deposits globally (Gustafson and Hunt, 1975; Seedorff et al., 2005; Proffett, 2009; Sillitoe, 2010). The veining history is more evident in simpler, smaller, and short-lived deposits than in deposits with a protracted history of magmatic-hydrothermal overprinting following multiple intrusions. Nonetheless, the crosscutting relationships of the different intrusions, veins, and halo types remain valuable for understanding the genesis these deposits. For this purpose, establishing a standard nomenclature based on the mineralogical, textural, morphological, and, most importantly, crosscutting relationships is critical for developing a genetic understanding across different porphyry deposits. This may also guide observations during mineral exploration of a porphyry deposit prospect and help infer and reconstruct its spatial zonation from fragmental data. Detailed SEM-CL, QEMSCAN, petrography, fluid inclusion, and other mineralogical and textural studies of each vein and halo type are very much needed. These studies should be reconciled with crosscutting relationships and the spatial distribution of veins, halos, and associated wall-rock hydrothermal alteration at the deposit scale. Further investigation is required to understand better the differences in veining zonation at both the deep low-Cu-grade core and shallow areas above the Cu ore. The thermal histories of A-vein-type versus early-halo-type porphyry deposits should continue to be studied.

Acknowledgments

We thank First Quantum Minerals LTD for supporting Federico Cernuschi's Ph.D. work and Antofagasta Minerals LTD for supporting Jaime Osorio's M.Sc. research, both at Oregon State University. First Quantum Minerals' continued research efforts during routine mineral exploration and the initiative to share data and findings enabled Federico to continue working on the research presented in this manuscript. He recognizes the support from Mike Christie, Markku Lappalainen, Tim Ireland, Steve Andersson, Raymond Rivera, Sebastian Benavides, Matt Hope, Miguel Ponce, and James Banyard. We also thank Santiago Gigola, Raymond Rivera, Tim Ireland, Juan Burlando, Richard Sillitoe, and David Cooke for excellent discussions about porphyry geology; Brian Rusk and Andreas Audétat for the discussions about SEM-CL imaging and limitations of the Ti-in-quartz geothermometry; Jim Reynolds, Thomas Monecke, Michael Schirra, and Christoph Heinrich for discussions about the timing of Cu-Fe sulfide deposition; and Stephanie Grocke and Dick Tosdal for reviews of early versions of this manuscript. We thank Larry Meinert and reviewers David Cooke, Thomas Monecke, Melissa Gregory, and Andreas Audétat and one anonymous reviewer for valuable feedback.

REFERENCES

Acosta, M.D., Watkins, J.M., Reed, M.H., Donovan, J.J., and DePaolo, D.J., 2020, Ti-in-quartz: Evaluating the role of kinetics in high temperature crystal growth experiments: Geochimica et Cosmochimica Acta, v. 281, p. 149–167, doi: 10.1016/j.gca.2020.04.030.

Alva-Jimenez, T., Tosdal, R.M., Dilles, J.H., Dipple, G., Kent, A.J., and Halley, S., 2020, Chemical variations in hydrothermal white mica across the Highland Valley porphyry Cu-Mo district, British Columbia, Canada: Economic Geology, v. 115, p. 903–926.

Atkinson, W.W., Souviron, A., Vehrs, T.I., and Faunes, G.A., 1996, Geology and mineral zoning of the Los Pelamberes porphyry copper deposit, Chile: Society of Economic Geologists, Special Publication 5, p. 131–156.

Audétat, A., and Günther, D., 1999, Mobility and H_2O loss from fluid inclusions in natural quartz crystals: Contributions to Mineralogy and Petrology, v. 137, p. 1–14.

Audétat, A., Pettke, T., Heinrich, C.A., and Bodnar, R.J., 2008, The composition of magmatic-hydrothermal fluids in barren and mineralized intrusions: Economic Geology, v. 103, p. 877–908.

Barnes, H.L., 1979, Solubilities or ore minerals, *in* Barnes, H.L., ed., Geochemistry of hydrothermal ore deposits, 2nd ed.: New York, Wiley, p. 404–454.

Barton, P.B., Jr., and Skinner, B.J., 1967, Sulfide mineral stabilities, *in* Barnes, H.L., ed., Geochemistry of hydrothermal ore deposits: New York, Holt, Rinehart, and Winston, p. 236–333.

Beane, R.E., and Titley, S.R., 1981, Porphyry deposits Part II. Hydrothermal alteration and mineralization: Economic Geology 75th Anniversary Volume, p. 235–269.

Benavides, S., 2017, Characterisation of sericitic alteration at the Taca Taca Bajo porphyry Cu deposit, Argentina: Unpublished M.S. thesis, Tasmania, Australia, University of Tasmania, 162 p.

Bierlein, F.P., Potma, W., Cernuschi, F., Brauhart, C., Robinson, J., Bargmann, C.J., Bullen, W., Henriquez, J.F., Davies, I., and Kennedy, A., 2020, New insights into the evolution and age of the Neoproterozoic Jebel Ohier porphyry copper deposit, Red Sea Hills, northeastern Sudan: Economic Geology, v. 115, p. 1–31, doi: 10.5382/econgeo.4691.

Blundy, J., Mavrogenes, J., Tattich, B., Sparks, S., and Gilmer, A., 2015, Generation of porphyry copper deposits by gas-brine reaction in volcanic arcs: Nature Geoscience, v. 8, p. 235–240, doi: 10.1038/NGEO2351.

Bodnar, R.J., 1995, Fluid inclusion evidence for a magmatic source for metals in porphyry deposits: Mineralogical Association of Canada, Short Course 23, p. 139–152.

Bodnar, R.J., Lecumberri-Sanchez, P., Moncada, D., and Steele-MacInnis, M., 2014, Fluid inclusions in hydrothermal ore deposits, *in* Turekian, K.K., and Holland, H.D., eds., Treatise on geochemistry: Elsevier, p. 119–142, doi: 10.1016/B978-0-08-095975-7.01105-0.

Brimhall, G.H., 1972, Early hydrothermal wall-rock alteration at Butte, Montana: Ph.D. dissertation, Berkeley, University of California, 103 p.

——1977, Early fracture-controlled disseminated mineralization at Butte, Montana: Economic Geology, v. 72, p. 37–59.

Brimhall, G.H., Ague, C., and Stoffregen, R., 1985, The hydrothermal conversion of hornblende to biotite: The Canadian Mineralogist, v. 23, p. 369–379.

Burnham, C.W., 1985, Energy release in subvolcanic environments; implications for breccia formation: Economic Geology, v. 80, p. 1515–1522.

Candela, J.S., and Holland, H.D., 1984, The partitioning of copper and molybdenum between silicate melts and aqueous fluids: Geochimica et Cosmochimica Acta, v. 48, p. 373–380.

Carten, R.B., 1986, Sodium-calcium metasomatism: Chemical, temporal, and spatial relationships at the Yerington, Nevada, porphyry copper deposit: Economic Geology, v. 81, p. 1495–1519.

Cernuschi, F., 2015, The geology and geochemistry of the Haquira east porphyry copper deposit of southern Peru: Insights on the timing, temperature and lifespan of the magmatic-hydrothermal alteration and mineralization: Unpublished Ph.D. dissertation, Corvallis, United States, Oregon State University, 256 p.

Cernuschi, F., Einaudi, M.T., Dilles, J.H., Heather, K.B., and Barr, N.C., 2012, Hydrothermal veins, porphyry geochemistry and mineralization zonation of the Haquira East porphyry Cu-Mo deposit, Peru: Society of Economic Geologists, SEG 2012: Integrated Exploration and Ore Deposits, Lima, Peru, September 23–26, 2012, Proceedings.

Cernuschi, F., Dilles, J.H., and Creaser, R., 2013, Hydrothermal alteration, SWIR-mineral mapping, vein distribution and age of the Haquira-East Cu-Mo porphyry: Society for Geology Applied to Mineral Deposits (SGA), Biennial Meeting, 12th, Uppsala, Sweden, August 12–15, 2013, Proceedings, v. 2, p. 782–785.

Cernuschi, F., Dilles, J.H., Grocke, S.B., Valley, J.W., Kitajima, K., and Tepley, F.J., 2018, Rapid formation of porphyry deposits evidenced by diffusion of oxygen and titanium in quartz: Geology, v. 46, p. 611–614, doi: 10.1130/G40262.1.

Cernuschi, F., Rivera, R., Dilles, J.H., Benavides, S., and Kouzmanov, K., 2019, Mineralogical variations in early halo alteration selvages of porphyry

deposits from North and South America [abs.]: Society of Economic Geologists, SEG 2019: South American Metallogeny: Sierra to Craton, Santiago, Chile, October 7–10, 2019, Proceedings.

Cernuschi, F., Gigola, S., Brownscombe, W., Ireland, T., Banyard, J., Arribasplata, D., Schorr, J., Gonnet, P., Sosa, P., and Duran, M., in press, Hydrothermal alteration chemistry and mineralogy of the Maricunga-style Vendaval Central Cu-Au porphyry [ext. abs.]: Society for Geology Applied to Mineral Deposits (SGA), Biennial Meeting, Zurich, August 28-September 1, 2023, Proceedings, 4 p.

Chambefort, I., Dilles, J.H., and Kent, J.R., 2008, Anhydrite-bearing andesite and dacite as a source for sulfur in magmatic-hydrothermal mineral deposits: Geology, v. 36, no. 9, p. 719–722.

Cline, J.S., and Bodnar, R.J., 1991, Can economic porphyry copper mineralization be generated by a typical calc-alkaline melt?: Journal of Geophysical Research, v. 96, p. 8113–8126.

Clode, C., Proffett, J., Mitchell, P., and Munajat, I., 1999, Relationships of intrusion, wall-rock alteration and mineralization in the Batu Hijau copper-gold porphyry deposit: Australasian Institute of Mining and Metallurgy (AusIMM), Publication Series, no. 4/99, p. 485–498.

Dilles, J.H., 1984, The petrology and geochemistry of the Yerington batholith and the Ann-Mason porphyry copper deposit, Western Nevada: Unpublished Ph.D. dissertation, Stanford, Stanford University, 389 p.

——1987, Petrology of the Yerington batholith, Nevada: Evidence for evolution of porphyry copper ore fluids: Economic Geology, v. 82, p. 1750–1789.

Dilles, J.H., and Einaudi, M.T., 1992, Wall-rock alteration and hydrothermal flow paths about the Ann-Mason porphyry copper deposit, Nevada: A 6-km vertical reconstruction: Economic Geology, v. 87, p. 1963–2001.

Dilles, J.H., and John, D.A., 2021, Porphyry and epithermal mineral deposits, *in* Alderton, D., and Elias, S.A., eds., Encyclopedia of geology, 2nd ed.: Academic Press, p. 847–866, doi: 10.1016/B978-0-08-102908-4.00005-9.

Dilles, J.H., Einaudi, M.T., Proffett, J.M., Jr., and Barton, M.D., 2000, Overview of the Yerington porphyry copper district: Magmatic to non-magmatic sources of hydrothermal fluids: Their flow paths and alteration effects on rocks and Cu-Mo- Fe-Au ores: Society of Economic Geologists Guidebook Series, v. 32, p. 55–66.

Driesner, T., and Heinrich, C.A., 2007, The system H_2O-NaCl. Part I: Correlation formulae for phase relations in temperature-pressure-composition space from 0 to 1000°C, 0 to 5000 bar, and 0 to 1 XNaCl: Geochimica et Cosmochimica Acta, v. 71, p. 4880–4901.

——2019, Revised model of porphyry-Cu formation: Ore forms at the porphyry to epithermal transition, overprinting barren stockwork veining and potassic alteration: Society for Geology Applied to Mineral Deposits (SGA), Biennial Meeting, 15th, Glasgow, Scotland, August 27–30, 2019, Proceedings.

Einaudi, M.T., 1997, Mapping altered and mineralized and rocks: An introduction to the Anaconda method: Stanford, Stanford University, Unpublished Short Course Notes, 19 p.

Field, C.W., and Gustafson, L.B., 1976, Sulfur isotopes in the porphyry copper deposit at El Salvador, Chile: Economic Geology, v. 71, p. 1533–1548.

Field, C.W., Zhang, L., Dilles, J.H., Rye, R.O., and Reed, M.H., 2005, Sulfur and oxygen isotopic record in sulfate and sulfide minerals of early, deep, pre-main stage porphyry Cu-Mo and late main stage base-metal mineral deposits, Butte district, Montana: Chemical Geology, v. 215, p. 61–93.

Fournier, R.O., 1967, The porphyry copper deposit exposed in the Liberty open-pit mine near Ely, Nevada; Part 1, syngenetic formation: Economic Geology, v. 62, p. 57–81, doi: 10.2113/gsecongeo.62.1.57.

——1985, The behavior of silica in hydrothermal solutions: Reviews in Economic Geology, v. 2, p. 45–61.

Frank, M.R., Candela, P.A., and Piccoli, P.M., 1998, K-feldspar-muscovite-andalusite-quartz-brine phase equilibria: An experimental study at 25 to 60 MPa and 400 to 550°C: Geochimica et Cosmochimica Acta, v. 62, p. 3717–3727.

Garwin, S., 2002, The geologic setting of intrusion-related hydrothermal systems near the Batu Hijau porphyry copper-gold deposit, Sumbawa, Indonesia: Society of Economic Geologists, Special Publication 9, p. 333–366.

Gregory, M.J., 2017, A fluid inclusion and stable isotope study of the Pebble porphyry copper-gold-molybdenum deposit, Alaska: Ore Geology Reviews, v. 80, p. 1279–1303, doi: 10.1016/j.oregeorev.2016.08.009.

Gustafson, L.B., and Hunt, J.P., 1975, The porphyry copper deposit at El Salvador, Chile: Economic Geology, v. 70, p. 857–912.

Gustafson, L.B., and Quiroga, J., 1995, Patterns of mineralization and alteration below the porphyry copper orebody at El Salvador, Chile: Economic Geology, v. 90, p. 2–16.

Halley, S.W., Dilles, J.H., and Tosdal, R.M., 2015, Footprints: Hydrothermal alteration and geochemical dispersion around porphyry deposits: Society of Economic Geologists, SEG Newsletter, no. 100, p. 12–17.

Hehnke, C., Ballantyne, G., Martin, H., Hart, W., Schwarz, A., and Stein, H., 2012, Geology and exploration progress at the Resolution porphyry Cu-Mo deposit, Arizona: Society of Economic Geologists, Special Publication 16, p. 147–166.

Hemley, J.J., and Hunt, J.P., 1992, Hydrothermal ore-forming processes in the light of studies in rock-buffered systems; II. Some general geologic applications: Economic Geology, v. 87, p. 23–43.

Hemley, J.J., and Jones, W.R., 1964, Chemical aspects of hydrothermal alteration with emphasis on hydrogen metasomatism: Economic Geology, v. 59, p 538–569.

Hemley, J.J., Montoya, J.W., Marinenko, J.W., and Luce, R.W., 1980, Equilibria in the system Al_2O_3-SiO_2-H_2O and some general implications for alteration/mineralization processes: Economic Geology, v. 75, p. 210–228.

Hemley, J.J., Cygan, G.L., Fein, J.B., Robinson, G.R., and d'Angelo, W.M., 1992, Hydrothermal ore-forming processes in the light of studies in rock-buffered systems; I. Iron-copper-zinc-lead sulfide solubility relations: Economic Geology, v. 87, p. 1–22.

Henley, R.W., King, P.L., Wykes, J.L., Renggli, C.J., Brink, F.J., Clark, D.A., and Troitzsch, U., 2015, Porphyry copper deposit formation by sub-volcanic sulphur dioxide flux and chemisorption: Nature Geoscience, v. 8, p. 210–215, doi: 10.1038/NGEO2367.

Huang, R., and Audétat, A., 2012, The titanium-in-quartz (Ti-in-quartz) thermobarometer: A critical examination and re-calibration: Geochimica et Cosmochimica Acta, v. 84, p. 75–89.

Hutchinson, M., and Dilles, J.H., 2019, Evidence for magmatic anhydrite in porphyry copper intrusions: Economic Geology, v. 114, no. 1, p. 143–152.

Irwin, J.J., and Roedder, E., 1995, Diverse origins of fluid in magmatic inclusions at Bingham (Utah, USA), Butte (Montana, USA), St-Austell (Cornwall, UK), and Ascension-Island (Mid-Atlantic, UK), indicated by laser microprobe analysis of Cl, K, Br, I, Ba Plus Te, U, Ar, Kr, and Xe: Geochimica et Cosmochimica Acta, v. 59, p. 295–312.

Jensen, K.R., Campos, E., Wilkinson, J.J., Wilkinson, C.C., Kearsley, A., Miranda-Díaz, G., and Véliz, W., 2022, Hydrothermal fluid evolution in the Escondida porphyry copper deposit, northern Chile: Evidence from SEM-CL imaging of quartz veins and LA-ICP-MS of fluid inclusions: Mineralium Deposita, v. 57, p. 279–300, doi: 10.1007/s00126-021-01058-z.

Kirkham, R.V., and Sinclair, W.D., 1988, Comb quartz layers in felsic intrusions and their relationship to the origin of porphyry deposits: Canadian Institute of Mining and Metallurgy, Special Volume 39, p. 50–71.

Klemm, L.M., Pettke, T., Heinrich, C.A., and Campos, E., 2007, Hydrothermal evolution of the El Teniente deposit, Chile: Porphyry Cu-Mo ore deposition from low-salinity magmatic fluids: Economic Geology, v. 102, p. 1021–1045, doi: 10.2113/gsecongeo.102.6.1021.

Landtwing, M.R., Pettke, T., Halter, W.E., Heinrich, C.A., Redmond, P.B., Einaudi, M.T., and Kunze, K., 2005, Copper deposition during quartz dissolution by cooling magmatic-hydrothermal fluids: The Bingham porphyry: Earth and Planetary Science Letters, v. 235, p. 229–243.

Landtwing, M.R., Furrer, C., Redmond, P.B., Pettke, T., Guillong, M., and Heinrich, C.A., 2010, The Bingham Canyon porphyry Cu-Mo-Au deposit. III. Zoned copper-gold ore deposition by magmatic vapor expansion: Economic Geology, v. 105, p. 91–118.

Leach, T.M., 1999, Evolution of selected porphyry copper-gold systems in the southwest Pacific region and its relevance to exploration: Australasian Institute of Mining and Metallurgy (AusIMM), Publication Series, no. 4/99, p. 211–225.

Lecumberri-Sanchez, P., Steele-MacInnis, M., Weis, P., Driesner, T., and Bodnar, R.J., 2015, Salt precipitation in magmatic-hydrothermal systems associated with upper crustal plutons: Geology, v. 43, p. 1063–1066.

Lerchbaumer, L., and Audétat, A., 2012, High Cu concentrations in vapor-rich inclusions: An artifact?: Geochimica et Cosmochimica Acta, v. 88, p. 255–274.

Mao, W., Rusk, B., Yang, F., and Zhang, M., 2017, Physical and chemical evolution of the Dabaoshan porphyry Mo deposit, South China: Insights from fluid inclusions, cathodoluminescence, and trace elements in quartz: Economic Geology, v. 112, p. 889–918.

Maydagán, L., Franchini, M., Rusk, B., Lentz, D.R., McFarlane, C., Impiccini, A., Rios, F.J., and Rey, R., 2015, Porphyry to epithermal transition in the Altar Cu-(Au-Mo) deposit, Argentina, studied by cathodoluminescence, LA-ICP-MS, and fluid inclusion analysis: Economic Geology, v. 110, p. 889–923.

Mercer, C.N., and Reed, M.H., 2013, Porphyry Cu-Mo stockwork formation by dynamic, transient hydrothermal pulses: Mineralogic insights from the deposit at Butte, Montana: Economic Geology, v. 108, p. 1347–1377, doi: 10.2113/econgeo.108.6.1347.

Mercer, C.N., Reed, M.H., and Mercer, C.M., 2015, Time scales of porphyry Cu deposit formation: Insights from titanium diffusion in quartz: Economic Geology, v. 110, p. 587–602.

Meyer, C., 1965, An early potassic type of wall rock alteration at Butte, Montana: American Mineralogist, v. 50, p. 1717–1722.

Meyer, C., Shea, E.P., Goddard, C.C., and staff, 1968, Ore deposits at Butte, Montana, *in* Ridge, J.D., ed., Ore deposits of the United States, 1933–1967: New York, American Institute of Mining, Metallurgical and Petroleum Engineers, p. 1373–1416.

Monecke, T., Monecke, J., Reynolds, T.J., Tsuruoka, S., Bennett, M.M., Skewes, W.B., and Palin, R.M., 2018, Quartz solubility in the H_2O-NaCl system: A framework for understanding vein formation in porphyry deposits: Economic Geology, v. 113, p. 1007–1046, doi: 10.5382/econgeo.2018.4580.

Monecke, T., Monecke, J., and Reynolds, T.J., 2019, The influence of CO_2 on the solubility of quartz in single-phase hydrothermal fluids: Implications for the formation of stockwork veins in porphyry copper deposits: Economic Geology, v. 114, no. 6, p. 1195–1206, doi: 10.5382/econgeo.4680.

Montoya, J.W., and Hemley, J.J., 1975, Activity relations and stabilities in alkali feldspar and mica alteration reactions: Economic Geology, v. 70, p. 577–583.

Müller, A., Herrington, R., Armstrong, R., Seltman, R., Kirwin, D., Stenina, N., and Kronz, A., 2010, Trace elements and cathodoluminescence of quartz in stockwork veins of Mongolian porphyry-style deposits: Mineralium Deposita, v. 45, p. 707–727.

Müller, A., Kirwin, D., and Seltmann, R., 2023, Textural characterization of unidirectional solidification textures related to Cu-Au deposits and their implication for metallogenesis and exploration: Mineralium Deposita, doi: 10.1007/s00126-023-01175-x.

Muntean, J.L., and Einaudi, M.T., 2000, Porphyry gold deposits of the Refugio district, Maricunga belt, northern Chile: Economic Geology, v. 95, p. 1445–1472.

——2001, Porphyry-epithermal transition: Maricunga belt, northern Chile: Economic Geology, v. 96, p. 743–772.

Norton, D., 1978, Sourcelines, sourceregions, and pathlines for fluids in hydrothermal systems related to cooling plutons: Economic Geology, v. 73, p. 21–28, doi: 10.2113/gsecongeo.73.1.21.

Ohmoto, H., and Rye, R.O., 1979, Isotopes of sulfur and carbon, *in* Barnes, H.L., ed., Geochemistry of hydrothermal ore deposits, 2nd ed.: New York, Wiley Interscience, p. 509–567.

Osorio, J., 2017, Intrusion sequence and hydrothermal fluid evolution of Encuentro porphyry Cu-Mo-Au deposit, northern Chile: Unpublished M.Sc. thesis, Corvallis, Oregon, Oregon State University, 179 p.

Osorio, J., and Dilles, J., 2019, Relationships between veins abundance and distribution, timing of mineralization, and ore shells geometry, Encuentro porphyry Cu-Au-Mo deposit, northern Chile. [ext. abs.]: Society of Economic Geologists, SEG 2019: South American Metallogeny: Sierra to Craton, Santiago, Chile, October 7–10, 2019, Proceedings, 3 p.

Osorio, J., Dilles, J., and Collao, S., 2018, Hydrothermal fluid evolution of the Encuentro porphyry Cu-Au-Mo deposit, northern Chile. [ext. abs.]: Society of Economic Geologists, SEG 2018: Metals, Minerals, and Society, Keystone, Colorado, USA, September 22–25, 2018, Proceedings, 1 p.

Ossandón, G., Fréraut, R., Gustafson, L.B., Lindsay, D.D., and Zentilli, M., 2001, Geology of the Chuquicamata mine: A progress report: Economic Geology, v. 96, p. 249–270.

Perelló, J., Sillitoe, R.H., Mpodozis, C., Brockway, H., and Posso, H., 2012, Geologic setting and evolution of the porphyry copper-molybdenum and copper-gold deposits at Los Pelambres, central Chile: Society of Economic Geologists, Special Publication 16, p. 79–104.

Pirrie, D., Butcher, A.R., Power, M.R., Gottlieb, P., and Miller, G.L., 2004, Rapid quantitative mineral and phase analysis using automated scanning electron microscopy (QEMSCAN): Potential applications in forensic geoscience: Geological Society, London, Special Publication 232, p. 123–136.

Porter, J.P., Schroeder, K., and Austin, G., 2012, Geology of the Bingham Canyon porphyry Cu-Mo-Au deposit, Utah: Society of Economic Geologists, Special Publication 16, p. 127–146, doi: 10.5382/SP.16.06.

Proffett, J.M., 1973, Structure of the Butte district, Montana: *in* Miller, R.N., ed., Guidebook for the Butte field meeting of the Society of Economic Geologists: Butte, Montana, The Anaconda Company, p. G-1–G-12.

——1979, Ore deposits of the western United States: A summary: Nevada Bureau of Mines and Geology, Report 33, p. 13–32.

——2003, Geology of the Bajo de la Alumbrera porphyry copper-gold deposit, Argentina. Economic Geology, v. 98, p. 1535–1574.

——2009, High Cu grades in porphyry Cu deposits and their relationship to emplacement depth of magmatic sources: Geology, v. 37, p. 675–678, doi:10.1130/G30072A.1.

——2019, Early mineralization with high copper grades in porphyry deposits: Its characteristics and its genetic and economic significance (ext. abs.): Society of Economic Geologists, SEG 2019, South American Metallogeny: Sierra to Craton, Santiago, Chile, Conference Proceedings, Distinguished Lecture, no. S04.07, 4 p.

Redmond, P.B., and Einaudi, M.T., 2010, The Bingham Canyon porphyry Cu-Mo-Au deposit. I. Sequence of intrusions, vein formation, and sulfide deposition: Economic Geology, v. 105, p. 43–68.

Redmond, P.B., Einaudi, M.T., Inan, E.E., Landtwing, M.R., and Heinrich, C.A., 2004, Copper deposition by fluid cooling in intrusion-centered systems; new insights from the Bingham porphyry ore deposit, Utah: Geology, v. 32, p. 217–220.

Reed, M.H., 1999, Zoning of metals and early potassic and sericitic hydrothermal alteration in the Butte, Montana, porphyry Cu-Mo deposit [abs.]: Geological Society of America Abstracts with Programs, v. 31, p. A381.

Reed, M., and Dilles, J., 2020, Ore deposits of Butte, Montana: Montana Bureau of Mines and Geology, Special Publication 122, v. 2, 41 p.

Reed, M., Rusk, B., and Palandri, J., 2013, The Butte magmatic-hydrothermal system: One fluid yields all alteration and veins: Economic Geology, v. 108, p. 1379–1396, doi: 10.2113/econgeo.108.6.1379.

Rees, C., Riedell, K.B., Proffett, J.M., Macpherson, J., and Robertson, S., 2015, The Red Chris porphyry copper-gold deposit, northern British Columbia, Canada: Igneous phases, alteration and controls of mineralization: Economic Geology, v. 110, p. 857–888.

Riedell, K.B., Sandberg, J.R., Guthrie, J.O., Gorecki, A.D., Lambiotte, J.M., Reynolds, S.J., Proffett, J.M., Ybarra, S.J., and Pulter, J.E., 2013, Early halo type porphyry and breccia Cu-Mo mineralization at Copper Creek, Pinal County, Arizona: Society of Economic Geologists, SEG 2013: Geoscience for Discovery, Whistler, British Columbia, September 24–27, 2013, Proceedings.

Rivera, S.L., Alcota, H., Proffett, J., Díaz, J., Leiva, G., and Vergara, M., 2012, Update of the geologic setting and porphyry Cu-Mo deposits of the Chuquicamata district, northern Chile: Society of Economic Geologists, Special Publication 16, p. 19–54.

Roberts, S.A., 1973, Pervasive early alteration in the Butte district, Montana, *in* Miller, R.N., ed., Guidebook for the Butte field meeting of the Society of Economic Geologists: Butte, Montana, The Anaconda Company, p. HH1-HH8.

——1975, Early hydrothermal alteration and mineralization in the Butte district, Montana: Unpublished Ph.D. thesis, Cambridge, Massachusetts, Harvard University, 173 p.

Roedder, E., 1971, Fluid inclusion studies on the porphyry ore deposits at Bingham, Utah, Butte, Montana, and Climax, Colorado: Economic Geology, v. 66, p. 98–118.

——1984, Fluid inclusions: Reviews in Mineralogy, v. 12, 644 p.

Rottier, B., and Casanova, V., 2021, Trace element composition of quartz from porphyry systems: A tracer of the mineralizing fluid evolution: Mineralium Deposita, v. 56, no. 5, p. 843–862, doi: 10.1007/s00126-020-01009-0.

Rusk, B., 2012, Cathodoluminescent textures and trace elements in hydrothermal quartz, *in* Götze, J., and Möckel, R., eds., Quartz: Deposits, mineralogy and analytics: Berlin, Springer, p. 307–329.

Rusk, B.G., and Reed, M.H., 2002, Scanning electron microscope-cathodoluminescence analysis of quartz reveals complex growth histories in veins from the Butte porphyry copper deposit, Montana: Geology, v. 30, p. 727–730.

Rusk, B.G., Reed, M.R., Dilles, J.H., and Kent, A.J.R., 2006, Intensity of quartz cathodoluminescence and trace-element content in quartz from the porphyry copper deposit at Butte, Montana: American Mineralogist, v. 91, p. 1300–1312, doi: 10.2138/am.2006.1984.

Rusk, B.G., Lowers, H.A., and Reed, M.H., 2008a, Trace elements in hydrothermal quartz: Relationships to cathodoluminescent textures and insights into vein formation: Geology, v. 36, p. 547–550, doi: 10.1130/G24580A.1.

Rusk, B.G., Reed, M.H., and Dilles, J.H., 2008b, Fluid inclusion evidence for magmatic-hydrothermal fluid evolution in the porphyry copper-molybdenum deposit at Butte, Montana: Economic Geology, v. 103, p. 307–334.

Schirra, M., Heinrich, C., and Driesner, T., 2017, Fluid evolution of the Batu Hijau porphyry Cu-Au deposit, Indonesia [ext. abs.]: Society of Economic

Geologists, SEG 2017, Ore Deposits of Asia: China and Beyond, Beijing, September 17–20, 2017, Proceedings, 1 p.
Schirra, M., Driesner, T., and Heinrich, C.A., 2019, Relative timing of sulfide precipitation at the Batu Hijau porphyry Cu-Au deposit, Sumbawa, Indonesia: Society for Geology Applied to Mineral Deposits (SGA), Biennial Meeting, 15th, Proceedings, v. 3, p. 1009–1012.
Schirra, M., Laurent, O., Zwyer, T., Driesner, T., and Heinrich, C.A., 2022, Fluid evolution at the Batu Hijau porphyry Cu-Au deposit, Indonesia: Hypogene sulfide precipitation from a single-phase aqueous magmatic fluid during chlorite–white-mica alteration: Economic Geology, v. 117, p. 979–1012, doi: doi: 10.5382/econgeo.4921.
Seedorff, E., and Einaudi, M.T., 2004, Henderson porphyry molybdenum system, Colorado: I. Sequence and abundance of hydrothermal mineral assemblages, flow paths of evolving fluids, and evolutionary style: Economic Geology, v. 99, p. 3–37.
Seedorff, E., Dilles, J.H., Proffett, J.M. Jr., Einaudi, M.T., Zurcher, L., Stavast, W.J.A., Johnson, D.A., and Barton, M.D., 2005, Porphyry deposits: Characteristics and origin of hypogene features: Economic Geology 100th Anniversary Volume, p. 251–298.
Seo, J.H., Guillong, M., and Heinrich, C.A., 2012, Separation of molybdenum and copper in porphyry deposits: The roles of sulfur, redox, and pH in ore mineral deposition at Bingham Canyon: Economic Geology, v. 107, p. 333–356, doi: 10.2113/econgeo.107.2.333.
Sepp, M.D., 2022, What lies beneath? Origin and transition from the shallow epithermal Au-Ag lithocap to deeper porphyry Cu environment: Insights from the magmatic hydrothermal deposits at Yerington, Nevada, and Summitville, Colorado: Unpublished Ph.D. dissertation, Corvallis, Oregon, Oregon State University, 297 p.
Setyandhaka, D., Arif, J., and Proffett, J., 2008, Characteristics of the roots of a classic Cu-Au porphyry system: the Batu Hijau porphyry deposit, Indonesia [ext. abs.]: PACRIM Congress, Australia, 2008, Proceedings, p. 445–450.
Sillitoe, R.H., 2010, Porphyry copper systems: Economic Geology, v. 105, p. 3–41.
Sillitoe, R.H., Marquardt, J.C., Ramírez, F., Becerra, H., and Gómez, M., 1996, Geology of the concealed MM porphyry copper deposit, Chuquicamata district, northern Chile: Society of Economic Geologists, Special Publication 5, p. 59–69.
Skinner, B.J., 1966, Thermal expansion: Geological Society of America, Memoir 97, p. 75–96.
Spencer, E.T., Wilkinson, J.J., Creaser, R.A., and Seguel, J., 2015, The distribution and timing of molybdenite mineralization at the El Teniente Cu-Mo porphyry deposit, Chile: Economic Geology, v. 110, p. 387–421.
Stefanova, E., Driesner, T., Zajacz, Z., Heinrich, C.A., Petrov, P., and Vasilev, Z., 2014, Melt and fluid inclusions in hydrothermal veins: The magmatic to hydrothermal evolution of the Elatsite porphyry Cu-Au deposit, Bulgaria: Economic Geology, v. 109, p. 1359–1381, doi: 10.2113/econgeo.109.5.1359.
Steinberger, I., Hinks, D., Driesner, T., and Heinrich, C.A., 2013, Source plutons driving porphyry copper ore formation: Combining geomagnetic data, thermal constraints, and chemical mass balance to quantify the magma chamber beneath the Bingham Canyon deposit: Economic Geology, v. 108, p. 605–624.
Streck, M.J., and Dilles, J.H., 1998, Sulfur content of oxidized arc magmas as recorded in apatite from a porphyry copper batholith: Geology, v. 26, no. 6, p. 523–526.
Sun, M., Monecke, T., Reynolds, T.J., and Yang, Z., 2021, Understanding the evolution of magmatic-hydrothermal systems based on microtextural relationships, fluid inclusion petrography, and quartz solubility constraints: insights into the formation of the Yulong Cu-Mo porphyry deposit, eastern Tibetan Plateau, China: Mineralium Deposita, v. 56, p. 823–842.
Thomas, J.B., and Watson, E.B., 2012, Application of the Ti-in-quartz thermobarometer to rutile-free systems. Reply to: A comment on: Ti-in-quartz under pressure: The effect of pressure and temperature on the solubility of Ti in quartz by Thomas et al.: Contributions to Mineralogy and Petrology, v. 164, p. 1–6.
Titley, S.R., and Beane, R.E., 1981, Porphyry deposits Part I. Geologic settings, petrology, and tectogenesis: Economic Geology 75th Anniversary Volume, p. 214–234.
Tosdal, R.M., and Dilles, J.H., 2020, Creation of permeability in the porphyry Cu environment: Reviews in Economic Geology, v. 21, p. 173–204, doi: 10.5382/rev.21.05.
Tsuruoka, S., Monecke, T., and Reynolds, T.J., 2021, Evolution of the magmatic-hydrothermal system at the Santa Rita porphyry Cu deposit, New Mexico, USA: Importance of intermediate-density fluids in ore formation: Economic Geology, v. 116, p. 1267–1284, doi: 10.5382/econgeo.4831.
Uribe-Mogollon, C., and Maher, K., 2018, White mica geochemistry of the Copper Cliff porphyry Cu deposit: Insights from a vectoring tool applied to exploration: Economic Geology, v. 113, p. 1269–1295, doi: 10.5382/econgeo.2018.4591.
Vry, V.H., Wilkinson, J.J., Seguel, J., and Millan, J., 2010, Multistage intrusion, brecciation, and veining at El Teniente: Evolution of a nested porphyry system: Economic Geology, v. 105, p. 119–153.
Wark, D.A., and Watson, E.B., 2006, TitaniQ: A titanium-in-quartz geothermometer: Contributions Mineralogy and Petrology, v. 152, p. 743–754.
Weis, P., Driesner, T., and Heinrich, C.A., 2012, Porphyry-copper ore shells form at stable pressure-temperature fronts within dynamic fluid plumes: Science, v. 338, article 1613, doi: 10.1126/science.1225009.
Zwyer, T., 2010, Temporal and spatial evolution of hydrothermal, ore-related fluids in the Batu Hijau porphyry copper-gold deposit, Sumbawa (Indonesia): Unpublished M.S. thesis, Switzerland, ETH Zürich, 57 p.

Federico Cernuschi is an independent consultant specializing in the geology and geochemistry of magmatic and hydrothermal processes, with a focus on porphyry deposits. He integrates classic hand-lens observations and Anaconda-style mapping with trace element geochemistry, spectroscopy, and other analytical techniques. Fede provides continued support to First Quantum Minerals and services to companies like Rio Tinto, Fortescue, and several juniors. In these roles, he has worked on exploration projects of varied geology and age across more than 20 countries and has provided training to multiple global exploration teams. His education includes the University of the Republic (UDELAR), Uruguay (B.S.), and Oregon State University, USA (M.S. and Ph.D.).